NOAA Technical Report NESDIS 154

DOI: 10.25923/p9de-yw97

Report for
Dedicated JPSS VIIRS Ocean Color Calibration/Validation Cruise
September 2019

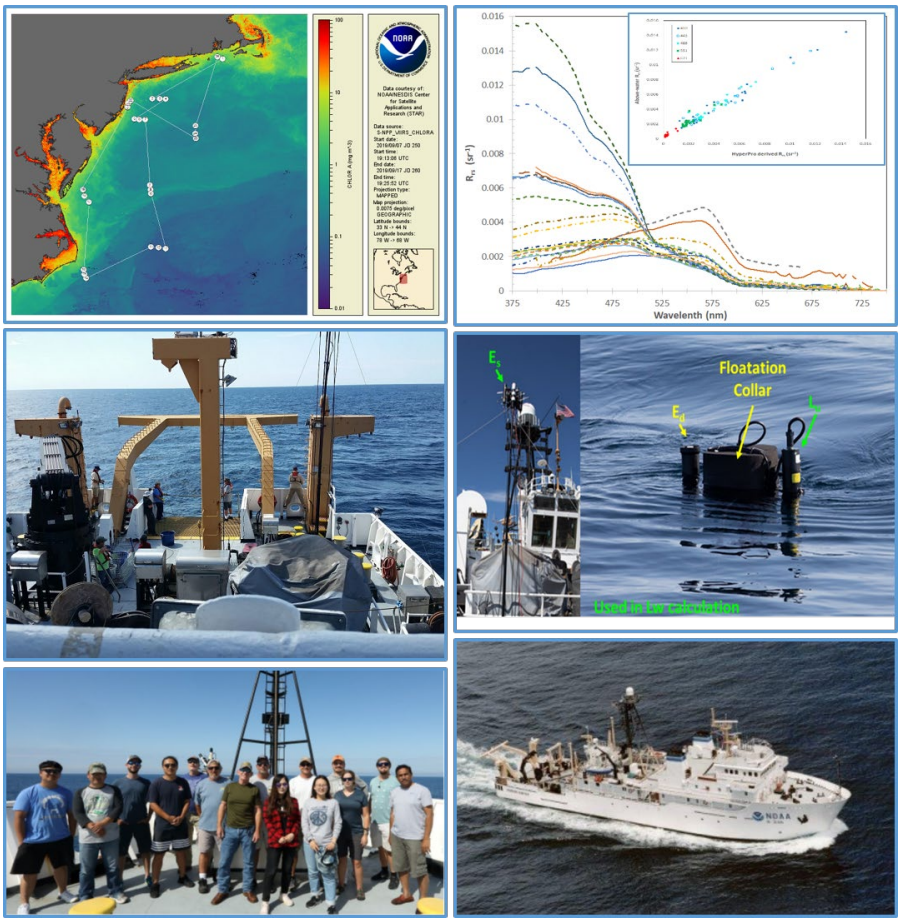

Washington, D.C.
February 2021

US DEPARTMENT OF COMMERCE
National Oceanic and Atmospheric Administration
National Environmental Satellite, Data, and Information Service

NOAA TECHNICAL REPORTS
National Environmental Satellite, Data, and Information Service

The National Environmental Satellite, Data, and Information Service (NESDIS) manages the Nation's civil Earth-observing satellite systems, as well as global national databases for meteorology, oceanography, geophysics, and solar-terrestrial sciences. From these sources, it develops and disseminates environmental data and information products critical to the protection of life and property, national defense, the national economy, energy development and distribution, global food supplies, and the development of natural resources.

Publication in the NOAA Technical Report series does not preclude later publication in scientific journals in expanded or modified form. The NESDIS series of NOAA Technical Reports is a continuation of the former NESS and EDIS series of NOAA Technical Reports and the NESC and EDS series of Environmental Science Services Administration (ESSA) Technical Reports.

Copies of other NESDIS Technical reports may be available by contacting NESDIS Chief of Staff, NOAA/ NESDIS, 1335 East-West Highway, SSMC1, Silver Spring, MD 20910, (301) 713-3578.

Previous NESDIS Technical Reports on the Dedicated JPSS VIIRS Ocean Color Calibration/Validation Cruise Series:

Report #146	**November 2014**	**doi: 10.7289/V52B8W0Z**
Report #148	**December 2015**	**doi: 10.7289/V5/TR-NESDIS-148**
Report #151	**October 2016**	**doi: 10.7289/V5/TR-NESDIS-151**
Report #152	**May 2019**	**doi: 10.25923/scyb-qf42**

*Cover image: (Clockwise from top left): 1) 2019 VIIRS Cal/Val cruise station locations overlaid onto NOAA MSL12 VIIRS SNPP science quality full spatial resolution (~750 m) mapped 10-day composite (7 September 2019 to 17 September 2019) of chlorophyll-*a*; 2) representative remote sensing reflectance spectra for all stations; (inset) plot of relationship of different measuring methods for remote sensing reflectance; 3) floating radiometer; 4) OMAO stock photo of NOAA Ship *Gordon Gunter*; 5) Photo of scientific crew; 6) deploying four profiling radiometers simultaneously from the aft deck.

NOAA Technical Report NESDIS 154

DOI: 10.25923/p9de-yw97

Report for Dedicated JPSS VIIRS Ocean Color Calibration/Validation Cruise September 2019

Edited by Veronica P. Lance[1*]
NOAA/NESDIS Center for Satellite Applications and Research (STAR), 5830 University Research Court, College Park, MD 20740, USA

*Corresponding Editor: veronica.lance@noaa.gov

Contributing authors:

Michael Ondrusek[1]*, Veronica P. Lance[1], Menghua Wang[1], Eric Stengel[1], Charles Kovach[1,2],
[1]NOAA/NESDIS Center for Satellite Applications and Research (STAR), 5830 University Research Court, College Park, MD 20740, USA
[2]Global Science and Technology, Inc., 7855 Walker Drive, Suite 200, Greenbelt, MD 20770, USA
*michael.ondrusek@noaa.gov

And (alphabetical by group lead last name):

Scott Freeman* and Antonio Mannino
NASA Goddard Space Flight Center, Greenbelt, MD
*scott.freeman@nasa.gov

Alex Gilerson*, Carlos Carrizo, Philipp Grötsch, Eder Herrera, Mateusz Malinowski, Sam Ahmed
City College of the City University of New York, 160 Convent Ave, New York, NY 10031, USA
*gilerson@ccny.cuny.edu

Joaquim I. Goes*, Jinghui Wu, Helga do Rosario Gomes and Kali McKee
Lamont Doherty Earth Observatory at Columbia University, 61 Route 9W, Palisades, NY, 10964, USA
*jig@ldeo.columbia.edu

Chuanmin Hu*, Jennifer Cannizzaro, Yingjun Zhang, Yang Zhang, David English
College of Marine Science, University of South Florida, 140 7th Avenue South, St. Petersburg, FL 33701, USA
*huc@usf.edu

Sherwin Ladner*, Wesley Goode
Naval Research Laboratory, Stennis Space Center, MS 39529, USA
*sherwin.ladner@nrlssc.navy.mil

Zhongping Lee*, Jianwei Wei, Shuai Zhang
School for the Environment, University of Massachusetts Boston, 100 Morrissey Blvd, Boston, MA 02125, USA
*zhongping.lee@umb.edu

Michael Twardowski* and Nicole Stockley, Christopher Strait
Harbor Branch Oceanographic Institute, Florida Atlantic University, Fort Pierce, FL 34946, USA
*mtwardowski@fau.edu

Kenneth J. Voss
Department of Physics, University of Miami, Knight Physics Building, Coral Gables, FL 33124, USA
*voss@physics.miami.edu

*Group corresponding contact

Washington, DC
February 2021

US DEPARTMENT OF COMMERCE
Wynn Coggins, Acting Agency Head

National Oceanic and Atmospheric Administration
Benjamin Friedman, Deputy Under Secretary for Operations, performing the duties of Under Secretary of Commerce for Oceans and Atmosphere and NOAA Administrator

National Environmental Satellite, Data, and Information Service
Dr. Stephen Volz, Assistant Administrator

Contents

List of Figures

List of Tables

List of Equations

Preface

The Ocean Color Team at the NOAA Center for Satellite Applications and Research (STAR) is focused on "end-to-end" production of high-quality satellite ocean color products. In situ validation of satellite data is essential to produce the high-quality, fit-for-purpose remotely sensed ocean color products that are required and expected by all NOAA line offices, as well as by external (both applied and research) users. In addition to serving the needs of its diverse users within the US, NOAA has a role in supporting the international ocean color community and is actively engaged in the International Ocean Colour Coordinating Group (IOCCG) with Menghua Wang as the NOAA representative.

NOAA/STAR scientists have been acquiring in situ data throughout all of the ocean color satellite missions. Since the launch in October 2011 of the Visible Infrared Imaging Radiometer Suite (VIIRS) aboard the Suomi National Polar-orbiting Partnership (SNPP) platform, part of the US Joint Polar Satellite System (JPSS) program, the NOAA/STAR Ocean Color Team has been making in situ measurements routinely in support of validation and algorithm development activities. The second VIIRS sensor was successfully launched in November 2017 onboard the NOAA-20 satellite. To date, five Dedicated JPSS VIIRS Ocean Color Calibration/Validation (Cal/Val) Cruises have been conducted. Over time support has been provided by: 1) the JPSS program for funding the STAR ocean color team and many of the participating groups; 2) the NOAA Office of Marine and Aviation Operations (OMAO) for ship time; and 3) NOAA/NESDIS/STAR with some supplemental in kind support by external Cal/Val team members and in kind support from NASA. This report covers the fifth dedicated VIIRS Cal/Val cruise that took place in September 2019 along the US mid-Atlantic and northeast coast. A sixth cruise was originally scheduled for March 2020 in Hawaii but was postponed and then completely cancelled due to the COVID-19 pandemic. The next dedicated VIIRS Cal/Val Cruise is planned for April 2021 in the Northern Gulf of Mexico near the National Aeronautics and Space Administration (NASA) AErosol RObotic NETwork for Ocean Color (AeroNET-OC) site named "WavCIS (CSI-06)" for inter-comparison. For FY22, OMAO ship time has been requested in Hawaii to sample oligotrophic waters near the Marine Optical Buoy (MOBY), the NOAA operational in situ vicarious calibration system, to cross-calibrate the in situ optical measurements made from the ship with MOBY observations.

These dedicated ocean color validation field campaigns provide in situ measurements needed to produce the best quality, fit-for-purpose ocean color remote sensing data and data products for NOAA applications and for users beyond NOAA. These observations support validation activities for the current JPSS VIIRS sensors on SNPP and NOAA-20 satellites, which are now the primary sources for NOAA operational remotely sensed ocean color data products. The data collected may also be used in support of non-NOAA US (e.g., NASA and United States Geological Survey (USGS)) and international ocean color related satellite missions (e.g., the Ocean and Land Colour Instrument (OLCI) aboard Sentinel-3 of the European Union's Copernicus mission and the Second Generation Global Imager (SGLI) aboard Global Climate Observation Mission-Climate (GCOM-C) mission from the Japan Aerospace Exploration Agency). Through the NOAA mission of science, service and stewardship, and in collaboration with the international ocean community, we aim to provide ocean satellite data products that improve our understanding of global and coastal ocean and inland water optical, biological, and biogeochemical properties and that support applications to benefit society.

Menghua Wang
Chief, Marine Ecosystems & Climate Branch; VIIRS Ocean Color Cal/Val Team Lead; NOAA Representative to the IOCCG
Paul DiGiacomo
Chief, Satellite Oceanography & Climatology Division; JPSS Ocean EDR Lead

Page vii is inserted for print format.

NOAA Technical Report NESDIS 154
Report for
Dedicated JPSS VIIRS Ocean Color Calibration/Validation Cruise September 2019

ABSTRACT

After a delay and change of port of call due to Hurricane Dorian, the fifth NOAA Dedicated JPSS VIIRS Ocean Color Calibration/Validation (Cal/Val) Cruise took place aboard the NOAA Ship Gordon Gunter (OMAO cruise identification #GU-19-03, https://www.ncei.noaa.gov/metadata/geoportal/rest/metadata/item/gov.noaa.nodc%3A0202840/html) from 8 September to 17 September 2019, round trip through Newport, Rhode Island. Overall, 26 stations were occupied in a variety of water types in the US mid-Atlantic and northeast coastal and continental shelf regions of the Western Atlantic. Nine research groups, 15 scientists, including 5 PhD students, conducted measurements. The overall aim of these VIIRS Cal/Val cruises [Ondrusek et al., 2015; Ondrusek et al., 2016; Ondrusek et al., 2017; Ondrusek et al., 2019] is to support improvements in the extent and accuracy of satellite remotely sensed ocean color parameters in the near surface ocean. The primary objective of these cruises is to collect high quality in situ optical and related biological and biogeochemical data for the purpose of validating satellite ocean color radiometry and derived products from the Visible Infrared Imaging Radiometer Suite (VIIRS) aboard the Suomi National Polar-orbiting Partnership (SNPP) platform, [Wang et al., 2013; Wang et al., 2014; Wang et al., 2017], the US Joint Polar Satellite System (JPSS) program NOAA-20 platform, and the follow-on JPSS missions. Many cloud-free days following the passage of Hurricane Dorian resulted in an impressive, record number of in situ measurements that matched with VIIRS observations ("match-ups") compared with all earlier VIIRS dedicated Cal/Val cruises. Match-ups for VIIRS SNPP overpasses were 24 out of 26 stations and match-ups for VIIRS NOAA-20 overpasses were 23 out of 26 stations.

1 Summary of Cruise and Purpose

After a delay and change of port of call due to Hurricane Dorian, the fifth dedicated VIIRS Cal/Val cruise for 2019 took place aboard the NOAA Ship *Gordon Gunter* (OMAO cruise identification #GU-19-03, https://www.ncei.noaa.gov/metadata/geoportal/rest/metadata/item/gov.noaa.nodc%3A0202840/html) from 8 September to 17 September 2019, round trip through Newport, Rhode Island. Overall, 26 stations were occupied in a variety of water types in the US mid-Atlantic and northeast coastal and continental shelf regions of the Western Atlantic.

The overall aim of the annual NOAA Dedicated JPSS VIIRS Ocean Color Calibration/Validation (Cal/Val) Cruises [Ondrusek et al., 2015; Ondrusek et al., 2016; Ondrusek et al., 2017; Ondrusek et al., 2019] is to support improvements in the extent and accuracy of satellite remotely sensed ocean color parameters in the near surface ocean. The primary objective of these cruises is to collect high quality in situ optical and related biological and biogeochemical data for the purpose of validating satellite ocean color radiometry and derived products from the Visible Infrared Imaging Radiometer Suite (VIIRS) aboard the Suomi National Polar-orbiting Partnership (SNPP) platform, [Wang et al., 2013; Wang et al., 2014; Wang et al., 2017], the US Joint Polar Satellite System (JPSS) program NOAA-20 platform, and the follow-on JPSS missions. Data can also be used to validate ocean color from non-NOAA missions (e.g., OLCI on Sentinel-3; SGLI on GCOM-C). The second objective is to quantify the confidence intervals of optical measurement protocols. The third objective is to characterize the optical signatures of a variety of water masses (i.e., coastal, near-shore, cross-shelf, eddies, fronts, filaments, blue water, etc.).

All results shown in this report should be considered preliminary and are included here to illustrate examples of measurements and observations. Post-processing and sample analyses are on-going. Results

are expected to be published as peer-reviewed literature in scientific journals as work is completed. The cruise dataset will be formally archived through NOAA/NESDIS National Centers for Environmental Information (NCEI) as required by NOAA. Cruise data will also be available to the ocean community through NOAA CoastWatch.

2 Principal Investigators and Participants

Nine research groups participated in the cruise. Table 1 lists the principal investigators, their associated institutions and abbreviations for the groups. These abbreviations will be used throughout this report. Fifteen scientists (Table 2) including five PhD students, sailed and conducted measurements with the support of officers and crew of the NOAA Ship *Gordon Gunter*. In addition to onboard activities, optical instruments were calibrated before and after the cruise at the NOAA/STAR optical laboratory in College Park, MD. The NOAA/STAR optical laboratory maintains an ongoing collaboration with the National Institute of Standards and Technology (NIST) to validate the NOAA/STAR radiometric scales in support of cruise activities, and to provide traceable calibration services.

Table 1. Principal investigators

Investigator Name (Last, First)	Participating Institutions	Research Group Abbreviation
Gilerson, Alex	City College of New York	CCNY
Goes, Joaquim	Lamont Doherty Earth Observatory at Columbia University	LDEO
Hu, Chuanmin	University of South Florida, Optical Oceanography Laboratory	USF
Ladner, Sherwin	Naval Research Laboratory, Stennis Space Center	NRL
Lee, ZhongPing	University of Massachusetts, Boston	UMB
Mannino, Antonio	NASA Goddard Space Flight Center, Ocean Ecology Group	NASA
Ondrusek, Michael	NOAA/NESDIS/Center for Satellite Applications and Research	NOAA/STAR
Twardowski, Michael	Harbor Branch Oceanographic Institute at Florida Atlantic University	HBOI
Voss, Kenneth	University of Miami	U. Miami

Table 2. List of science party personnel aboard the NOAA Ship *Gordon Gunter* (alphabetical order).

Name (Last, First)	Title	Research Group/Home Institution
Carrizo, Carlos	Student	CCNY
Freeman, Scott	Researcher	NASA
Goes, Joaquim	Professor	LDEO
Goode, Wesley	Researcher	NRL
Grötsch, Philipp	Researcher	CCNY
Ladner, Sherwin	Researcher	NRL
Ondrusek, Michael	Chief Scientist	NOAA/STAR
Stengel, Eric	Researcher	NOAA/STAR
Stockley, Nicole	Researcher	HBOI
Strait, Christopher	Researcher	HBOI
Wei, Jianwei	Researcher	UMB
Wu, Jinghui	Student	LDEO
Zhang, Shuai	Student	UMB
Zhang, Yang	Student	USF
Zhang, Yingiun	Student	USF

3 Background

NOAA has been supporting satellite ocean color validation and calibration since the development and launch of the Coastal Zone Color Scanner (CZCS) [Gordon et al., 1980; Hovis et al., 1980] in the late 1970's and was instrumental in the development of the Marine Optical BuoY (MOBY) [Clark et al., 1997] in the Sea-viewing Wide Field-of-view Sensor (SeaWiFS) era [Gordon, 2010]. MOBY, now supported by NOAA, is the primary vicarious calibration reference standard for satellite ocean color sensors worldwide [Clark et al., 2002; Brown et al., 2007]. In addition to high quality satellite sensor and vicarious calibrations from MOBY, in situ radiometric measurements from a variety of ocean optical conditions are essential to the production of accurate remotely sensed ocean color products.

The JPSS VIIRS-SNPP satellite ocean color Cal/Val science plan calls for in situ observations for developing and validating ocean color Environmental Data Records (EDRs) for global and coastal

regions. Since 2014, the NOAA/STAR ocean color group has lead five annual dedicated NOAA VIIRS Ocean Color Cal/Val Cruises (Table 3 and references within) to validate VIIRS satellite ocean color data [Arnone et al., 2012; Wang et al., 2013; Arnone et al., 2014; Wang et al., 2014], quantify the variability of in situ measurements and study the optical signatures of oceanic processes.

Table 3. List of the five dedicated VIIRS Cal/Val cruises to date.

Nominal Date	Nominal Location	NOAA Ship; OMAO Cruise Identification Number	NOAA/NESDIS Report Number	Citation
2019 September	US Mid-Atlantic and northeast coastal and continental shelf	*Gordon Gunter*; GU-19-03	154	This Report
2018 May	Gulf of Mexico, the Florida Straits and in the coastal Atlantic.	*Okeanos Explorer*; EX-18-04	152	[Ondrusek et al., 2019]
2016 October	off the coast of Charleston directly following Hurricane Mathew	*Nancy Foster*; NF-16-08	151	[Ondrusek et al., 2017]
2015 December	US Mid-Atlantic Coast and across the Gulf Stream and included some stations in the Tongue of the Ocean (Bahamian waters)	*Nancy Foster*; NF-15-13	148	[Ondrusek et al., 2016]
2014 November	US Mid-Atlantic Coast and across the Gulf Stream	*Nancy Foster*; NF-14-09	146	[Ondrusek et al., 2015]

4 Cruise Objectives

Shipboard observations of apparent optical properties (AOPs, i.e., radiances) and inherent optical properties (IOPs, e.g., absorption, beam attenuation, backscattering, etc.) and additional biological and biogeochemical measurements support three major objectives:

1) the validation of the VIIRS ocean color observations and derived products;
2) the characterization of the sources of uncertainty of in situ ocean color (remote sensing reflectance and IOPs) associated with nearly concurrent measurements by a variety of instruments and protocols; and
3) the characterization of optical properties of ocean variability (i.e., coastal, near-shore, cross-shelf, eddies, fronts, filaments, blue water) toward the future aim of using remotely sensed satellite ocean color data to monitor and study various ocean processes.

Objectives are briefly discussed further below. Greater detail can be found in previous cruise reports [Ondrusek et al., 2015; Ondrusek et al., 2016; Ondrusek et al., 2017; Ondrusek et al., 2019].

1) Validate VIIRS ocean color satellite remote sensing

Satellite sensor performance is evaluated, or validated, by matching up satellite observations with in situ observations, which are considered as the "true" values for this purpose. The primary properties derived from ocean color satellite observations are AOPs including spectral normalized water-leaving radiance ($nL_w(\lambda)$) and spectral remote sensing reflectance ($R_{rs}(\lambda)$), where λ represents the specified nominal center wavelength being measured. Therefore, in situ measurements for satellite validation are focused primarily on these AOP radiometric properties. By applying algorithms to $nL_w(\lambda)$ spectra, other satellite ocean color remote sensing products can be estimated. Products including the concentration of chlorophyll-*a* (Chl-*a*) and IOPs such as coefficients of spectral absorption ($a(\lambda)$), scattering ($b(\lambda)$), backscattering ($b_b(\lambda)$) and beam attenuation ($c(\lambda)$) are also validated using the in situ measurements of these parameters. The sub-pixel variability of the IOP within VIIRS satellite pixels is examined using continuous flow-through measurements to validate satellite ocean color.

2) Characterize and quantify sources of uncertainty associated with in situ ocean color measurements

Sources of uncertainty for in situ measurements include errors associated with instruments, deployment and processing protocol differences and variances associated with the variability of the shipboard environment and the natural environment. Laboratory calibration of instruments (measurement conditions of repeatability [GUM, 1995]) and shipboard experiments (measurement conditions of reproducibility [GUM, 1995]) were conducted to quantify these differences [Johnson et al., 2014]. The reproducibility

experiments measured differences associated with: a) parallel observations from multiple instruments of the same or similar models deployed at the same time and in a small spatial range (within meters of each other); b) observations of the same in situ parameters by using different types of instruments (i.e., profiling in-water versus above-water versus hybrid floating instruments); c) different deployment protocols for sample collection; d) different post-processing methods for the in situ data; and e) observations made under different environmental conditions (i.e., stations in different water masses and sky conditions).

3) Characterize the optical properties of dynamic ocean processes
The third objective of this cruise is to observe in situ optical characteristics of ocean variability related to dynamic processes in the open ocean and coastal waters for exploring the utility of VIIRS ocean color satellite products in identifying and monitoring oceanographic processes from space. The cruise data will be used to evaluate and demonstrate the ability of VIIRS ocean color products to differentiate the variations of spectral features produced by physical and biological states and processes.

5 Cruise Track, Stations and JPSS VIIRS Coverage

The fifth dedicated VIIRS Cal/Val cruise for 2019 had been confirmed for 15 May to 24 May 2019 aboard the NOAA Ship *Nancy Foster*. However, due to unexpected major repairs needed on the *Nancy Foster*, the NOAA Office of Marine and Aviation Operations (OMAO) re-allocated ship time for the cruise to later in 2019 aboard the NOAA Ship *Gordon Gunter* (OMAO cruise identification #GU-19-03, https://www.ncei.noaa.gov/metadata/geoportal/rest/metadata/item/gov.noaa.nodc%3A0202840/html). The revised project instructions allowed for 10 days at sea, departing 7 September 2019 and returning 16 September, beginning and ending in Norfolk, VA. Then, due to Hurricane Dorian, the port of call was moved to Newport, RI with a one-day delay in sailing. Actual cruise dates were 8 September to 17 September 2019. Overall, 26 stations were occupied in a variety of water types in the US Mid-Atlantic and northeast coastal and continental shelf regions of the Western Atlantic (Figure 1; Table 4 and Table 5).

Many cloud-free days following the passage of Hurricane Dorian resulted in an impressive, record number of in situ measurements that matched with VIIRS cloud-free observations ("match-ups") compared with all previous VIIRS dedicated Cal/Val cruises (some of which had exemplary number of match-ups themselves). Satellite observations by the VIIRS sensors aboard the JPSS polar-orbiting satellites SNPP and NOAA-20 occur daily, crossing the equator at local time of approximately 13:30 and crossing the cruise region approximately 2 h earlier. The orbit patterns of each satellite provide the opportunity for occasional overlapping of coverage at a particular location. With both SNPP and NOAA-20 flying, between two and four overpasses per day at a given location are possible. Not every overpass will result in an ocean color observation mainly due to clouds, sunglint or high sensor-zenith angle [Mikelsons and Wang, 2019]. Match-ups for VIIRS SNPP overpasses were 24 stations out of 26 stations and match-ups for VIIRS NOAA-20 overpasses were 23 stations out of 26 stations.

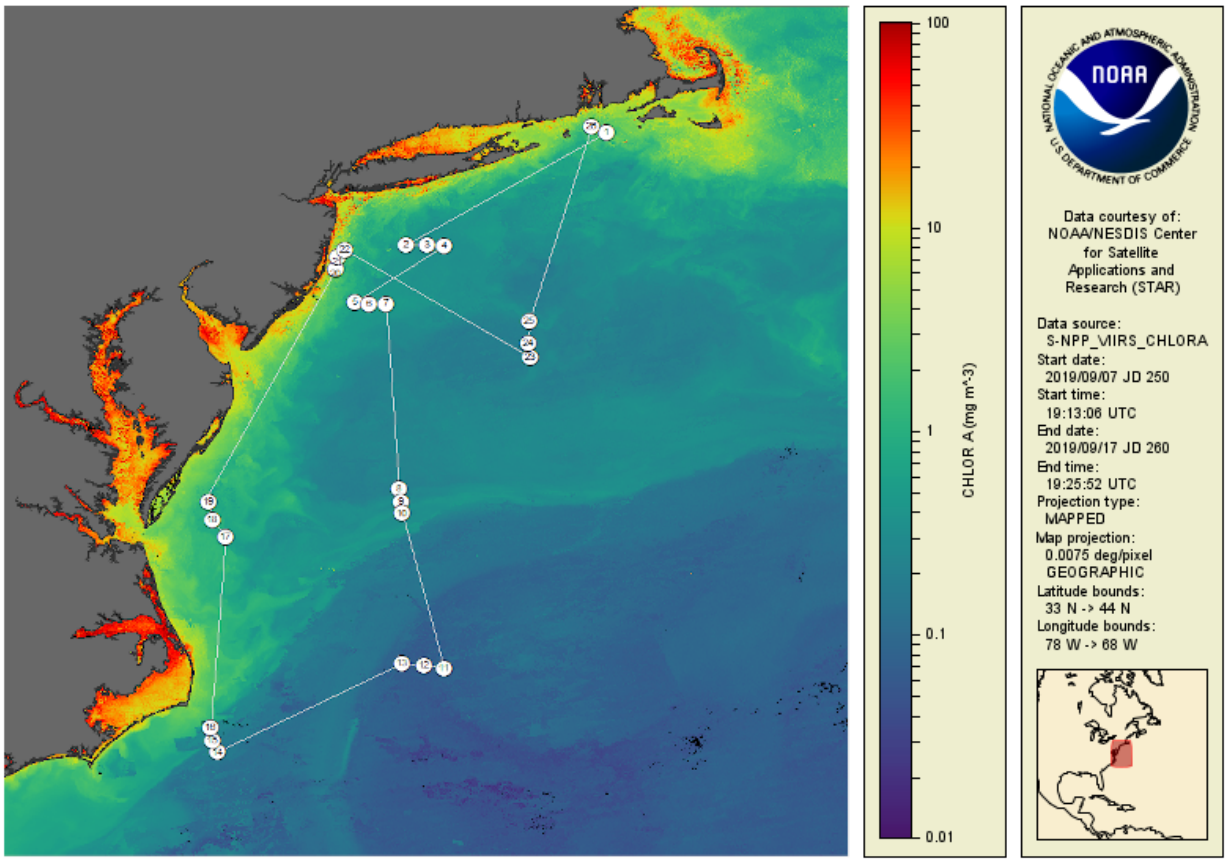

Figure 1. Stations overlaid on NOAA MSL12 VIIRS SNPP science quality full spatial resolution (~750 m) mapped 10-day composite (7 September 2019 to 17 September 2019) chlorophyll-*a*. Figure provided by NOAA CoastWatch.

Table 4. Station descriptions and operations for Station 1 through Station 13. Date is date in September 2019; Time, hh:mm, UTC; Lat for latitude, decimal degrees N; Long for longitude, decimal degrees E; n.d. for not done; n/a for not available; CBAY is for Chesapeake Bay; IW is for in-water profiling radiometer deployments; AW is for above-water handheld radiometer deployments; Floats is for surface floating instrument packages; HYP is for HyperPro profiling radiometers; ASD, SEV, SVC and GER are for specific handheld radiometers as detailed in Section 8.4.

Station	**01**	**02**	**03**	**04**	**05**	**06**	**07**	**08**	**09**	**10**	**11**	**12**	**13**
Date	**08**	**09**	**09**	**09**	**10**	**10**	**10**	**11**	**11**	**11**	**12**	**12**	**12**
Day of Year	**251**	**252**	**252**	**252**	**253**	**253**	**253**	**254**	**254**	**254**	**255**	**255**	**255**
Time_ Arrive	16:30	13:45	16:45	20:09	13:25	15:55	19:02	13:30	16:40	20:00	12:32	15:50	19:20
Time_ Leave	19:30	15:07	19:08	21:20	14:50	17:45	20:38	15:23	19:15	22:10	14:45	17:52	21:16
Lat_ Arrive	41.1757	40.0368	40.0272	40.0171	39.4279	39.4325	39.4098	37.4922	37.3345	37.2349	35.6013	35.6310	35.6712
Lat_ Leave	41.2072	40.0243	40.0194	40.0179	39.4325	39.4113	39.4239	37.4870	37.3563	37.2572	35.6280	35.6730	35.6562
Long_ Arrive	-71.1844	-73.2334	-72.9897	-72.8455	-73.7551	-73.6083	-73.4421	-73.3102	-73.2967	-73.2958	-72.8087	-73.0501	-73.2873
Long_ Leave	-71.1278	-73.2524	-73.0191	-72.8408	-73.7750	-73.6399	-73.4581	-73.3146	-73.3034	-73.2225	-72.8554	-73.0642	-73.2563
Location Descrip-tion	off Rhode Island @ buoy	off coast Long Island	East of Hudson River	South of Station 3	North of Atlantic City	East of Station 5	East of Station 6	East of CBAY	South of Station 8, East of CBAY	South of Station 9, East of CBAY	South-west of CBAY	Outer Banks	Moving West toward shore
Water Depth [m]	75	45	50	17	26	36	36	1390	995	1201	4045	3939	3792
Cloud cover [%]	30	60	50	30	50	40	30	10	20	50	30	40	20
Wave Height [m]	1	1	1	1	1	1	1	1	1	1	0	1	1
Water Color	green	blue	blue	blue green	blue/green	blue	blue	blue	blue	blue	blue	blue	blue
Wind Speed [knots]	5.79	3.71	7.92	4.6	2.56	3.7	2.86	1.56	2	4.0	2.23	4	2.11
Wind Direction [degrees N]	240	107	88	86	88	84	135	106	115	220	189	216	271
Practical Salinity [unitless]	32.05	31.8	32.02	32.44	31.63	31.596	31.63	34.65	34.4	33.05	36.42	36.8	36.33
Sea Temp-erature [°C]	19.3	22.3	22.4	22.6	22.6	23.1	22.9	25.7	25.2	24.9	28.1	28.5	28.9

Station	**01**	**02**	**03**	**04**	**05**	**06**	**07**	**08**	**09**	**10**	**11**	**12**	**13**
Date	**08**	**09**	**09**	**09**	**10**	**10**	**10**	**11**	**11**	**11**	**12**	**12**	**12**
Day of Year	**251**	**252**	**252**	**252**	**253**	**253**	**253**	**254**	**254**	**254**	**255**	**255**	**255**
Secchi Depth [m]	n.d.	19.5	n.d.	15	19	20	n.d.	26	28	28	38	>30	n.d.
Package Deploy-ment Order	CTD, IOP, IW, Floats/AW, CTD	IOP, CTD, Floats, AW, IW	CTD, IOP, IW, AW, Floats	AW, IW, Floats	CTD, IOP, Float, AW, IW	CTD, IOP, IW, AW, Floats	IW, AW, Floats, CTD, IOP	CTD, IOP, Floats, IW, AW	IW, AW, Floats	IW, AW, Floats, CTD, IOP	CTD, IOP, Floats, AW, IW	CTD, IOP, IW, AW, Floats	IW, AW, Floats, IOP, CTD
IW_ time_start	18:06	14:30	17:47	20:20	14:15	16:49	19:10	14:30	17:00	20:12	14:15	16:55	19:22
IW_ time_end	18:37	14:56	18:45	20:42	14:45	17:16	19:48	15:16	17:33	20:38	14:42	17:20	19:50
IW_ Lat_in	41.1880	40.0254	40.0253	40.0173	39.4315	39.4087	39.4115	37.4839	37.3414	37.2368	35.6178	35.6321	35.6712
IW_ Lat_out	41.1988	40.0246	40.0235		39.4325		39.4185	37.4851	37.3489	37.2422	35.6280	35.6550	35.6693
IW_ Long_in	-71.1569	-73.2420	-73.0169	-72.8424	-73.7704	-73.6202	-73.4441	-73.3078	-73.2978	-73.2080	-72.8448	-73.0573	-73.2862
IW_ Long_out	-71.1423	-73.2523	-73.0268		-73.7742		-73.4530	-73.3137	-73.2996	-73.2729	-72.8554	-73.0594	-73.2780
IW Instru-ments	HYPx3, C-OPS	HYPx3, C-OPS	HYPx3, C-OPS	HYPx2, C-OPS	HYPx3, C-OPS	HYPx3, C-OPS	HYPx3, C-OPS	HYPx3, C-OPS	HYPx3, C-OPS	HYPx3, C-OPS	HYPx3, C-OPS	HYPx3, C-OPS	HYPx3, C-OPS
AW_ time_start	18:50	14:30	17:55	20:15	14:15	16:58	19:17	14:35	17:07	20:10	14:15	16:55	19:25
AW_ time_ end	19:20	15:00	18:20	20:38	14:35	17:12	19:36	15:00	17:20	20:42	14:40	17:15	19:50
AW_ Lat_start	41.2059	40.0254	40.0263	40.0170	39.4315	39.4090	39.4130	37.4839	37.3437	37.2366	35.6178	35.6488	35.6712
AW_ Lat_end	n/a	40.0246	40.0245	40.0172	39.4325	39.4098	39.4165	37.4850	37.3498	37.2423	35.6268	35.6550	35.6694
AW_ Long_start	-71.1314	-73.2420	-73.0194	-72.8452	-73.7704	-73.6216	-73.4492	-73.3078	-73.2979	-73.2920	-72.8448	-73.0573	-73.2861
AW_ Long_ end	n/a	-73.2523	-73.0271	-72.8405	-73.7750	-73.6294	-73.4506	-73.3113	-73.2987	-73.2727	-72.8543	-73.0594	-73.2780
AW Instru-ments	ASDx2, GER, SVCx2, SEV	ASDx2, GER, SVCx2, SEV	ASDx2, SEV, GER, SVCx2	ASDx2, SEV, GER, SVCx2	ASDx2, SEV, SVCx2, GER	ASDx2, SEV, SVCx2, GER	ASDx2, SEV, SVCx2, GER	ASDx2, SEV, SVCx2, GER	ASDx2, SEV, SVCx2, GER	ASDx2, SEV, SVCx2, GER	ASDx2, SEV, SVCx2, GER	ASDx2, SEV, SVCx2, GER	ASDx2, SEV, SVCx2, GER
FLOAT_ Time_start	18:55	14:00	18:55	20:54	13:50	17:20	19:55	13:40	17:43	20:44	13:45	17:30	19:57
FLOAT_ Time_end	19:16	14:16		21:02	14:01	17:40	20:10	14:19	17:57	21:05	13:56	17:52	20:14
FLOAT_ Lat_start	41.2072	40.0301	40.0206	40.0178	39.4294	39.4111	39.4203	37.4850	37.3514	37.2434	35.6096	35.6647	35.6684

Station	**01**	**02**	**03**	**04**	**05**	**06**	**07**	**08**	**09**	**10**	**11**	**12**	**13**
Date	**08**	**09**	**09**	**09**	**10**	**10**	**10**	**11**	**11**	**11**	**12**	**12**	**12**
Day of Year	**251**	**252**	**252**	**252**	**253**	**253**	**253**	**254**	**254**	**254**	**255**	**255**	**255**
FLOAT_ Lat_end		40.0275					39.4239	37.4839	37.3548	37.2469	35.6123		35.6650
FLOAT_ Long_start	-71.1278	-73.2321	-73.0206	-72.8402	-73.7648	-73.6390	-73.4549	-73.3031	-73.3007	-73.2695	-72.8319	-73.0618	-73.2751
FLOAT_ Long_end		-73.2373					-73.4581	-73.1744	-73.3026	-73.2469	-72.8368		-73.2686
Floating Instru-ments	HYP, SBAx2, RAMSES	SBAx2, RAMSES, HYP	SBAx1, HYP, RAMSES	SBAx2, HYP, RAMSES	HYP, SBAx2, RAMSES	HYP, SBAx2, RAMSES	SBAx2, HYP, RAMSES	SBAx2, HYP, RAMSES, NURADS	SBAx2, HYP, RAMSES	SBAx2, HYP, RAMSES	SBAx2, HYP, RAMSES, NURADS	SBAx2, HYP, RAMSES, NURADS	SBAx2, HYP, RAMSES, NURADS
IOP_ time_start	16:34	13:45	16:45	21:00	13:25	16:11	20:13	12:30	18:00	21:15	12:32	15:55	20:21
IOP_ time_end	17:25	14:00	17:30	21:20	13:40	16:35	20:38	13:30	19:00	22:05	13:30	16:50	21:12
IOP_ Lat _in	41.1754	40.0368	40.0265	40.0171	39.4279	39.4325	39.4255	37.4922	37.3563	37.2572	35.6013	35.6310	35.6635
IOP_ Lat _end	41.1788					39.4093		37.4854			35.6077		
IOP_ Long _in	-71.1839	-73.2334	-73.0079	-72.8408	-73.7551	-73.6083	-73.4599	-73.3102	-73.3034	-73.2225	-72.8087	-73.0501	-73.2658
IOP_ Long _end	-71.1722					-73.6165		-73.3023			-72.8261		
IOP Profiling Instru-ments	CTD, IOPx2	CTD, IOPx2	CTD, IOPx2	CTD, IOPx2	CTD, IOPx2	CTD, IOPx2	CTD, IOPx2	CTD, IOPx2	CTD, IOPx2	CTD, IOPx2	CTD, IOPx2	CTD, IOPx2	CTD, IOPx2
Comments	check out station		Issue w/ Mike's (NOAA, IW) Hyperpro losing power, only 1 SBA float deployed	Quick station due to time of day		Fluor = 0.237 mg $m^{-}3$; Beam Trans-mission = 94 %		ASD Ladner 0-4 sky w/some saturation	Flat seas w/ swells. Re-located due to front line	Shadows on the bow. surface glint w/ flat sea state	Small patches sea weed, ASD Ladner 10-14 had radiance changes, 15-24 saturated, 25-29 good.	Hazy overhead, NRL HYP tangled with RAMSES	Hazy

Table 5. Same as for Table 4 for Station 14 through Station 26.

Station	**14**	**15**	**16**	**17**	**18**	**19**	**20**	**21**	**22**	**23**	**24**	**25**	**26**
Date	**13**	**13**	**13**	**14**	**14**	**14**	**15**	**15**	**15**	**16**	**16**	**16**	**17**
Day of Year	**256**	**256**	**256**	**257**	**257**	**257**	**258**	**258**	**258**	**259**	**259**	**259**	**260**
Time_ Arrive	13:05	16:20	19:46	14:00	16:05	19:24	16:00	18:20	20:40	12:35	15:55	19:33	12:44
Time_ Leave	15:05	18:40	21:10	14:30	18:00	21:15	17:20	20:00	22:00	14:40	18:00	21:30	14:50
Lat_ Arrive	34.7249	34.8605	34.8692	36.9872	37.1653	37.3442	39.4638	39.8988	39.8383	38.8742	38.9993	39.2253	41.2452
Lat_ Leave	34.7556	34.8692	35.0018	36.9873	37.1800	37.3602	39.7757	39.9140	39.9882	38.8525	39.0140	39.2277	-71.3103
Long_ Arrive	-75.2605	-75.2690	-75.2367	-75.1257	-75.2572	-75.3007	-74.1250	-73.9472	-73.8835	-71.9440	-71.9638	-71.9607	-71.3093
Long_ Leave	-75.1970	-75.2367	-75.2737	-75.1247	-75.2688	-75.3037	-73.9743	-73.9520	-73.8820	-71.9592	-71.9662	-71.9365	-71.2555
Location Descrip-tion	Off Cape Hatteras	Closer to Cape Hatteras	Closer to coast	East of CBAY	North of CBAY	North of Station 18	North of Delaware Bay	East of NY	North of Station 23	Offshore from NY due south of RI	Offshore East of NY	North of Station 24	Buoy off Rhode Island - Checkout Station
Water Depth [m]	2433	1106	160	33	24	26	18	17.5	9	2575	2371	1575	32
Cloud cover [%]	60	60	80	10	10	20	80	30	10	30	40	50	n/a
Wave Height [m]	1	1	2	1.5	2	1	1	1	1	1	1	1	1
Water Color	blue	blue	green	green	green	green	green	brownish green	brownish green	blue	blue	blue	green
Wind Speed [knots]	3.47	7.1	8.0	15.0	5	3	2.4	3.72	5	3	1	4	1
Wind Direction [degrees N]	301	28	295	146	166	88	338	190	244	260	157	188	123
Salinity	36.10	36.33	32.26	31.6	31.52	31.06	30.5	30.76	30.87	35.2	34.64	35.26	31.56
Sea Temp-erature [°C]	28.4	28.2	26.8	22.9	23.6	24.6	22.7	23.6	23.3	24.8	25	25.4	20.2
Secchi Depth [m]	>30	23	n.d.	n.d.	11	13.5	7	6	9	27	25	25	14

Station	**14**	**15**	**16**	**17**	**18**	**19**	**20**	**21**	**22**	**23**	**24**	**25**	**26**
Date	**13**	**13**	**13**	**14**	**14**	**14**	**15**	**15**	**15**	**16**	**16**	**16**	**17**
Day of Year	**256**	**256**	**256**	**257**	**257**	**257**	**258**	**258**	**258**	**259**	**259**	**259**	**260**
Package Deploy-ment Order	CTD, IOP, Floats, IW, AW	IW, AW, Floats, CTD, IOP	IW, AW, CTD, IOP	IW, AW, CTD, IOP	IW, AW, Floats, CTD, IOP	IW, AW, Floats, CTD, IOP	CTD, IOP, IW, AW, Floats	IW, AW, Floats, CTD, IOP	IW, AW, Floats, CTD, IOP	CTD, IOP, Floats, AW, IW	IW, AW, Floats, CTD, IOP	IW, AW, Floats, CTD, IOP	CTD, IOP, Floats, IW, AW
IW_ time_start	14:30	17:35	19:53	14:03	16:05	19:28	16:45	18:25	20:45	14:12	15:58	19:38	14:10
IW_ time_end	15:00	18:15	20:11	14:30	16:45	19:50	17:05	18:40	21:02	14:34	16:23	20:03	14:28
IW_ Lat_in	34.7465	34.8648	35.0020	36.9872	37.1653	37.3442	39.7718	39.9007	39.9727	38.8548	38.9997	39.2265	41.2503
IW_ Lat_out	34.7531	34.8673		36.9869	37.1683	37.3536	39.7750	39.9048	39.9790	38.8490	38.0037	39.2302	41.2553
IW_ Long_in	-75.2147	-75.2578	-75.2738	-75.1258	-75.2572	-75.3007	-73.9695	-73.9470	-73.8830	-71.9490	-71.9642	-71.9593	-71.3075
IW_ Long_out	-75.2016	-75.2432		-75.1265	-75.2597	-75.2987	-73.9727	-73.9478	-73.8815	-71.9553	-71.9678	-71.8713	-71.3103
IW Instru-ments	HYPx3, C-OPS	HYPx3, C-OPS	HYPx3, C-OPS	HYPx1	HYPx3, C-OPS	HYPx3, C-OPS	HYPx3, C-OPS	HYPx3, C-OPS	HYPx3, C-OPS	HYPx3, C-OPS	HYPx3, C-OPS	HYPx3, C-OPS	HYPx3, C-OPS
AW_ time_start	14:30	17:30	19:48	14:05	16:05	19:25	16:45	18:25	20:45	13:45	16:05	19:42	14:10
AW_ time_ end	15:00	18:00	20:11	14:30	16:34	19:55	17:10	18:55	21:05	14:22	16:25	20:00	14:40
AW_ Lat_start	34.7465	34.8640	35.0022	36.9873	37.1653	37.3442	39.7718	39.9007	39.9727	38.8605	39.0003	39.2237	41.2503
AW_ Lat_end	34.7531	34.8655			37.1670	37.3543	39.7750	39.9063	39.9790	38.8523	39.0040	39.2210	41.2555
AW_ Long_start	-75.2147	-75.2635	-75.2737	-75.1260	-75.2572	-75.3007	-73.9712	-73.9470	-73.8830	-71.9460	-71.9643	-71.9588	-71.3075
AW_ Long_ end	-75.2016	-75.2508			-75.2587	-75.2988	-73.9727	-73.9483	-73.8715	-71.9517	-71.9682	-71.9558	-71.3103
AW Instru-ments	ASDx2, SEV, SVCx2, GER	ASDx2, SEV, SVCx2, GER	ASDx2, SEV, SVCx2, GER	ASDx2, SEV, GER, SVCx2	ASDx2, SEV, SVCx2, GER	ASDx2, SEV, SVCx2, GER	ASDx2, SEV, SVCx2, GER	ASDx2, SEV, SVCx2, GER	ASDx2, SEV, SVCx2, GER	ASDx2, SEV, SVCx2, GER	ASDx2, SEV, SVCx2, GER	ASDx2, SEV, SVCx2, GER	ASDx2, SEV, SVCx2, GER
FLOAT_ Time_start	14:05	18:25	n.d.	n.d.	16:56	19:55	17:05	18:48	21:06	13:45	16:30	20:15	13:48
FLOAT_ Time_end	14:20	18:40	n.d.	n.d.	17:08	20:20	17:20	19:05	21:23	13:59	16:45	20:30	14:04
FLOAT_ Lat_start	34.7388	34.8690	n.d.	n.d.	37.1710	37.3537	39.7752	39.9063	39.9795	38.8605	39.0043	39.2302	41.2477

Station	**14**	**15**	**16**	**17**	**18**	**19**	**20**	**21**	**22**	**23**	**24**	**25**	**26**
Date	**13**	**13**	**13**	**14**	**14**	**14**	**15**	**15**	**15**	**16**	**16**	**16**	**17**
Day of Year	**256**	**256**	**256**	**257**	**257**	**257**	**258**	**258**	**258**	**259**	**259**	**259**	**260**
FLOAT_ Lat_end	34.7427	34.8692	n.d.	n.d.	37.1733	37.3577		39.9035	39.9830	38.8578	39.0062	39.2212	41.2488
FLOAT_ Long_start	-75.2297	-75.2385	n.d.	n.d.	-75.2500	-75.2998	-73.9728	-73.9483	-73.8822	-71.9460	-71.9683	-71.9522	-71.3052
FLOAT_ Long_end	-75.2221	-75.2367			-75.2634	-75.3026		-73.9505	-73.8812	-71.9477	-71.9700	-71.9485	-71.3073
Floating Instru-ments	SBAx2, HYP, RAMSES	SBAx2, HYP, RAMSES, NURADS	n.d.	n.d.	SBAx2, HYP, RAMSES, NURADS	SBAx2, HYP, RAMSES, NURADS	SBAx2, HYP, RAMSES, NURADS	SBAx2, HYP, RAMSES, NURADS	SBAx2, HYP, RAMSES, NURADS	SBAx2, HYP, RAMSES, NURADS	SBAx2, HYP, RAMSES, NURADS	SBAx2, HYP, RAMSES, NURADS	SBAx2, HYP, RAMSES, NURADS
IOP_ time_start	13:05	16:33	20:23	14:20	17:29	20:32	16:00	19:25	21:39	12:40	17:15	20:32	12:44
IOP_ time_end	14:00	17:20	21:10	14:28	17:55	21:15	16:36	19:55	22:00	13:35	17:55	21:27	13:32
IOP_ Lat _in	34.7249	34.8618	35.0018	36.9869	37.1777	37.3602	39.4638	39.9140	39.9862	38.8743	39.0103	39.2203	41.2452
IOP_ Lat _end	34.7366										39.0140	39.2277	41.2443
IOP_ Long _in	-75.2605	-75.2670	-75.2737	-75.1257	-75.2652	-75.3037	-74.1250	-73.9520	-73.8802	-71.9440	-71.9697	-71.9485	-71.3093
IOP_ Long _end	-75.2344										-71.9662	-71.9365	-71.3032
Profile	CTD, IOPx2	CTD, IOPx2	CTD, IOPx2	IOPx1	CTD, IOPx2	CTD, IOPx2	CTD, IOPx2	CTD, IOPx2	CTD, IOPx2	CTD, IOPx2	CTD, IOPx2	CTD, IOPx2	CTD, IOPx2

Station	14	15	16	17	18	19	20	21	22	23	24	25	26
Date	13	13	13	14	14	14	15	15	15	16	16	16	17
Day of Year	256	256	256	257	257	257	258	258	258	259	259	259	260
Comments	AW sky variable.	ASD-L some sun, SEV overcast / diffuse	ASD Ladner extra set of water, sky variable. Rain started at 2011 GMT. IW and AW cut short. Surface layer to 12 m.	Quick Station. Extra ASD set for Mike O. ASD ship moved while collecting + some shadow on plaque.	Extra water spectra for Mike O. ASD (saturated 10-14). SEV 571-580 jellyfish + bucket (white) SEV 581-590 bucket only (white) SEV 591-600 jellies w/ black back-ground SEV 601-610 black back-ground	SEV641-650 jellies in black garbage can. SEV 651-660 can and water only.	Lots of clouds & haze. Radiance condition stable during AW. 2nd round = blue sky (better)	Great cond-itions.	Low sun angle, glint & stack smoke. Question-able SEV plaque due to shadow.	Flat surface w/ swells. Layer @ 39 m	More clouds for SEV. Layer @ 48 m	Haze, glinted surface. Layer @ 45 m	Windy, breaking waves, foam, bad cond-itions.

6 Sampling Strategies

A station is composed of a series of discrete activities that take place while the ship is stationary or attempts to maintain its position. Station activities generally include deploying instruments over the side (into the seawater). Underway bio-optical flow-through sampling occurs continuously by instruments plumbed into the ship's flow-through sea water system. Underway above water observations are made continuously (or semi continuously, depending on the ship's heading) with instruments mounted on the bow and side rail of the ship. Additionally, water samples are collected from the rosette at stations and underway from the flow-through sea water system for biogeochemical analyses of several environmental properties. More details regarding measurements follow here in Section 7 and in the individual reports on each group's activities in Section 11.

Discrete Station Activities

Discrete stations were conducted daily, weather conditions permitting, during daylight hours between ~0900 EDT and ~1700 EDT local time (between ~1300 UTC and ~2100 UTC). Several activities routinely took place at each station, including:

- Profiling instrument packages that measured continuously and/or at discrete depths vertically through the water column, generally within the first 2 optical depths or to the physical mixed layer,
- Floating instrument packages configured to float at the water's surface,
- Above-water handheld instruments deployed on the ship's bow.
- Conductivity Temperature Depth (CTD)/Rosette package that collected water samples into 12 Niskin bottles (5 L), usually from two discrete depths, nominally one near surface and a second near the chlorophyll-*a* maximum depth within the first optical depth. The CTD instruments collect profile data as well.
- Deck mounted instruments and instruments plumbed into ships flow-through system collected surface measurements continuously while on station as well as underway.

Underway and Flow-Through Sampling

A series of bio-optical and hydrographic instruments for continuous (underway and during station operations) sampling were mounted on deck and also plumbed into the ship's sea water flow-through system. The sea chest intake was at a depth of 3 m. Observational data were synchronized with time and location and were monitored in real time for determining station locations. The flow-through data will also be used for spatial variability analyses.

7 Observations and Measured Parameters

7.1 Introduction to Observations and Measured Parameters

Brief descriptions of observations and measurements are itemized in this section. Table 6 shows observations made at each station and underway (continuously). Further details of instruments and deployment and processing protocols are provided in Section 8 and in individual group sub-sections within Section 11. An instrument list is consolidated in Table A-2 of the Appendix.

> *Note that commercial equipment, instruments, or materials are identified in this report to document activities and foster understanding. Such identification does not imply recommendation or endorsement by NOAA, NIST or any of the participating institutions, nor does it imply that the materials or equipment identified are necessarily the best available for the purpose.*

7.2 AOPs

AOPs measured include downwelling irradiance ($E_d(\lambda)$), upwelling radiance ($L_u(\lambda)$) and incoming solar irradiance ($E_s(\lambda)$) spectrally (λ) across a range of wavelengths (e.g., 300 nm to 900 nm). These properties are used to determine in situ $nL_w(\lambda)$ and $R_{rs}(\lambda)$ (which are comparable with the satellite products).
As light from the sun passes through seawater, its spectral shape and intensity are changed. Some of the light that enters the ocean is eventually re-emitted. This re-emitted light is part of the light that the ocean color satellite sensor "sees". An in-water profiling radiometer is essentially a pair of spectrometers, one, upward looking, which measures $E_d(\lambda)$, and another, downward looking, which measures $L_u(\lambda)$, both mounted on an instrument that is dropped through the water column. An above-water reference sensor simultaneously measures $E_s(\lambda)$. These measurements are used to calculate $R_{rs}(\lambda)$ and $nL_w(\lambda)$, which is the parameter retrieved from ocean color satellites. These $nL_w(\lambda)$ are used to validate satellite ocean color radiances and to derive other ocean color products such as Chl-*a* or SPM concentrations used in ecological studies [Ondrusek et al., 2012].

- $nL_w(\lambda)$, $R_{rs}(\lambda)$ measured using multiple instruments representing several sampling types deployed in a variety of ways:
    - On station
        - Water column profiles: four free-falling hyperspectral AOP profiling packages;
        - Sea surface, floating: four instrument packages with hyperspectral radiometric sensors configured to float at the sea surface
        - Above surface, on deck: six handheld radiometers deployed from the bow to make concurrent observations under identical environmental conditions using common deployment protocols
    - Continuous, on deck: an imaging camera system and a deck mounted radiometer for continuous measurements from the 02-deck
- Secchi depth (Z_{sd})
- Aerosol optical thickness (AOT, a component of atmospheric correction algorithms) using handheld sun photometers
- Radiance distribution of $L_u(\lambda)$
- Daily solar $E_d(\lambda)$ integrated from 400 nm to 700 nm, the photosynthetically available radiation (PAR) spectral region (E_d (PAR)) and $E_s(\lambda)$

7.3 IOPs

Several optical in situ instrument packages measured IOPs. During stations, some packages profiled the water column, others floated at the water surface and still others were plumbed into the underway, flow-through system. Instrument packages had unique combinations of sensors and are described in more detail within the specific group's sub section in Section 11.

7.3.1 Water Column – profiling (on station)

Measurements from dedicated IOP packages:

- Hyperspectral absorption coefficients: total ($a_t(\lambda)$); particulate ($a_p(\lambda)$); detrital ($a_d(\lambda)$); gelbstoff ($a_g(\lambda)$)
- Hyperspectral beam attenuation coefficient ($c(\lambda)$)
- Backscatter coefficient ($b_b(\lambda)$)
- Fluorescence
- Volume scattering function (VSF)

IOPs included on AOP packages:

- Chlorophyll *a* (Chl-*a*) fluorescence
- Chromophoric Dissolved Organic Material (CDOM) fluorescence
- Phycoerythrin fluorescence
- Scattering ($b(\lambda)$ at 443 nm, 530 nm and 860 nm by NOAA/STAR and at 660 nm by USF).

IOP on the *Explorer's* CTD/Rosette package:

- Chl-*a* fluorescence

7.3.2 Continuous – near surface (underway flow-through and deck-mounted)

Flow-through:

- Hyperspectral $a(\lambda)$ and $c(\lambda)$
- $b_b(\lambda)$ at 470 nm, 572 nm and 670 nm
- Chl-*a* and ultraviolet (UV) fluorescence (ship)
- CDOM fluorescence
- Phycobilipigments fluorescence
- Phytoplankton functional types (PFTs; imaging)
- Phytoplankton photo-physiology from variable fluorescence

Deck mounted:

- E_d(PAR)

7.4 Discrete water sampling

These parameters were determined from analyses of discrete water samples collected from Niskin bottles on the CTD/Rosette or from the underway flow-through system:

- Extracted fluorometric Chl-*a* (fluorometry)
- Suspended Particulate Material (SPM; mass)
- $a(\lambda)$ (including constituents) by filter pad technique (FPT; spectrophotometry) and by point-source integrating-cavity meter (PSICAM)
- CDOM (spectrophotometry)
- Phytoplankton pigments by high performance liquid chromatography (HPLC)
- Nutrients; N (nitrate and nitrite), P and Si (colorimetry)
- Preserved samples for phytoplankton assemblage characterization (microscopy)
- Phytoplankton automated imagery
- Phytoplankton size class
- Phycobilipigment types
- Photosynthetic efficiency (F_v/F_m; variable fluorometry)

7.5 Other ship measurements

These additional parameters were observed by onboard instrumentation maintained by the ship.

- Profiling CTD-rosette package
    - Salinity
    - Sea surface temperature
    - Dissolved O_2
- Air temperature
- Currents (Acoustic Doppler Current Profiler; ADCP)
- Meteorology
    - Wind speed

- Wind direction
- Sea state
- Air temperature

- Ocean Acidification
  - Partial pressure (p) and fugacity (f) of CO_2 and other necessary ancillary data were measured under the direction of OAR/AOML Ocean Chemistry and Ecosystems Division on behalf the NOAA Ocean Acidification Program. Rik Wanninkhof and Denis Pierrot are the Principal Investigators.

While the pCO_2 and fCO_2 are not discussed further in this report, the existence of these concurrent data is worth noting for potential future research.

Table 6. Accounting of measurements made at stations and underway from the flow-through system.

GU-19-03 Station ID#	**01**	**02**	**03**	**04**	**05**	**06**	**07**	**08**	**09**	**10**	**11**	**12**	**13**	**14**	**15**	**16**	**17**	**18**	**19**	**20**	**21**	**22**	**23**	**24**	**25**	**26**	**Underway**
Date in September 2019	**08**	**09**	**09**	**09**	**10**	**10**	**10**	**11**	**11**	**11**	**12**	**12**	**12**	**13**	**13**	**13**	**14**	**14**	**14**	**15**	**15**	**15**	**16**	**16**	**16**	**17**	**8 to 17**
Day of Year	**251**	**252**	**252**	**252**	**253**	**253**	**253**	**254**	**254**	**254**	**255**	**255**	**255**	**256**	**256**	**256**	**257**	**257**	**257**	**258**	**258**	**258**	**259**	**259**	**259**	**260**	**251 to 260**
***$L_u(\lambda)$, $R_{rs}(\lambda)$, $nL_w(\lambda)$* profiles**																											
NOAA-HyperPro	x	x	x	x	x	x	x	x	x	x	x	x	x	x	x	x	x	x	x	x	x	x	x	x	x	x	
NASA - HyperPro	x	x	x		x	x	x	x	x	x	x	x	x	x	x	x		x	x	x	x	x	x	x	x	x	
USF- HyperPro	x	x	x	x	x	x	x	x	x	x	x	x	x	x	x	x		x	x	x	x	x	x	x	x	x	
NASA - C-OPS	x	x	x	x	x	x	x	x	x	x	x	x	x	x	x	x		x	x	x	x	x	x	x	x	x	
***$L_u(\lambda)$, $R_{rs}(\lambda)$, $nL_w(\lambda)$* surface (floating)**																											
NRL HTSRB		x	x	x	x	x	x	x	x	x	x	x	x	x	x			x	x	x	x	x	x	x	x	x	
UMB SBA	x	x	x	x	x	x	x	x	x	x	x	x	x	x	x	x		x	x	x	x	x	x	x	x	x	
NOAA SBA	x	x		x	x	x	x	x	x	x	x	x	x	x	x	x		x	x	x	x	x	x	x	x	x	
RAMSES	x	x	x	x		x	x	x	x	x	x	x	x	x	x			x	x	x	x	x	x	x	x	x	
(NURADS) radiance distribution								x			x	x	x		x			x	x	x	x	x	x	x	x	x	
***$L_u(\lambda)$, $R_{rs}(\lambda)$, $nL_w(\lambda)$* Above water**																											
CCNY Imager	x	x	x	x	x	x	x	x	x	x	x	x	x	x	x	x	x	x	x	x	x	x	x	x	x	x	x
NASA HyperSAS	x	x	x	x	x	x	x	x	x	x	x	x	x	x	x	x	x	x	x	x	x	x	x	x	x	x	x
NRL SEV	x	x	x	x	x	x	x	x	x	x	x	x	x	x	x	x	x	x	x	x	x	x	x	x	x	x	
USF SVC	x	x	x	x	x	x	x	x	x	x	x	x	x	x	x	x	x	x	x	x	x	x	x	x	x	x	
NRL ASD	x	x	x	x	x	x	x	x	x	x	x	x	x	x	x	x	x	x	x	x	x	x	x	x	x	x	
NOAA ASD	x	x	x	x	x	x	x	x	x	x	x	x	x	x	x	x	x	x	x	x	x	x	x	x	x	x	
NOAA SVC	x	x	x	x	x	x	x	x	x	x	x	x	x	x	x	x	x	x	x	x	x	x	x	x	x	x	
CCNY GER	x	x	x	x	x	x	x	x	x	x	x	x	x	x	x	x	x	x	x	x	x	x	x	x	x	x	

GU-19-03 Station ID#	**01**	**02**	**03**	**04**	**05**	**06**	**07**	**08**	**09**	**10**	**11**	**12**	**13**	**14**	**15**	**16**	**17**	**18**	**19**	**20**	**21**	**22**	**23**	**24**	**25**	**26**	**Underway**
Date in September 2019	**08**	**09**	**09**	**09**	**10**	**10**	**10**	**11**	**11**	**11**	**12**	**12**	**12**	**13**	**13**	**13**	**14**	**14**	**14**	**15**	**15**	**15**	**16**	**16**	**16**	**17**	**8 to 17**
Day of Year	**251**	**252**	**252**	**252**	**253**	**253**	**253**	**254**	**254**	**254**	**255**	**255**	**255**	**256**	**256**	**256**	**257**	**257**	**257**	**258**	**258**	**258**	**259**	**259**	**259**	**260**	**251 to 260**
***E_d*(PAR)**	x	x	x	x	x	x	x	x	x	x	x	x	x	x	x	x	x	x	x	x	x	x	x	x	x	x	x
Profiling IOP optical sensors																											
$a_t(\lambda)$*, *$a_d(\lambda)$*, *$a_g(\lambda)$*, *$a_p(\lambda)$	x	x	x	x	x	x	x	x	x	x	x	x	x	x	x	x	x	x	x	x	x	x	x	x	x	x	x
$c(\lambda)$	x	x	x	x	x	x	x	x	x	x	x	x	x	x	x	x	x	x	x	x	x	x	x	x	x	x	x
$b_b(\lambda)$	x	x	x	x	x	x	x	x	x	x	x	x	x	x	x	x	x	x	x	x	x	x	x	x	x	x	x
Flow-through IOP optical sensors																											
$a_t(\lambda)$*, *$a_d(\lambda)$*, *$a_g(\lambda)$*, *$a_p(\lambda)$	x	x	x	x	x	x	x	x	x	x	x	x	x	x	x	x	x	x	x	x	x	x	x	x	x	x	x
$c(\lambda)$	x	x	x	x	x	x	x	x	x	x	x	x	x	x	x	x	x	x	x	x	x	x	x	x	x	x	x
$b_b(\lambda)$	x	x	x	x	x	x	x	x	x	x	x	x	x	x	x	x	x	x	x	x	x	x	x	x	x	x	x
$b(\lambda)$	x	x	x	x	x	x	x	x	x	x	x	x	x	x	x	x	x	x	x	x	x	x	x	x	x	x	x
CDOM fluorescence	x	x	x	x	x	x	x	x	x	x	x	x	x	x	x	x	x	x	x	x	x	x	x				
VSF - yes, check stations	x	x	x	x	x	x	x	x	x	x	x	x	x	x	x	x	x	x	x	x	x	x	x	x	x	x	-
CDOM (spectrophotometry)	x	x	x	x	x	x	x	x	x	x	x	x	x	x	x	x	x	x	x	x	x	x	x	x	x	x	
***$a_p(\lambda)$*, *$a_d(\lambda)$*, *$a_g(\lambda)$*, filter pad technique**	x	x	x	x	x	x	x	x	x	x	x	x	x	x	x	x	x	x	x	x	x	x	x	x	x	x	
Chl-*a* and UV fluorescence	x	x	x	x	x	x	x	x	x	x	x	x	x	x	x	x	x	x	x	x	x	x	x	x	x	x	
Chl-*a* extracted	x	x	x	x	x	x	x	x	x	x	x	x	x	x	x	x	x	x	x	x	x	x	x	x	x	x	
SPM	x	x	x	x	x	x	x	x	x	x	x	x	x	x	x	x	x	x	x	x	x	x	x	x	x	x	
HPLC pigments	x	x	x	x	x	x	x	x	x	x	x	x	x	x	x	x	x	x	x	x	x	x	x	x	x	x	
Nutrient concentrations (N, P, Si)	x	x	x	x	x	x	x	x	x	x	x	x	x	x	x	x	x	x	x	x	x	x	x	x	x	x	
Microscopy	x	x	x	x	x	x	x	x	x	x	x	x	x	x	x	x	x	x	x	x	x	x	x	x	x	x	
Phycoerythrin flourescence	x	x	x	x	x	x	x	x	x	x	x	x	x	x	x	x	x	x	x	x	x	x	x	x	x	x	
F_v/F_m* and *σ_{PSII}	x	x	x	x	x	x	x	x	x	x	x	x	x	x	x	x	x	x	x	x	x	x	x	x	x	x	x
Phycobiligment types (PE1, PE2, PE3)	x	x	x	x	x	x	x	x	x	x	x	x	x	x	x	x	x	x	x	x	x	x	x	x	x	x	
Secchi depth		x		x	x	x		x	x	x	x			x				x	x	x				x	x		
AOT (microtops)	x	x	x	x	x	x	x	x	x	x	x	x	x	x	x	x	x	x	x	x	x	x	x	x	x	x	
Currents	x	x	x	x	x	x	x	x	x	x	x	x	x	x	x	x	x	x	x	x	x	x	x	x	x	x	x
Wind speed and direction	x	x	x	x	x	x	x	x	x	x	x	x	x	x	x	x	x	x	x	x	x	x	x	x	x	x	x
Air temperature	x	x	x	x	x	x	x	x	x	x	x	x	x	x	x	x	x	x	x	x	x	x	x	x	x	x	x

GU-19-03 Station ID#	01	02	03	04	05	06	07	08	09	10	11	12	13	14	15	16	17	18	19	20	21	22	23	24	25	26	Underway
Date in September 2019	08	09	09	09	10	10	10	11	11	11	12	12	12	13	13	13	14	14	14	15	15	15	16	16	16	17	8 to 17
Day of Year	251	252	252	252	253	253	253	254	254	254	255	255	255	256	256	256	257	257	257	258	258	258	259	259	259	260	251 to 260
Salinity	x	x	x	x	x	x	x	x	x	x	x	x	x	x	x	x	x	x	x	x	x	x	x	x	x	x	x
SST	x	x	x	x	x	x	x	x	x	x	x	x	x	x	x	x	x	x	x	x	x	x	x	x	x	x	x
Dissolved O2																											x
Water depth	x	x	x	x	x	x	x	x	x	x	x	x	x	x	x	x	x	x	x	x	x	x	x	x	x	x	x
Cloud cover	x	x	x	x	x	x	x	x	x	x	x	x	x	x	x	x	x	x	x	x	x	x	x	x	x	x	

8 Common Radiometric Measurements: Methods and Protocols

8.1 Overview of in situ radiometry methods

During the 2019 Cal/Val cruise, in situ observations were made using multiple spectroradiometric instruments that can be grouped by three distinct approaches: 1) in-water profiling, 2) surface floating, and 3) above-water, handheld. Each approach has fundamental strengths and weaknesses [e.g., see especially Ondrusek et al., 2019]).

Multiple profiling radiometers, floating radiometers and handheld spectrometers were deployed by groups using an agreed-upon set of protocols and common processing methods. These multi-instrument common deployments are described in the next three sections (Section 8.2, Section 8.3, and Section 8.4). Sometimes, individual researchers made additional observations using different protocols to test the effects of protocol on measurements, which are discussed within the respective group's section (sub-sections of Section 11).

The profiling radiometers were calibrated before and after the cruise from 350 nm to 900 nm as described in Ondrusek et al. [2019].

8.2 In-water profiling radiometry

Four profiling radiometers were deployed simultaneously during this 2019 Cal/Val cruise. Three were HyperPro (Satlantic Sea-Bird) instruments (NOAA/STAR; NASA instrument operated by NOAA/STAR; and USF) and a C-OPS (Biospherical Laboratories, Inc.) profiling radiometer (NASA). Deployments occurred in a similar fashion to those of the previous Cal/Val cruises [Ondrusek et al., 2015; Ondrusek et al., 2016; Ondrusek et al., 2017; Ondrusek et al., 2019], following recommended protocols [Satlantic, 2004, 2012], keeping them away from the ship and each other, and avoiding ship shadowing. At each station, the ship was positioned so that the sun was directly off the stern. The four profiling instruments, which were weighted to produce a descent rate of approximately 0.1 m s^{-1} to 0.3 m s^{-1}, were positioned evenly spaced across the stern and lowered together to the sea surface. The ship steamed at approximately 1 knot as the cables were let out until the profilers were at least 20 m off the stern. After that, the ship kept just enough headway to maintain the heading, to prevent the profilers from closing in on the ship, and to prevent them from crossing cables while profiling. For each station, three to five multicast measurement sets were conducted. For each set, all four profilers were lowered to approximately 10 m to

15 m depth through the euphotic zone and raised together three to five times. If sky conditions changed significantly during the cast, the set was stopped and restarted when the conditions were favorable again.

The HyperPro system has a downward looking HyperOCR radiometer that measures $L_u(\lambda)$ and an upward looking HyperOCI irradiance sensor to measure $E_d(\lambda)$ in the water column. Each HyperOCR or HyperOCI has a 256-channel silicon photodiode array detector with 10 nm spectral resolution and spectral sampling of 3.3 nm pixel^{-1}. The HyperOCRs have dark signal corrections performed using shutter dark measurements collected every fifth scan. The above-water reference sensor was an upward looking HyperOCI irradiance sensor to measure $E_s(\lambda)$ used during data reduction. All of the E_s sensors (one for each instrument package) were mounted on a telescoping tower mounted on the 02-deck as pictured in Figure 18. Additional sensors incorporated into these profiling radiometer packages measure pressure, temperature, conductivity, and tilt. WET Labs ECO-Puck Triplet sensors for IOPs are also included in the profiling radiometer packages. Further details on the C-OPS instrument are discussed in Section 11.2. VSF was measured from WET Labs MASCOT on a profiling package along with $a_t(\lambda)$ and $a_g(\lambda)$.

For consistency, the data processing for all of the profiling HyperPro systems followed multi-cast protocols established by Michael Ondrusek of NOAA/STAR using Satlantic ProSoft processing software version 8.1.6. Details on the NOAA/STAR processing of HyperPro data can be found in prior cruise reports [Ondrusek et al., 2015; Ondrusek et al., 2016; Ondrusek et al., 2017; Ondrusek et al., 2019].

8.3 In-water floating (surface) radiometry

Three of the floating radiometer systems utilized during this cruise are HyperPros outfitted with floating collars that position the sensors at the ocean surface. One system (NRL) had the radiometers configured to measure $L_u(\lambda)$ just below the surface and $E_s(\lambda)$ just above the surface (Figure 18). Two systems (UMB and NOAA/STAR) were configured as a RISBA ([Lee et al., 2013]) where both the L_u and the E_s sensors are positioned just above the water and the $L_u(\lambda)$ is covered with a cone extending to the water surface allowing the direct measurement of $L_w(\lambda)$ while blocking skylight reflection. The three systems were deployed simultaneously off the stern, acquiring about 5 min to 15 min of data (cover image). A fourth radiometer, a TriOS RAMSES (Rastede, Germany), was deployed by HBOI group to measure scalar irradiance just below the surface of the water.

8.4 Above water radiometry with handheld instruments

Above-water handheld radiometry measurements were conducted on the bow using six handheld instruments (Table 7). Also, on the bow, sun photometer data to measure AOT were collected by NOAA and CCNY.

At each station, above-water measurements of the water reflectance were conducted. Six handheld radiometers were deployed near-coincidently (within ~40 min) on the bow using an agreed-upon standardized deployment protocol and the NRL 99% white reference plaque (Reference #99AA08-0618-0606, 8/h NIST traceable, calibrated by Labsphere on 29 August 2018). This common deployment was described in more detail in the previous cruise reports [Ondrusek et al., 2015; Ondrusek et al., 2016; Ondrusek et al., 2017; Ondrusek et al., 2019]. In addition, individual groups may have conducted above water measurements using other deployment protocols and 10% grey and 99% white reflectance plaques for additional comparative studies (see details in sub-sections of Section 11).

Table 7. Above-water, handheld spectroradiometers used for marine $R_{rs}(\lambda)$ determinations.

Instrument	Vendor	Serial Number	Spectral Range and Resolution [nm]	FOV [°]	Fiber Coupled	Institution
FieldSpecHandHeld 2	ASD	1847	350 to >1000; 3	10	No	NOAA
FieldSpecHandHeld 2	ASD	1897	325 to 1075; 1	10	No	NRL
GER 1500	Spectra Vista	2053	350 to 1050; 3	4	No	CCNY
HR-512i	Spectra Vista	916214	350 to 1050; 3	8	No	NOAA
HR-512i	Spectra Vista	2030	350 to 1050; 3	8	No	USF
PSR-1100F	Spectral Evolution	178-4475	320 to 1100; 1	8	Yes	NRL

The common above-water instrument configurations, reference plaque and measurement angles are as follows.

- Integration time was optimized for each target prior to collection (i.e., integration time of sensor was changed based on relative brightness of the target and new dark counts were taken to correct for instrument noise). Integration times ranged from 68 ms to 4352 ms.
- The reflectance plaque, referred to here as the "NRL white plaque," is a Labsphere 99% white Spectralon® card with a known directional/hemispherical reflectance and assumed to be a near-Lambertian surface. Its radiance is measured to provide a quantity proportional to E_s.
- Instruments were positioned to make the reference measurement at between ~30 cm and ~60 cm above the NOAA white plaque.
- Fore-optic attachments with field of view (FOV) angles unique to each instrument were used (see Table 7).
- Five to ten consecutive radiometric spectral measurements were taken of each of the following targets: NOAA white plaque (S_p), water (S_{sfc}), and sky (S_{sky}).
- All measurements were made on the bow of the ship. The exact location of sampling was dependent on the orientation of the ship relative to the sun to eliminate shadowing from the vessel and surface contamination.
- The desired optical sensor zenith angles for the NOAA white plaque (θ_p), water (θ_{sfc}) and sky (θ_{sky}) measurements were 40°, 40° and 40°, respectively. The desired relative-azimuth angle of the sensor to the sun ($\Delta\varphi$) was 90° up to 135° depending on sea conditions and ship orientation.

Processing of above-water data to retrieve $R_{rs}(\lambda)$ is being conducted using the group specific processing software that follows the guidelines of Mueller et al. [2003a] and utilizes different processing models for comparison including: R_{rs}_sfc (no NIR reflectance correction), R_{rs}_fresnel (Fresnel correction omitted), R_{rs} [Carder and Steward, 1985], R_{rs}_Lee [Lee et al., 1997], and R_{rs}_Gould [Gould et al., 2001]. More discussion of the methods can be found in the previous dedicated VIIRS Cal/Val cruise reports [Ondrusek et al., 2015; Ondrusek et al., 2016; Ondrusek et al., 2017; Ondrusek et al., 2019].

9 Intercomparison of in situ measured nL_w

Up to 9 instruments are shown (Figure 2) in the comparisons of $nL_w(\lambda)$, including three profiling HyperPros; three floating HyperPros including two RISBA; and three out of six handheld above-water instruments described in Section 8.4. Not all instruments were deployed at each station depending on conditions or time constraints (see Table 4, Table 5, and Table 6). Intercomparisons of the in situ $nL_w(\lambda)$ measurements from multiple methods at each station are shown to provide an estimate of in situ measurement variability. For each station, $nL_w(\lambda)$ are displayed for each instrument along with the average $nL_w(\lambda)$ of all instruments. The number of instruments varies for each station. Since spectral resolutions differ between instruments, all data were spectrally weighted to VIIRS spectral response function. For each station, instruments that gave measurements beyond one standard deviation (σ) from

the average of all instrument measurements at that station were omitted from the results. Table 8 gives the percent difference for each instrument at each band for all stations as well as the percent difference of individual instrument $nL_w(\lambda)$ relative to the average $nL_w(\lambda)$ of all instruments at each station.

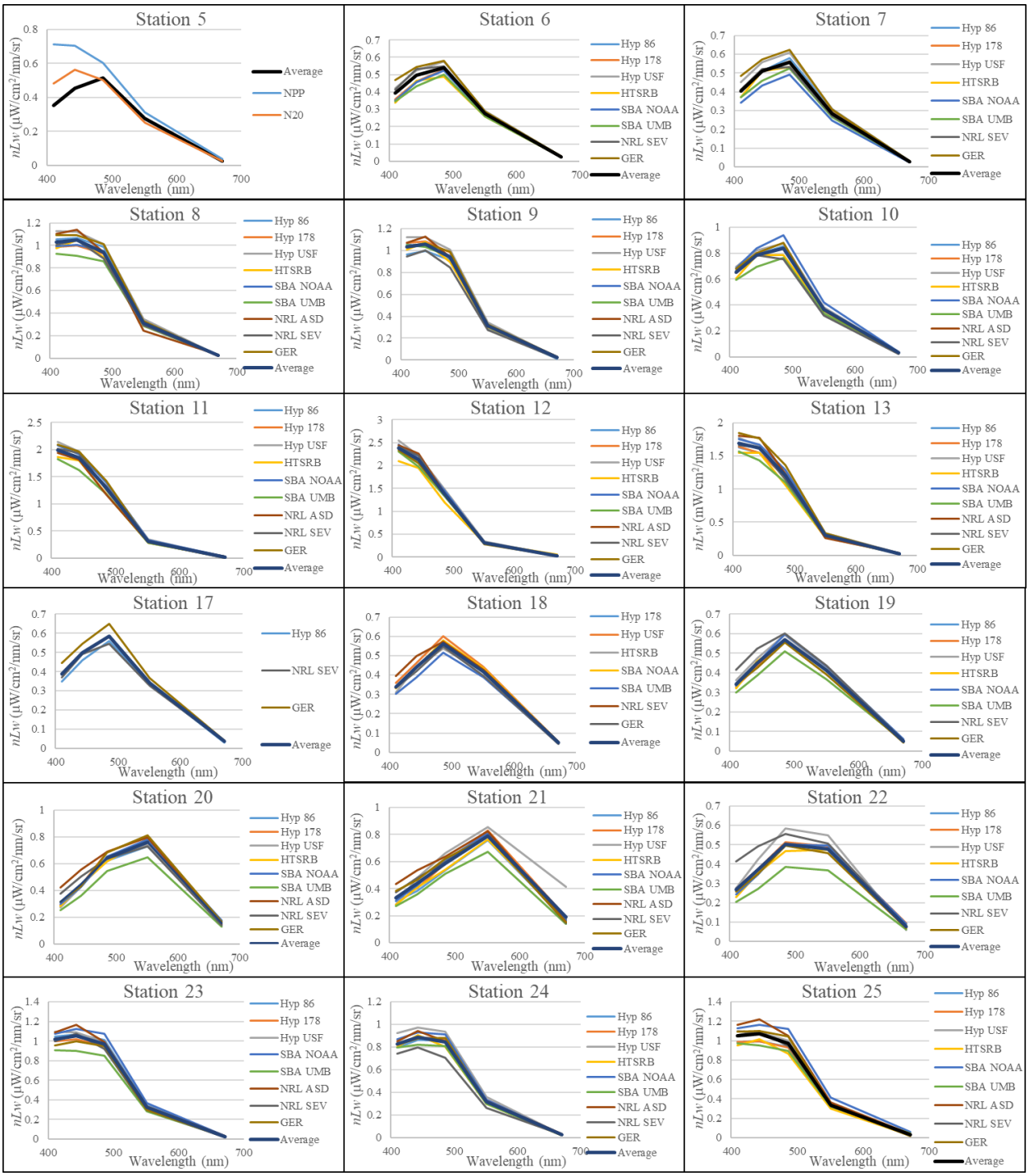

Figure 2. VIIRS band weighted $nL_w(\lambda)$ plots of each instrument (by color) and the average $nL_w(\lambda)$ of all instruments (average in black line) measured at each station with good satellite matchups. In the legends, Hyp are profiling HyperPros; HTSRB is a floating HyperPro; SBAs are the RISBA floating HyperPro; ASD, SEV, and GER are handheld above-water instruments described in Section 8.4.

Table 8. The average across all stations of the percent difference of individual instrument $nL_w(\lambda)$ relative to the average $nL_w(\lambda)$ of all instruments. Instrument abbreviations are as for Figure 2.

Band	Profilers	Floater	Above	Hyperpro	SBA	HTSRB	Hypersas	GER	Spec Ev	NOAA Hyp
410	-1	-8	9	-1	-7	-9	-	7	8	-4
443	-1	-6	7	-1	-8	-3	-	4	7	-4
486	2	-5	3	2	-3	-7	-	6	-2	-1
551	3	-3	0	3	-3	-3	-	1	-2	0
671	-3	3	3	-3	3	3	-	-7	-4	-10
Avg410-551	**1**	**-5**	**5**	**1**	**-5**	**-6**	**-**	**5**	**3**	**-2**

10 Validation of VIIRS ocean color data with in situ observations

To assess the performance of the VIIRS ocean color satellite sensors during the time of this cruise, the VIIRS SNPP and NOAA-20 $nL_w(\lambda)$ are compared to in situ data for each station. VIIRS SNPP and NOAA-20 data are processed by the STAR Ocean Color Science Team using MSL12. Processing version for SNPP was NPPSCINIR_L2; SCI_OC04.0_v1.21 and processing for NOAA-20 was J01_SCINIR_L2; SCI_OC4.0_v1.21_v1.30. The method for determining valid satellite data to use for matchups with in situ data follows Wang et al, [2009] and is briefly described as follows: For each in situ observation, $nL_w(\lambda)$ satellite data from a 5 pixel by 5 pixel box centered on the in situ sampling location are obtained. The average and σ of the $nL_w(\lambda)$ values of the 25 pixels in the box are calculated. Next, values with 1.5 or greater σ from the average are omitted. If the count of the remaining "good" values is greater than 50% of the original count (i.e., 13 or more out of 25), the average and σ are recalculated for the remaining "good" pixels. These results are then matched with the in situ observations. For the in situ measurements, up to 13 instruments were used to measure water-leaving radiances as described in Section 8. To remove outliers in the in situ data, the average and σ were calculated for all the instruments utilized at each station. Then, for each wavelength band, any data that were greater than one σ were removed and then the final average and σ were calculated. Spectral results for each station for the two VIIRS sensors and the quality average representation of all the in situ are shown in Figure 3.

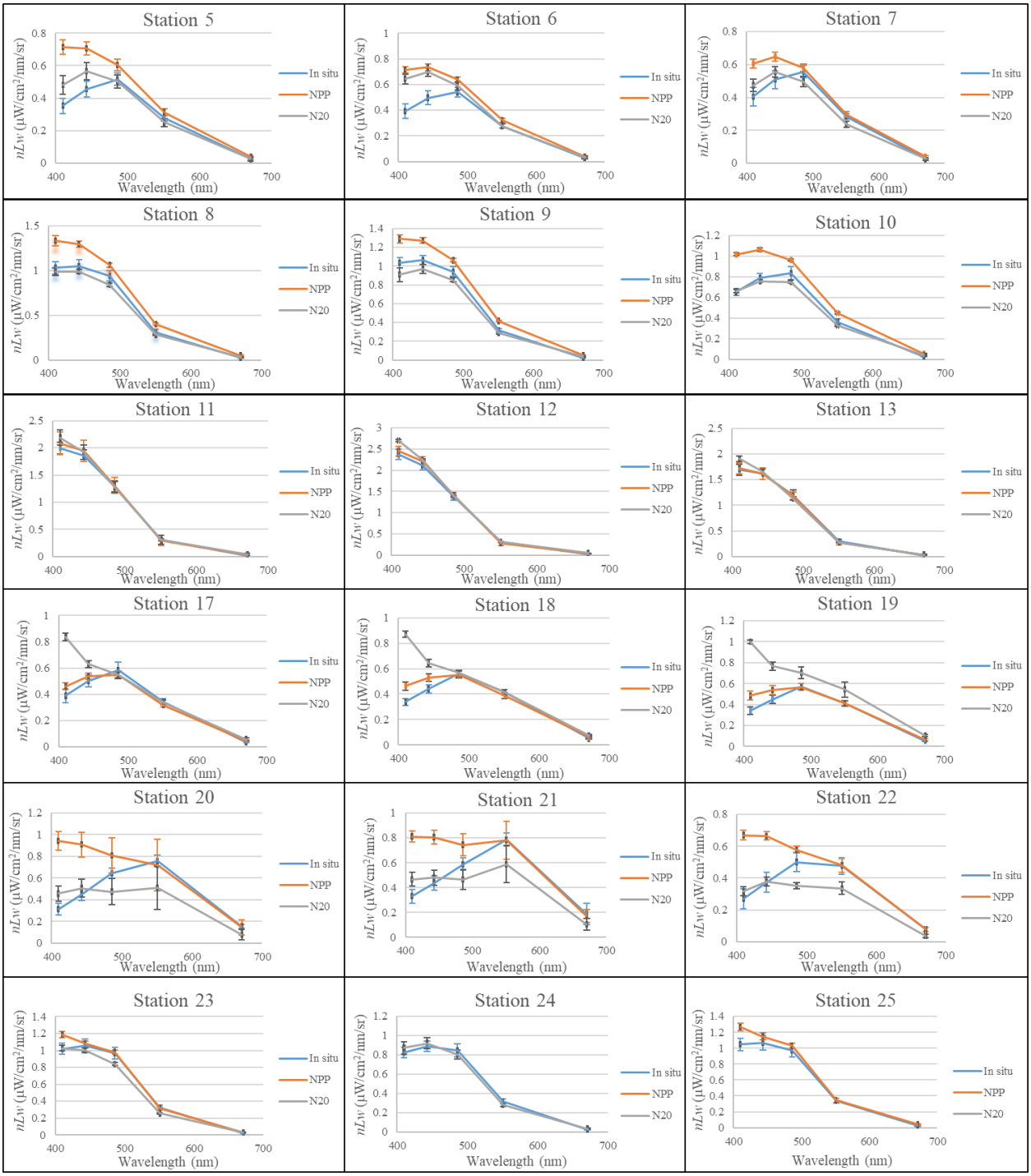

Figure 3. Preliminary MSL12 VIIRS 5 pixel by 5 pixel average (SNPP, shown as NPP, in orange and NOAA20, shown as N20, in grey) versus the average for all in situ measurements (blue) at each station for stations where there were good matchups.

11 Participating Science Groups' Unique Activities, Methods and Protocols

11.1 NOAA/STAR – Michael Ondrusek, Eric Stengel, and Charles Kovach

In-water and above-water radiometry

In addition to organizing and planning daily operations for the cruise, NOAA/STAR led the simultaneous deployment of the in-water profiling radiometry instruments as described in Section 8.2, participated in the in-water floating radiometry measurements as described in Section 8.3, participated in the above-water measurements as described in Section 8.4. We also deployed the bi-directional radiance distribution camera, NURADS, in collaboration with U. Miami. For the profilers, NOAA/STAR operated two HyperPro Profiler II packages each equipped with depth, temperature, and tilt sensors. The first profile system (serial number (SN) 179) was equipped with one ECO-Puck sensor that measured fluorescence to estimate concentrations of chlorophyll *a*, CDOM and phycoerythin, and one ECO-Puck sensor that measured b_b at 443 nm, 530 nm, and 860 nm. The second profiler was NASA GSFC's profiler (SN 178) which was equipped with a built-in CTD and no ECO-Puck. These two profilers were run simultaneously along with the USF HyperPro and a NASA C-OPS at 24 out of 26 stations, omitting Station 4 and Station 17. At Station 4 only two HyperPros and the C-OPS were run due to equipment malfunctions and at Station 17 only one HyperPro profiler was deployed due to weather and sea state conditions.

For the in-water floating measurements, the NOAA HyperPro SN 86 was outfitted with UMB's SBA hardware and deployed simultaneously with UMB's SBA, NRL's HTSRB, and NURADS. The SBA's and the HTSRB floaters were run at every station except Station 16 and Station 17 where sea conditions were too rough. NURADS was deployed at only 13 stations. Figure 4 shows an example of a comparison at Station 26 where the NOAA deployed two HyperPros and one SBA were deployed and processed.

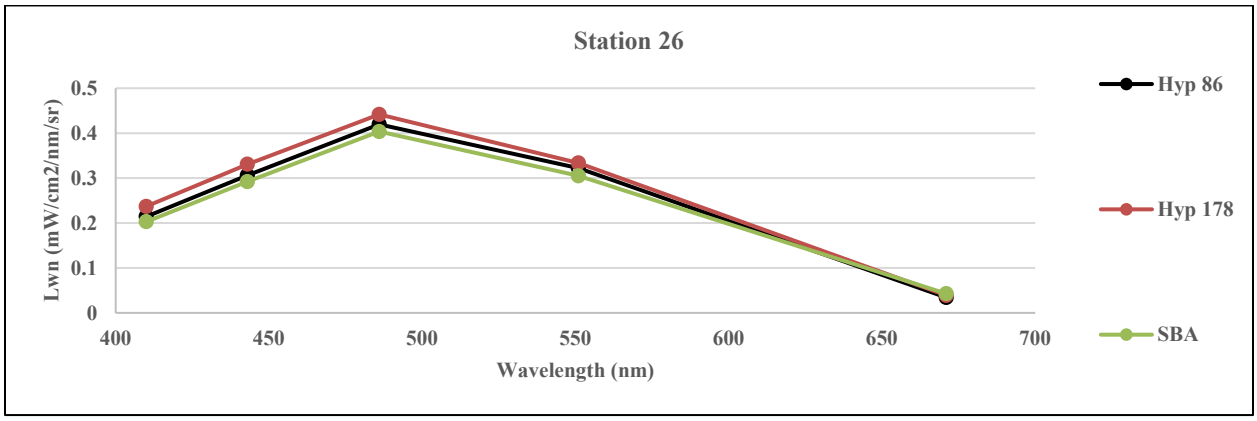

Figure 4. Normalized water-leaving radiances measured at Station 26 collected on September 17, 2019. Data is spectrally weighted to VIIRS visible bands. Station 26 was located near the outer channel marker buoy outside of Newport, RI and surface waters there had chlorophyll-*a* concentrations of 0.76 mg m^{-3}.

NOAA/STAR deployed two above-water handheld instruments during the cruise. One system was the ASD HandHeld2 and the other was the Spectra Vista 512i. The ASD has a spectral range of 325 nm to 1075 nm and a spectral resolution of less than 3 nm. This unit was equipped with a built in GPS and was equipped with fore-optics with a 10 degree FOV. The other system NOAA used was a Spectra Vista HR-512i. The NOAA HR-512i covers a spectral range of 350 nm to 1050 nm, a 3 nm spectral resolution, and an 8 degree FOV. Validation measurements were conducted at all stations on the bow simultaneously with the other team members above-water measurements typically while the floaters and profilers were deployed. The method of Mueller et al. [2003a] was utilized with a NOAA Spectralon white plaque with a nominal reflectance of 0.99. The water and plaque measurements were conducted at an angle of 40 to 45° from nadir and an azimuth angle to the sun of 90° to 135°. The sky was measured at a 40 ° to 45° zenith angle and at an azimuth angle to the sun of 90° to 135°.

Extracted fluorometric Chl-*a*
Chl-*a* concentrations were measured using a Turner 10 AU Fluorometer [Welschmeyer, 1994]. Surface samples were collected in duplicate at each station from the Rosette Sampler and several times a day while underway from the flow-through system to calibrate the underway chlorophyll fluorometers. From 100 mL to 500 mL of seawater was filtered on a 25 mm diameter, 0.7 μm glass microfiber filter (GF/F; Whatman). The filters were frozen in liquid nitrogen, then extracted in 90% acetone in a freezer for at least 48 h. The samples were vortexed then centrifuged for 5 min before being measured on the Turner 10 AU.

Suspended Particulate Matter (SPM)
SPM samples were collected in duplicate from the surface waters for each station. Up to 2 L of water were collected for each sample and processed according to techniques outlined by Hunter et al. [2006]. Water samples were filtered on pre-weighed 47 mm diameter GF/F filters. The volume of filtrate was then measured with a graduated cylinder and recorded. Filters were rinsed 3 times with distilled water, placed in 47 mm diameter Petri dishes and oven dried at 60 °C for 12 h then stored in a desiccator until analysis. Filters were weighed on a Sartorius CPA 2250 balance (with a precision of 0.01 μg) and weighed at least three times until consecutive readings were less than 0.055% variable [EPA, 1971].

HPLC Pigments
Surface water samples were collected from each CTD rosette cast at each station except Station 17 and Station 19 where they were collected from the ship's underway flow-through system. Water collected from the CTD Niskin bottles was transferred to 10 L carboys which were covered with black plastic bags to prevent high light exposure while awaiting filtration. For each sample, a known volume of water was filtered under gentle vacuum (~127 mm Hg) onto a 25 mm diameter Whatman GF/F filter (nominal pore size ~0.7 μm). The HPLC filter samples were wrapped in aluminum foil and stored in liquid nitrogen onboard. In the laboratory, the HPLC samples were stored at −80°C until analysis and were analyzed at the NASA Goddard Space Flight Center, Ocean Ecology Laboratory. The HPLC method is modified from Van Heukelem and Thomas [2001].

AOT
AOT was measured at 11 stations using a Microtops sun photometer. The data are delivered for processing to NASA as part of the AERONET Marine Aerosol Network program.

NURADS
The NURADS instrument was used to measure the spectral upwelling radiance distribution at Stations 8, 11 to 13, 15, and 18 to 26 using the method of Voss and Chapman [2005]. The NURADS instrument was calibrated immediately before the cruise using previously published protocols [Voss and Zibordi, 1989; Voss and Chapin, 2005]. When deployed, floats are attached to the instrument and the package is floated 20 m to 50 m away from the ship, at the surface (measurement depth is 0.75 m). During deployment, the instrument measures the upwelling radiance continuously, cycling through the 6 different wavelengths and associated dark measurements.

11.2 NASA/GSFC – Scott Freeman and Antonio Mannino

In-Water AOPs
In-water AOPs, both E_d and L_u, were measured using a Biospherical Instruments C-OPS profiling radiometer system. A matching reference radiometer measured E_s. The three radiometers have a spectral range from 300 nm to 900 nm, with 19 wavebands each, as listed below.

List of wavebands (n=19) measured by NASA's C-OPS profiling radiometer [nm]:

- 305
- 320
- 340
- 380
- 395
- 412
- 443
- 465
- 490
- 510
- 532
- 555
- 565
- 625
- 665
- 683
- 710
- 780
- 875

The L_u radiometer substitutes a broad natural chlorophyll fluorescence sensor (27 nm FWHM, centered at 683 nm) for the 875 nm sensor. All other wavelengths are 10 nm FWHM. The radiometers feature three gain stages, which provide 9 decades of dynamic range [Morrow et al., 2010].

Before each deployment, dark current measurements at each of the three gain stages and a pressure tare were made by capping the sensors and running the dark current procedure through the μProfile software (C-OPS manual). The C-OPS system was deployed at each station, measuring over 200 profiles of the water column in total. Each radiometer was calibrated at NOAA NESDIS, College Park before and after the cruise. The system was last calibrated at the manufacturer's facility in March, 2018.

Above-water AOPs

Above-water AOPs (E_s, L_{sky}, L_t) were measured using a Satlantic HyperSAS system. This system was on a turntable, which allowed rotation to the desired angle relative to the solar azimuth angle (90° to120°), within the limits of viewing angle. The HyperSAS radiometers were calibrated at NOAA NESDIS, College Parkboth before and after the cruise. The system was last calibrated at the manufacturer's facility in March to August of 2018. The hyperspectral radiometers have a spectral range of 305 nm to 1150 nm, and were calibrated for the full range. The data will be processed at NASA to obtain R_{rs} using software in development.

11.3 CCNY – Alex Gilerson, Carlos Carrizo, Philipp Grötsch, Eder Herrera, Mateusz Malinowski, Sam Ahmed

The primary instrument of CCNY group used for above water observations in the validation process was a GER 1500, SpectraVista, NY. Measurements were also made with the hyperspectral polarimetric imaging system, which included a snapshot hyperspectral imager UHD285 (Cubert, Germany) and polarization camera M2450 (Teledyne DALSA, Canada) as well as with the HyperSAS (Satlantic, Canada). In addition, AOT was measured by Microtops II sunphotometer (Solar Light, PA) at 5 wavelengths: 380 nm, 500 nm, 675 nm, 870 nm, 1020 nm.

Handheld spectroradiometer

The GER 1500, Field Portable Spectroradiometer, is a handheld spectroradiometer designed to provide fast spectral measurements covering the UV, Visible and NIR wavelengths from 350 nm to 1050 nm at 3 nm full width half maximum (FWHM) resolution. It uses a diffraction grating with a silicon diode array that has 512 discrete detectors and provides the capacity of reading 512 spectral bands. Subsequent download and analysis is done using a personal computer with a standard RS232 serial port and the GER 1500 licensed operating software. The GER 1500 is equipped and operated with a standard lens with 4° nominal FOV for above water observations. The GER 1500 is used in the field to calculate R_{rs} by measuring the total radiance (L_t) above the sea surface, the sky radiance (L_s) and the downwelling radiance (L_d) based on the radiance reflected from the white plaque.

The instrument has undergone radiometric and wavelength calibration in the optics mode (with the lens) at the manufacturer in March 2019. Generally, due to the nature of the measurement, calibration is not necessary. Main details of the data processing are available in the Cruise Report #152 [Ondrusek et al., 2019] which follow the Mobley [1999] approach. In addition, data were processed with the 3C model developed by Groetsch et al. [2017], which assumes spectrally dependent bias for R_{rs} spectra due the combination of the sky and sun glint.

Hyperspectral polarimetric imaging system

The Hyperspectral polarimetric imaging system included a snapshot hyperspectral imager with a filter wheel, which contained polarizing filters with different orientation and a polarization camera, with another filter wheel, which contained color filters (Figure 5). The system was operated by two laptop computers.

Figure 5. CCNY instrumentation on the ship: snapshot hyperspectral imager with polarization camera (left), HyperSAS (right).

Snapshot Hyperspectral Imager

An imaging spectrometer UHD285 with no moving parts permits acquisition of the spectral cube in the visible/NIR part of the spectrum with a field of view (FOV) of 40° [Carrizo et al., 2019]. In this instrument light from the object after the objective is divided by a 50:50 cubic non-polarizing beam splitter with one half directed to the first photodetector matrix for acquisition of a panchromatic image in the 450 nm to 1000 nm wavelength range with a spatial resolution of 1000 × 1000 pixels. The other half of the beam is modified by a micro-lens array, collimated, spectrally split using a prism, and finally focused on the second detector matrix. After processing with Cubert's proprietary algorithm, spectra are available for 50 × 50 spatial pixels and 138 wavelengths with a sampling interval of 4 nm. Since a prism is used as the dispersive element in the imager, the spectral bandwidth strongly depends on the wavelength with FWHM of ~5 nm at 450 nm and ~30 nm at 900 nm. The non-scanning feature eliminates the necessity of the continual movement required by push-broom imagers. The UHD285 imager underwent additional laboratory calibration at CCNY by the comparison of radiances reflected from a white Lambertian plaque standard (ZenithLiteTM, SphereOptics GmbH) with the radiances measured by the GER spectroradiometer. A typical integration time for ocean observations with the imager is 20 ms to 50 ms. The imager was installed on the tripod with the main axis at 90° (270°) azimuth angle from the Sun, typically 40° viewing angle from the nadir (with some measured deviations) for L_t measurements and at 40° viewing angle from the zenith for the sky measurements. Downwelling irradiance was measured independently by the HyperOCR E_d sensor installed on the pole in an unobstructed area on the ship. The imager had a filter wheel in front with three polarizers 50 mm diameter and 0°, 45°, and 90° orientation to the reference direction, one window on the wheel was unobstructed for measurements of the L_t and one was blocked to measure dark currents. Stokes vector components of the radiances I, Q and U were calculated by special processing of polarized radiances I0, I45 and I90 as described in Gilerson et al. [2020].

Polarization camera

A recently released Sony image polarization sensor with 2464 H (horizontal) × 2056 V (vertical) pixels where each 2 × 2 pixel area consists of four subpixels that are equipped with polarizers oriented at 0°, 90°, 45° and -45°, respectively was integrated by Teledyne DALSA into the M2450 camera and

calibrated by us together with the UHD285 snapshot imager. In our implementation, it was combined with a filter wheel (Finger Lakes Instrumentation, NY) containing six color band-pass filters (AVR Optics, NY) with rectangular transmission spectra at the following center wavelengths (bandwidths): 442 nm (42 nm), 494 nm (41 nm), 550 nm (32 nm), 655 nm (40 nm), 684 nm (24 nm) and 775 nm (46 nm). Camera and lens were assembled with the filter wheel to provide a rectangular FOV (HFOV × VFOV = 29.2° × 38.4°) similar to the FOV of the imager. Typical integration time was 2 ms for water measurements, 0.7 ms for sky measurements, and 0.05 ms for white plaque measurements. Videos of the water surface were acquired with a typical frame rate of about 30 to 40 frames/second and 8 bits digitization, standalone images were acquired with 8 bits and 12 bits digitization. The user interface provided by the manufacturer was integrated with the filter wheel interface to allow for automatic acquisition of videos and images of polarization components. These images and videos were then reprocessed to get images and videos of Stokes vector components, the degree of linear polarization (DoLP) and angle of linear polarization (AoLP), which were further used in the analysis in Gilerson et al. [2019]. Polarimetric measurements provide additional information relevant to the VIIRS NOAA-20 instrument, which has increased sensitivity to polarization [Sun et al., 2019]. These measurements should be also helpful in the characterization of ocean wave slopes [Zappa et al., 2008] and analysis of their variability in different open ocean and coastal areas as a function of wind speed.

HyperSAS

A Satlantic HyperSAS system was installed at the bow of the *Gordon Gunter* at approximately 10 m above the water surface. Three spectrometers observed sky radiance L_s (40° from zenith), L_s (0° from zenith), and total water-leaving radiance L_t (40° from nadir) in the wavelength range 305 nm to 905 nm with 180 equally spaced channels. The L_t and L_s radiance sensors had a 3° full-angle field-of-view and were oriented −67.5° from cruising direction, observing water and sky at 40° from nadir and zenith, respectively. This fixed observation geometry caused the relative azimuth angle (dAZ) between Sun and radiance sensor to be variable, with occasional high sun glint contributions to be expected. The $L_s(0°)$ sensor had been intended to add information on sky radiance distribution, but was of limited use due to a faulty dark current shutter. E_d was recorded from above the observation deck, with unobstructed sky views except for the radar mast at a distance of approximately 10 m. The cosine corrector could not be reached during the cruise and was therefore not cleaned regularly. However, no obvious contamination was found on the sensor upon retrieval after the cruise. Sensor calibrations were initially performed by Satlantic Inc. and were validated before and after the cruise against a NIST-traceable light source at the NOAA/STAR optics laboratory. HyperSAS observations were processed with the 3C method [Groetsch et al., 2017] to R_{rs}. The 3C method consists of a bio-optical inversion scheme that retrieves reflectance at high precision and low bias even when L_t observations are highly variable due to sun glint and wind-roughened water surfaces.

Examples of measured and processed data

Example comparisons of GER data with satellite data including VIIRS SNPP and VIIRS NOAA-20 processed by NOAA MSL12 code, and from VIIRS SNPP, VIIRS NOAA-20, and MODIS Aqua processed by NASA are shown for Station 1 (coastal water) and Station 12 (open ocean) in Figure 6. For coastal waters, above-water measured GER spectra were corrected by the standard Mobley 99 approach [Mobley, 1999], which should be adjusted by the subtraction of R_{rs} at 750 nm; it was separately processed also by the 3C model. Because of the spectrally dependent bias in the 3C model, these spectra differ especially in the blue. For the 3C model, R_{rs} in the NIR is also not necessarily equal to zero, which is typical for coastal waters. Comparisons for coastal waters indicate significant variability of the satellite spectra at 410 nm and 443 nm bands, which is most likely due to the different processing algorithms and also probably to the surface effects in the coastal waters [Gilerson et al., 2018; Carrizo et al., 2019]. Examples of the L_t spectra from the imager in unpolarized mode at viewing angles 20° to 60° and comparison with GER are shown in Figure 7 for Station 11 (open ocean) and Station 18 (coastal water).

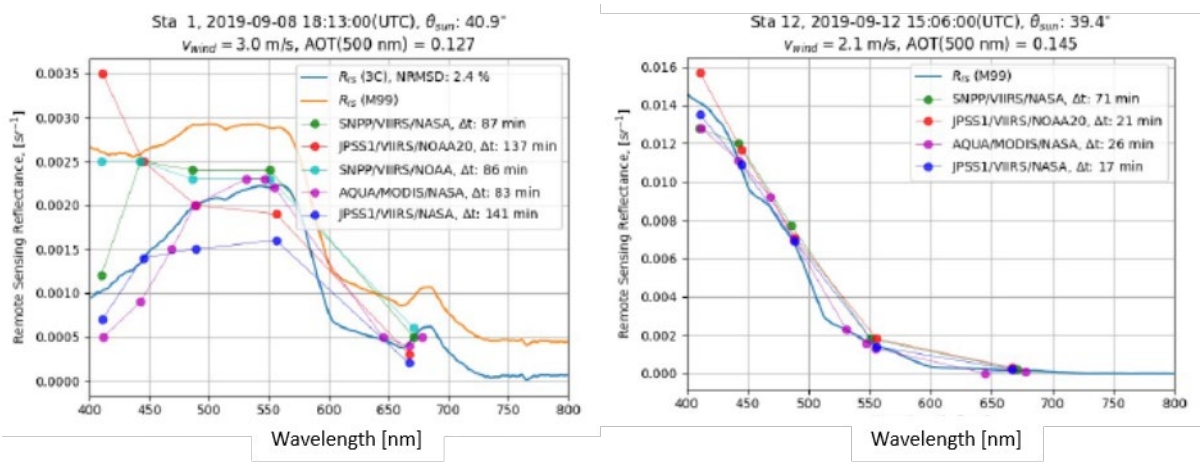

Figure 6. Comparison of measured spectra by GER with satellite data: a) coastal waters at Station 1 b) open ocean at Station 12. GER spectra are processed with reflectance coefficient from Mobley [1999] and the 3C model [Groetsch et al., 2017].

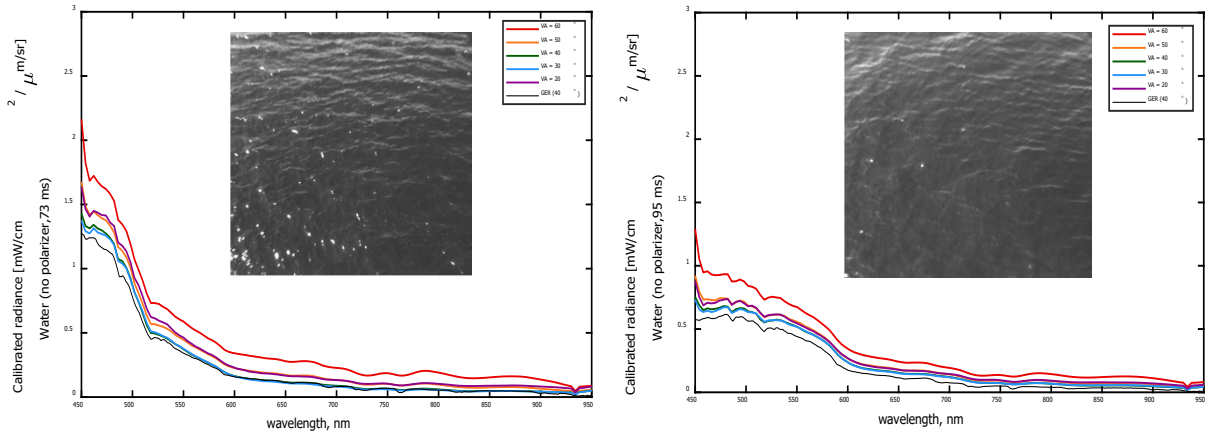

Figure 7. Example of the imager L_t spectra for different viewing angles and matchup with GER for two stations: a) Station 11 09/12/2019, 14:24 (UTC), W = 1 m s^{-1}, b) Station 18 09/14/2019, 16:24 (UTC), W = 2.6 m s^{-1}.

Examples of images from the polarization camera are shown in Figure 8, which include images of Stokes vector components I, Q and U, DoLP, AoLP, and an image in one of polarization channels (90°). Images were collected with the 442 nm (42 nm wide) filter. Following the methodology [Zappa et al., 2008], 100 frames of DoLP and AoLP were used to determine variances of wave slopes, which are compared with the values from Cox-Munk expression [Cox and Munk, 1954] in Figure 9. Processing was carried out from the images at 550 nm, where the impact of the polarization from the water leaving radiance and spatial non-uniformity of the DoLP and AoLP was minimal.

Examples of spectra from the HyperSAS processed by the 3C model are shown in Figure 10 for the cases with minimal sun glint and in Figure 11 with significant sun glint demonstrating ability of the 3C model R_{rs} retrieval even in conditions of the strong sun glint.

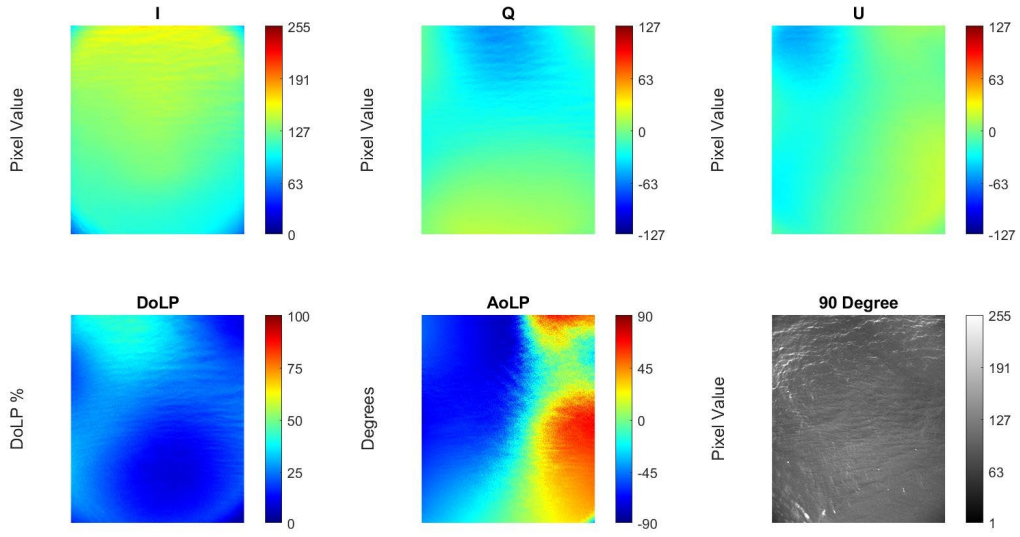

Figure 8. Example of the images from the polarization camera, Station 18, W = 2.6 m s^{-1}.

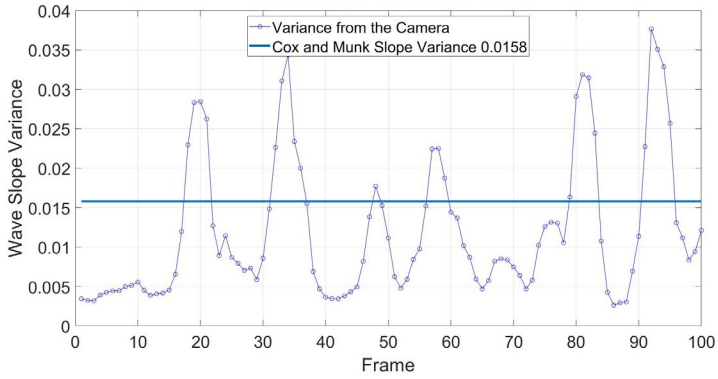

Figure 9. Example of time series of wave slope variances calculated from measurements of the polarization camera for Station 18.

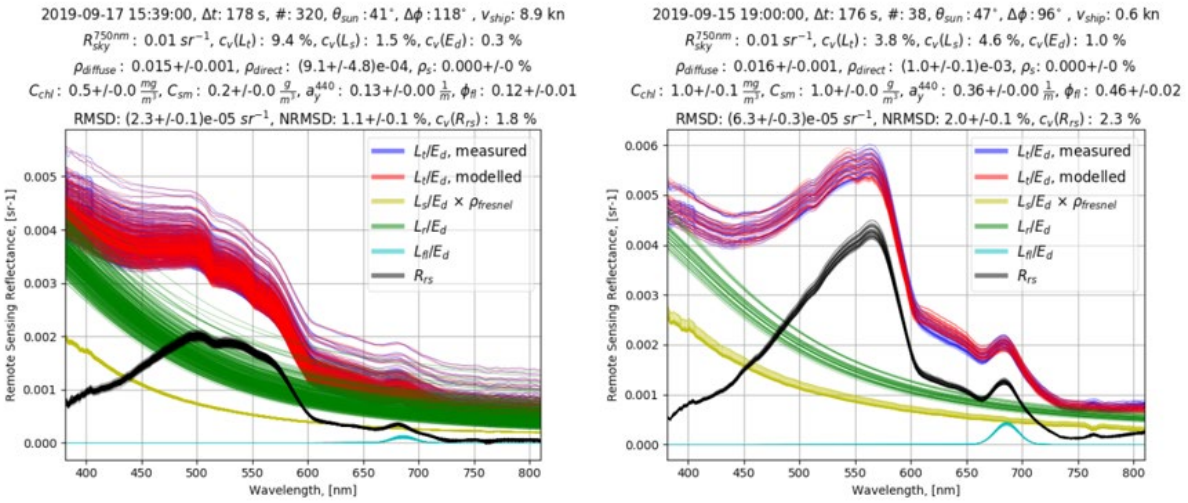

Figure 10. R_{rs} 3C retrieval results for HyperSAS observations recorded at sun glint-minimizing viewing geometries, i.e. ΔΦ=90° to 135°. Left panel is from 17 September. Right panel is from 15 September. Offsets in the near-infrared spectral region are accounted for in the inversion.

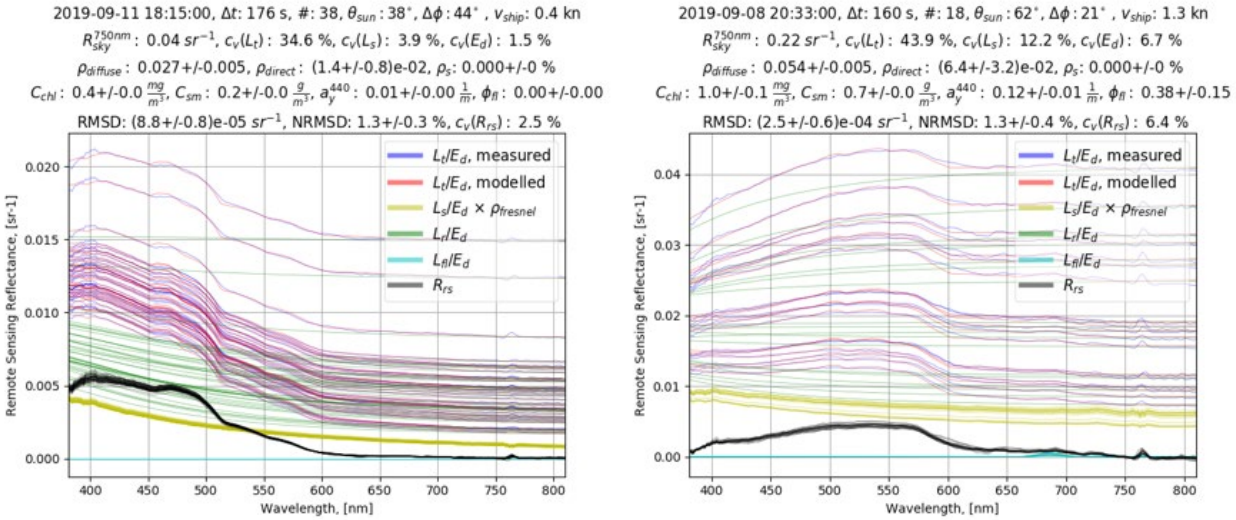

Figure 11. R_{rs} 3C retrieval results for HyperSAS observations recorded at sun glint-prone viewing geometries. Variability in L_t observations cv(L_t) was resolved in sky and sun glint contributions, allowing the derivation of reflectance at high precision (cv(R_{rs})) in both cases.

11.4 LDEO - Joaquim I. Goes, Jinghui Wu, Helga do Rosario Gomes and Kali McKee

The LDEO group undertook high-resolution measurements of chlorophyll, phytoplankton functional types, phytoplankton size classes and phytoplankton photosynthetic efficiencies in near surface (~5 m) samples from seawater that was pumped continuously through the NOAA Ship *Gordon Gunter's* uncontaminated seawater flow-through system. These measurements were repeated for discrete samples that were collected from three depths in the water column using a CTD rosette. In addition, samples from the three depths were pre-filtered for nutrient analyses to provide additional information about the biogeochemical conditions in the water column.

STATIONS Discrete Samples

Water samples were collected from a total of 26 stations along the cruise track. At each station seawater samples were obtained from 3 depths in the water column (coincident with sampling for fluorometric Chl *a*, HPLC pigments, CDOM and a^*_{ph}) for the following measurements:

i. Microscopic analysis of phytoplankton community composition and sizes.
ii. Counting, imaging and size estimations of phytoplankton and other detrital particles using a Fluid Imaging Technologies, Inc., FlowCAM [Jenkins et al., 2016].
iii. Estimates of phycobilipigments using a newly developed fluorescence technique developed at LDEO.
iv. Fluorescence based estimates of Chl-*a*, CDOM, Phycobilipigments and variable fluorescence (F_v/F_m), a measure of phytoplankton photosynthetic efficiency, using a WET Labs Advanced Laser Fluorometer (ALF) [Chekalyuk and Hafez, 2008; Chekalyuk et al., 2012; Goes et al., 2014].
v. Measurements of F_v/F_m and the functional absorption cross-section of Photosystem II (σ_{PSII}) and Electron Transport Rates (*ETR*) in a mini-Fluorescence Induction and Relaxation (FIRe)® Fast Repetition Rate Fluorometer (FRRF) [Gorbunov and Falkowski, 2004].
vi. Nutrients

i. Microscopy based phytoplankton identification and cell counts

For microscopic identification and enumeration of phytoplankton, samples were collected in 100 mL screw top hard plastic bottles from 3 depths at each of the 26 stations. Samples were fixed with 1% alkaline Lugol's iodine, preserved in 1.5% buffered formaldehyde solution and were stored in dark and cool conditions. Microscopic analysis is currently underway and includes overnight settling of 10 mL samples in an Ultermohl counting chamber and then counting the samples using a Nikon® inverted microscope at 200X and 400X magnifications. The smallest cells that can be enumerated by this method are ~5 µm in diameter. Phytoplankton identifications are based on standard taxonomic keys [Tomas, 1997]. Cryptophytes are identified by epifluorescence microscopy using their yellow-orange fluorescence signatures [Booth, 1993; MacIssac and Stockner, 1993; Goes et al., 2014].

ii. FlowCAM based phytoplankton identification, cell counts and cell sizes

In addition to the microscopic analysis of phytoplankton, 2 x 25 mL aliquots of the preserved samples have been analyzed for phytoplankton community composition and size structure analysis using a FlowCAM particle imaging system equipped with a 4X objective (UPlan FLN, Olympus®) and a 300 µm FOV flow cell. FOV flow cells ensure that the liquid passing through the flow cell is entirely encompassed within the camera's field of view. Phytoplankton cells within the preserved samples have been counted and imaged in auto-image mode with a peristaltic pump rate of approximately 0.32 mL min^{-1} to 0.44 mL min^{-1} as specified by the manufacturer. Cells will be classified to the genus level using the Visual Spreadsheet program v. 2.2.2, Fluid Imaging). The instrument provides the total number of particles imaged, together with the dimensions of each particle allowing estimations of phytoplankton community structure, particle size distribution of both phytoplankton and of detrital particles.

iii. Phycobilipigment collection and analysis

Approximately 1 L to 2 L of seawater samples from 2 depths were carefully filtered on to 4 x 25 mm Whatman GF/F filters for analysis of estimating phycoerythrin and phycourobilin pigments. Samples were immediately stored in liquid nitrogen for later analysis at LDEO using methods developed by us which rely on freezing, sonication and extraction of the phycobilipigments in phosphate buffer and analysis in a spectrofluorometer.

iv. Automated Laser Fluorescence (ALF) measurements of phytoplankton groups
The ALF combines high-resolution spectral measurements of blue (405 nm) and green (532 nm) laser-stimulated fluorescence with spectral deconvolution techniques to quantify the following:

- fluorescence of Chl-*a* (peak at 679 nm)
- three phycobilipigment types: Phycoerythrin-1 (PE-1; peak at 565 nm), Phycoerythrin-2 (PE-2; peak 578 nm) and Phycoerythrin-3 (PE-3; peak at 590 nm)
- CDOM (peak at 508 nm)
- F_v/F_m

All fluorescence values obtained are normalized to the Raman spectra of seawater and generally expressed as relative fluorescence units (RFU), whereas F_v/F_m is unitless. PE-1 type pigments are associated with blue water or oligotrophic cyanobacteria with high phycourobilin/phycoerythrobilin (PUB/PEB) ratios, PE-2 type phytoplankton with low PUB/PEB ratios are generally associated with green water cyanobacteria that usually thrive in coastal mesohaline waters, and PE-3 attributable to eukaryotic photoautotrophic cryptophytes [Chekalyuk and Hafez, 2008; Chekalyuk et al., 2012; Goes et al., 2014]. RFU values for Chl-*a* can be converted into mg m^{-3} Chl-*a* values using least square regressions of acetone or HPLC measured Chl-*a* with RFU values for Chl-*a* measured in an ALF.

All samples for the ALF were collected directly from the Niskin samplers into 500 mL acid-washed amber glass bottles and stored for about 30 min in the dark at temperatures close to the average surface seawater temperature at each station. Dark adaptation allows all of the Photosystem II (PSII) reaction centers and electron acceptor molecules of phytoplankton to become fully oxidized and hence available for photochemistry thus minimizing the impacts of non-photochemical quenching before analysis.

v. Fluorescence Induction and Relaxation (FIRe) measurements of photosynthetic competency
The FIRe instrument provides a comprehensive suite of photosynthetic and physiological characteristics of photosynthetic organisms [Gorbunov and Falkowski, 2004; Bibby et al., 2008]. This technique provides a set of parameters that characterize photosynthetic light-harvesting processes, F_v/F_m, the functional absorption cross-section of PSII (σ_{PSII}), and the electron transfer rate (ETR). All optical measurements by the FIRe are sensitive, fast, non-destructive, and can be done in real time and in situ and can provide an instant measure of the photosynthetic efficiency of the cells.

vi. Nutrient analysis
At each station, samples from discrete depths were collected directly from Niskin bottles attached to a Sea-Bird Electronics® CTD rosette. The samples were pre-filtered using a syringe filter and then transferred into acid-washed 50 ml Falcon tubes, which were immediately frozen on board. Samples will be analyzed for inorganic nutrients (SiO_3, NO_3+NO_2, and PO_4) with a SEAL AA3® nutrient auto analyzer using the methods proposed by Knap et al. [1994].

UNDERWAY FLOW-THROUGH MEASUREMENTS
Between stations, the ALF, the FlowCAM, the FIRe and a bbe Moldeanke AlgaeOnlineAnalyser [Richardson et al., 2010] were connected in parallel to the ship's seawater flow-through system, allowing for continuous in-water measurements of phytoplankton community composition, phytoplankton size, phycobilipigment types and photosynthetic efficiency. With the exception of a few breaks during stations and for reconditioning, all four instruments were operated over the entire cruise track, providing several thousand fluorescence based measurements of Chl-*a*, CDOM, PE-1, PE-2, PE-3, F_v/F_m, σ_{PSII}, and p (a measure of electron transport between the PSII and PSI. Continuous flow through measurements of phytoplankton species distribution and cell size distribution along the cruise track will provide useful information for interpreting the optical measurements for PFTs over the study area. The AlgaeOnlineAnalyser provides continuous measurements of Chl-*a*, plus determination of cyanobacteria, green algae, brown algae (diatoms and dinoflagellates) and cryptophytes fluorescence using colored light emitting diodes.

Preliminary data obtained with the flow-through instrumentation allow us to obtain a synoptic pictures of biological oceanographic conditions during the cruise (Figure 12). Waters closer to the coast were much fresher than those offshore, rich in CDOM and Chl-*a*, particularly off the coast of Delaware, near the mouth of the Delaware River and New Jersey (Figure 12a-d). A patch of blue water cyanobacteria (*Trichodesmium sp*.) was observed off the coast of Virginia (Figure 12e), whereas a patch of elevated coastal water cyanobacteria was observed at the mouth of the Delaware River (Figure 12f).

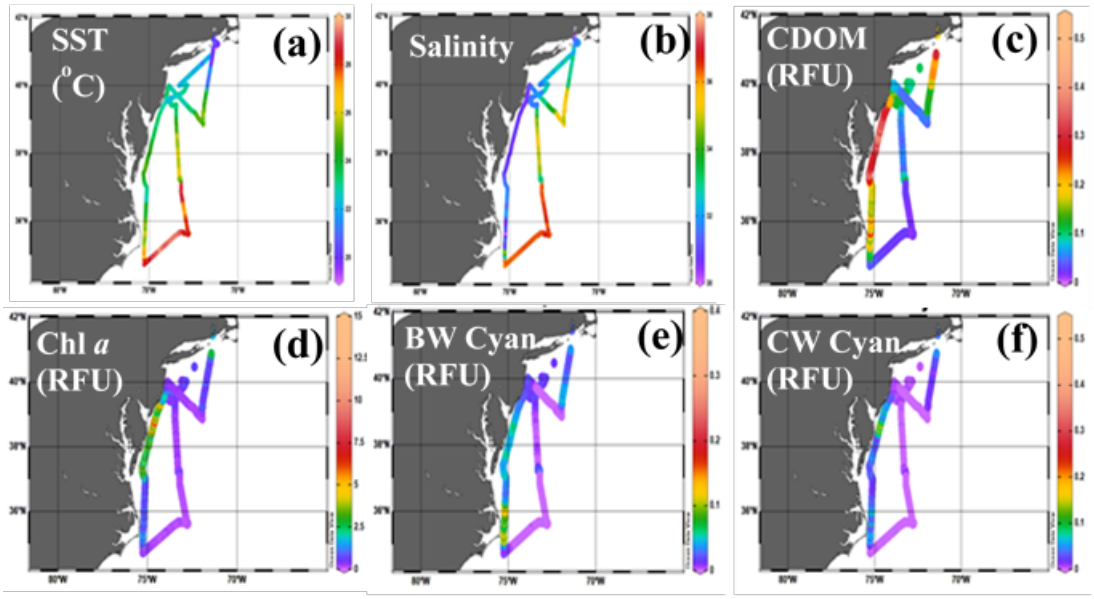

Figure 12. Distribution of a) sea surface temperature (SST), b) salinity, c) CDOM, d) Chl-*a*, e) blue water cyanobacteria, and f) coastal water cyanobacteria along the cruise track.

Values of F_v/F_m, σ_{PSII}, and p (Figure 13) were indicative of a population that was generally photosynthetically active and not stressed for nutrients except in the region close to the coast northeast of New Jersey.

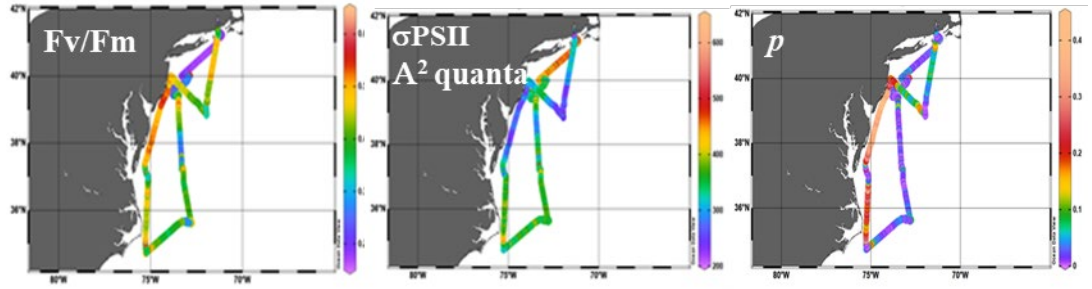

Figure 13. Distribution of photosynthetic rate parameters F_v/F_m (left), σ_{PSII} (middle), and p (right).

11.5 USF - Chuanmin Hu, Jennifer Cannizzaro, Yingjun Zhang, Yang Zhang, and David English

Spectral absorption and pigment determinations

Measurements of the light absorption due to the particulate and dissolved components of water samples are used for understanding and modeling of the underwater light field, as well as the development of remote sensing and primary productivity algorithms. Shortly after collection, a subset of the water samples from the CTD rosette or surface underway system were filtered through a glass fiber filter to allow later spectral measurements of the light absorption by particles in the water. A portion of the filtrate

was also reserved for a shore-based measurement of the spectral absorption of the dissolved material, $a_g(\lambda)$, in these water samples. The extraction of the particulate pigments allows the separation of the total particulate absorption, $a_p(\lambda)$, into a living or pigmented fraction, $a_{ph}(\lambda)$, and detrital fraction, $a_d(\lambda)$ [Kishino et al., 1985]. The extraction of the pigments also allows a fluorometric determination of the Chl-*a* concentration [Holm-Hansen and Riemann, 1978; Welschmeyer, 1994].

Table 9. Time and depth of water samples collected for particulate and dissolved absorption analysis.

Time (UTC)	Station or sample ID	Sample Depths (m)
9/08 17:00	1	2.0, 17.0
9/09 13:39	2	2.0, 23.5
9/09 16:45	3	2.0, 26.0
9/09 20:15	4	2.0, 31.5
9/10 13:25	5	2.7, 20.5
9/10 15:58	6	2.5, 24.0
9/10 20:18	7	2.5, 23.4
9/11 11:58	ALFA 001	~3
9/11 12:36	8	2.7, 43.0
9/11 18:05	9	2.7, 49.6
9/11 21:18	10	2.7, 51.0
9/12 12:33	11	2.6, 79.5
9/12 15:57	12	2.1, 137
9/12 20:25	13	2.7, 136
9/14 01:01	ALFA 002	~3
9/13 13:04	14	2.5, 36.1
9/13 16:31	15	2.1, 49.0
9/13 20:22	16	3.6, 37.0
9/14 14:20	17	~3
9/14 17:30	18	2.8, 16.9
9/15 16:06	20	2.5, 3.3
9/15 19:27	21	2.8, 8.9
9/15 21:41	22	2.7, 9.8
9/16 12:39	23	2.3, 39.0
9/16 17:16	24	2.2, 48.4
9/16 20:34	25	3.3, 44.0
9/17 13:04	26	3.0, 15.0

During the GU-19-03 cruise of September 2019, 51 water samples were filtered for particulate absorption analysis. There were 28 samples collected from surface waters and 23 from waters located at depths greater than 4 m (Table 9). These samples will be processed to determine $a_p(\lambda)$, $a_d(\lambda)$, $a_{ph}(\lambda)$, $a_g(\lambda)$ and Chl-*a* concentrations. Additionally, water samples from 24 of the stations were filtered for later HPLC analysis by NASA (see Section 11.2).

Above-water remote sensing reflectance

Above-water $R_{rs}(\lambda)$ was collected at most of the stations using a Spectra Vista Corp. (SVC) HR-512i spectroradiometer. The $R_{rs}(\lambda)$ measurements were made by comparing spectral radiance measurements of both the water's surface and the sky to a reference plaque [Carder and Steward, 1985; Mueller et al., 2003b]. The HR-512i with an 8° FOV and a white reflectance plaque (~98% reflectance) with measured spectral reflectance characteristics were used to determine $R_{rs}(\lambda)$. The HR-512i viewed the reflective reference from >30 cm above the reflectance plaque from nadir, while the sea-surface and sky measurements (Θ_w & Θ_s) were made with viewing angles of 35° to 40° from nadir and zenith, respectively. Since Θ_w is recorded by this HR-512i, the measured angle, rather than the suppositional angle, was incorporated into the selection of the surface's skylight reflectance value during the processing of the measurements.

Measurements for $R_{rs}(\lambda)$ using the HR-512i were made at all of the GU-19-03 stations, but shading of the reference panel by clouds and adverse conditions reduced the reliability of the results for several stations.

Of the measurements from the 26 stations, the $R_{rs}(\lambda)$ estimates from 7 stations were flagged as unreliable or suspect. $R_{rs}(\lambda)$ estimates for GU-19-03 stations are shown in Figure 14.

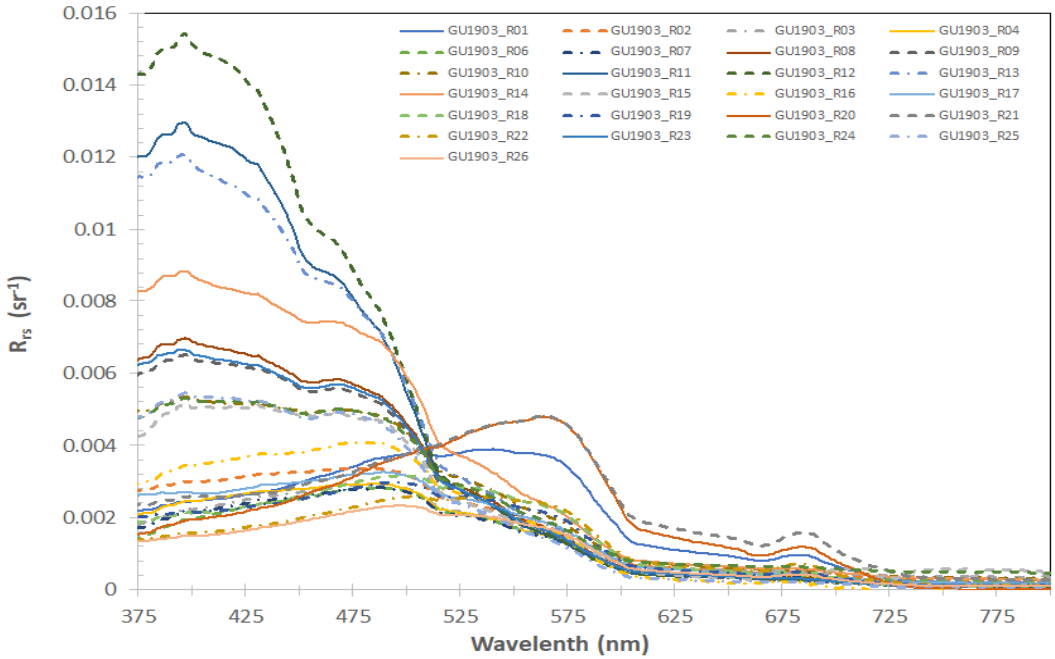

Figure 14. Preliminary above-water $R_{rs}(\lambda)$ from HR-512i measurements at 25 stations of GU-19-03.

In-water radiometry

Vertical profiles of the near-surface water light field were collected using a Satlantic HyperPro-II. The HyperPro-II includes $L_u(\lambda,z)$ and $E_d(\lambda,z)$ sensors, as well as sensors for measuring pressure, temperature, conductivity, $b_b(660)$, and both Chl-*a* and CDOM fluorescence. At 25 stations of GU-19-03, the $L_u(\lambda,z)$ and $E_d(\lambda,z)$, measurements from multiple casts were used to estimate sea surface conditions such as $L_w(\lambda,0+)$ and $E_d(\lambda,0+)$, $R_{rs}(\lambda)$, and $nL_w(\lambda)$. Figure 15 shows some of the $R_{rs}(\lambda)$ estimates derived from HyperPro-II measurements at each station. USF's HyperPro system was deployed using the manufacturer's recommended protocol [Satlantic, 2003, 2004] in coordination with the HyperPro profiling group. Preponderantly good agreement was observed (Figure 16) between the estimates of R_{rs} for several satellite wavebands (410 nm, 443 nm, 486 nm, 551nm, and 671 nm) derived from HyperPro-II casts and above-water HR512i measurements.

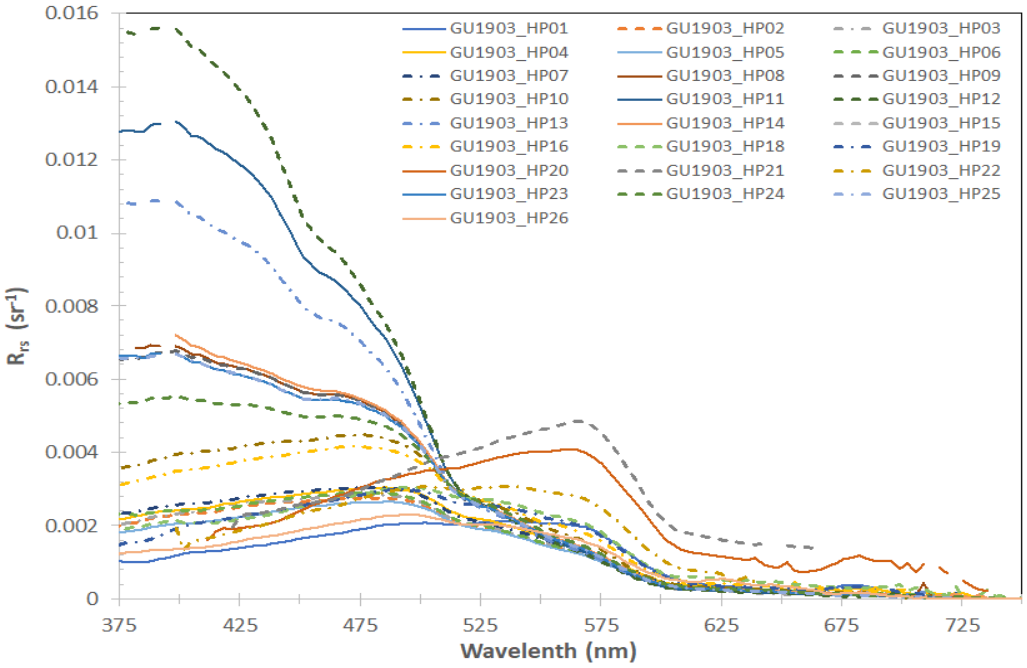

Figure 15. Preliminary $R_{rs}(\lambda)$ estimated from HyperPro-II profiles at GU-19-03 stations.

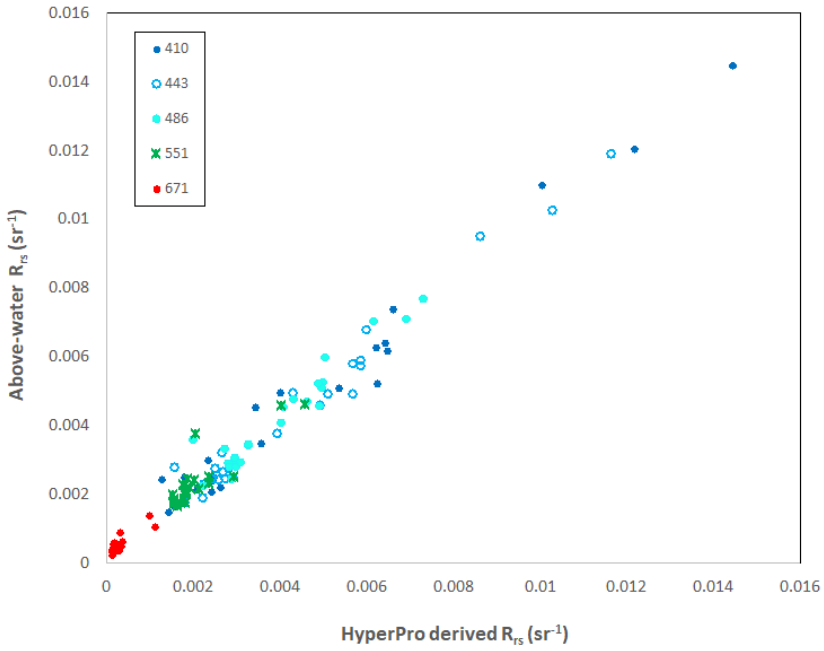

Figure 16. Comparison of HyperPro derived R_{rs} and above-water HR512i R_{rs} measurements during GU-19-03 for several satellite validation wavebands.

No Underway flow-through measurements using the WETLabs ALFA system

The WETLabs Aquatic Laser Fluorescence Analyzer, ALFA, is a laser stimulated fluorescence measuring system that uses blue (405 nm) and green (515 nm) lasers and spectral deconvolution software to assess phytoplankton pigment concentrations and physiological status and CDOM concentration. A component in the USF ALFA system failed during pre-cruise testing, and it could not be replaced before the cruise.

Thus, though USF's ALFA system was deployed on several of the previous NOAA VIIRS cal/val cruises, it was not operational during GU-19-03.

11.6 NRL - Sherwin Ladner and Wesley Goode

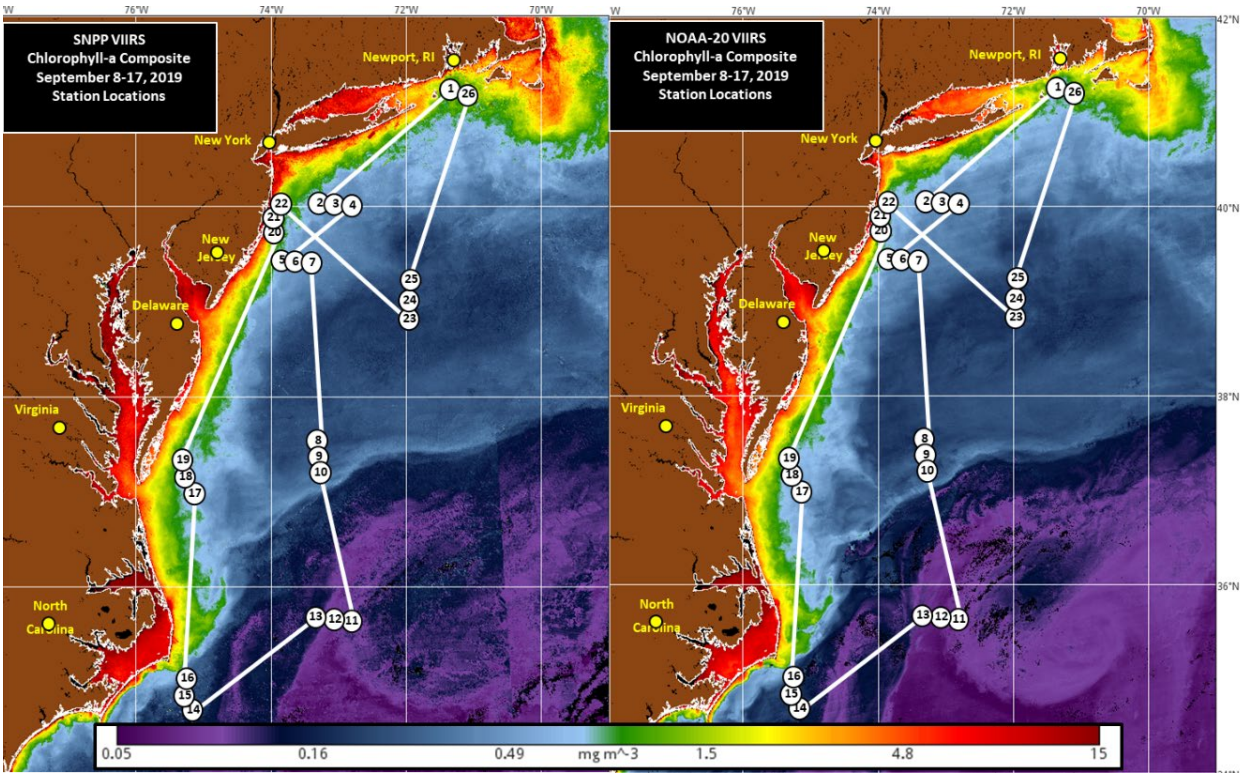

Figure 17. Chl-*a* images illustrating the NOAA Ship *Gordon Gunter* cruise track (solid line) and 26 stations (white circles) averaged daily for VIIRS SNPP(left) and VIIRS NOAA-20 (right) for the time period 8 to 17 September 2019. Both composite images in this figure were processed by NRL's Automated Processing System (APS) v6.10 and vicariously calibrated to the MOBY calibration and validation site in Hawaii. Note a variety of water-masses (coastal, shelf, offshore, Gulfstream) were collected.

The NOAA Ship *Gordon Gunter* cruise track from 8 to 17 September 2019 consisted of a total of 26 stations (white circles) over the 10 day period (Figure 17). Stations were adaptively planned and selected based on predicted (https://www.windy.com/) weather forecasts and clear sky conditions to increase the probability of obtaining satellite matchups. The NRL group provided individual daily Google Earth images of both VIIRS sensors (SNPP and NOAA-20) in near real-time along with daily composites that consisted of merging VIIRS SNPP, VIIRS NOAA-20, OLCI Sentinel-3A, and OLCI Sentinel-3B to plan next day's station locations and to determine if the day's stations were clear/valid for matchups with each sensor. The goals for the cruise sampling were same as the May 2018 cruise [Ondrusek et al., 2019]: evaluate and test methods for collection and processing protocols for in situ ocean color measurements from different instruments to improve the precision and reduce the variability across sensors in measurements and to improve in situ and satellite matchups for consistent and accurate satellite Cal/Val.

The NRL group sensor measurements included: 1) hyperspectral $R_{rs}(\lambda)$ using one floating HyperPro (HTSRB); 2) continuous underway hyperspectral IOPs from the ship's flow-through using two ac-s instruments (filtered for CDOM absorption and non-filtered for total absorption and beam attenuation), BB3 sensor and ship's CTD and fluorometer; and 3) hyperspectral $R_{rs}(\lambda)$ using two handheld

hyperspectral radiometers (ASD and Spectral Evolution Inc.). The collection protocols for the instruments were carried over from the May 2018 survey [Ondrusek et al., 2019].

NRL Measurements

Floating HyperPro (In-Water) Measurements

The NRL group utilized one floating HyperPro (NRL) on the cruise. The NRL instrument was deployed at 24 of the 26 stations omitting Station 16 and Station 17 due to time and weather contraints (Figure 17, Table 5, and Table 6). The spectral range of both E_d (SN 275) and L_u (SN 311) sensors is from 352 nm to 805 nm at 3.3 nm ±0.1 nm increments. The HyperPro instrument normally used for profiling was fitted with a molded floatation collar, allowing the observation of temporal variability of above-water and in-water measurements at a fixed depth just beneath the sea surface. The downwelling E_d sensor uses a cosine collector and is approximately 30 cm above the water surface, but it was not used for final $R_{rs}(\lambda)$ calculations. The L_u sensor is mounted approximately 30 cm below the water surface. The NRL E_s sensor (SN 376) also uses a cosine collector and was mounted along with all the participating groups' E_s sensors on the deck on a pole which was elevated above the ship's superstructure while on station for consistency (Figure 18). E_s from the ship mounted sensors was combined with L_u from floating HyperPro for computation of R_{rs}. The NRL HyperPro L_u, E_s and E_d sensors were calibrated by NOAA/STAR (Michael Ondrusek) based on NIST calibration protocols prior to cruise. The sensors were calibrated within a month of the cruise and those calibration coefficients were used for processing.

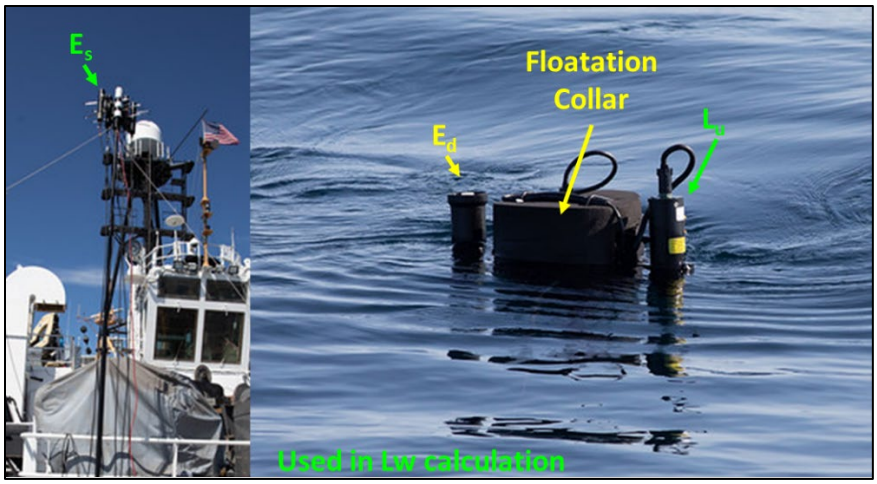

Figure 18. Labelled photographs of the NRL group's floating HyperPro system. The E_s sensor (left photo) onboard the ship and the L_u sensor on the buoy were used to calculate nL_w then coverted to R_{rs} (above water) using Prosoft v8.1.6 software.

The floating HyperPros were deployed from the starboard side of the ship. The instruments were allowed to float out a sufficient distance from the boat (20 m to 30 m) to prevent contamination from vessel-generated bubbles, ship shadowing and other potential contamination. Once the instrument was at a sufficient distance from the vessel, data was recorded for approximately 5 min. Post processing of this dataset was done using Satlantic's ProSoft v8.1.6 with pre-established protocols limiting the sensor tilt to 2° from nadir.

The pre-established processing protocols for deriving $R_{rs}(\lambda)$ from in-water radiometry follow Chapter 2 of Mueller, et al. [2003a]. $R_{rs}(\lambda)$ is computed as for Equation 1 below, where $\rho = 0.021$ is the Fresnel reflectance of the air sea interface, and $n = 1.34$ is the refractive index of seawater.

$$R_{rs} = L_u * factor / E_s, \text{ where } factor = (1- \rho) / (n^2) \qquad (1)$$

Above Water Radiometry Measurements

Above-water remote sensing reflectance measurements were taken using Analytical Spectral Devices FieldSpec Handheld2 hyperspectral spectroradiometer (ASD) and Spectral Evolution Inc. PSR-1100F hyperspectral spectroradiometer on the bow of the NOAA Ship *Gordon Gunter*. Each spectroradiometer was calibrated for spectral radiance using NIST-traceable standards by their respective manufacturers. The bow location was selected to reduce the amount of contamination from the ship's structure on the collection of the calibrated reference plaques (NRL White) and the water's surface.

Above water measurements were acquired during all 26 stations using the Spectral Evolution spectroradiometer. Issues occurred with the NRL ASD at Stations 1, 3, 4, 5, 7, 10, 14, 15, 17, 18, 19, 22 and 26 resulting in 13 valid ASD stations due to instrument malfunction with the automated optimization of integration time. The above water measurements were made using only the NRL white 99% reflectivity 10x10 Labsphere Inc. plaque during the standard sky, water, and reference plaque sequence for deriving the above-water R_{rs}. The NRL white plaque was used as the standard reference to compute the above-water $R_{rs}(\lambda)$. The white plaque has a known BRDF and is used to normalize the un-calibrated irradiance measurements for E_s. Answers may vary due to instrument type and calibration, warm up time, shadowing of the plaques, BRDF differences for plaque, etc.

The above-water measurement activities took place on the bow of the NOAA Ship *Gordon Gunter*. At the start of each station, the reference plaque was placed on the bow's bollard posts (Figure 19). The plaque was occasionally partially obscured from the full hemisphere by the ship's bridge, participants, and the bow rail. The magnitude of this bias will depend on how much of the diffuse component is blocked. The NRL group recorded station metadata (time, latitude, longitude, instrument base filenames, spectra target assignments and numbers, ocean parameters from ship's flow-through, physical water characteristics, meteorology, etc.) on hand written log sheets during each station. Other personnel took photographs of the sky conditions and the participants in action. Observers attempted to make concurrent measurements using multiple instrument types (ASDx2, Spectral Evolution, GER and SVCx3). At the end of each station, the plaque and the radiometers (powered off) were placed in a water tight storage box on the bow. At the end of each day they were taken back into the lab to download data and stored in their respective cases.

Figure 19. NRL group collection sequence (sky, plaque and water) during above water spectroradiometer (ASD and Spectral Evolution) data collection activities.

The NRL group ASD instrument was configured to average 10 spectra and save five spectra for each target. The Spectral Evolution is designed to collect one spectra at a time and has to be triggered for each individual scan (10 scans per target). During each station, five consecutive radiometric spectrum with dark measurements subtracted were taken of each of the following targets: 1) sky, 2) NRL white plaque and 3) water for the ASD. The same sequence was collected for the Spectral Evolution with 10 radiometric spectra per target. For both the ASD and Spectral Evolution instruments, an 8 degree fore optic was attached, integration time was optimized for each target prior to collection (i.e., integration time of sensor was changed based on relative brightness of the target and new dark counts were taken to correct for instrument noise). The sensor zenith angles for the θ_p, θ_{sfc}, and θ_{sky} measurements were 40°, 40° and 40°, respectively. The relative azimuth angle of the sensor to the sun ranged from 90° to 135° depending on visual surface contamination (sea foam, glint, bubble, shadows, etc.).

The post processing of the ASD and Spectral Evolution above-water data collected by the NRL group was performed by NRL using code developed by NRL for the 26 stations collected and $R_{rs}(\lambda)$ was computed using the NRL white plaque using same collection protocols for both instruments to look at inter-sensor differences. The NRL software was modified to process the above water instruments using a baseline-subtraction protocol and the calculation of the surface reflectance correction ρ, based on the solar azimuth and wind speed calculation [Mobley, 2015]. This approach is a substantial improvement over using a constant ρ of 0.021 to minimize the reflected sunlight contribution and inherited from the MatLab software developed at Oregon State University by Ivan Lalovic and Nick Tufillaro to process their respective Spectral Evolution data.

Above Water Processing Protocols

The ASD spectroradiometer measures light at 1.0 nm sampling over the 325 nm to 1075 nm spectral range. The Spectral Evolution PSR-1100-F spectroradiometer measures light at 1.0 nm sampling over the 320 nm to 1100 nm spectral range. Processing follows the equation

$$R_{rs} = (S_{w+s} - S_{sky}\,\rho(\theta))/(\,\pi S_p/refl) \qquad (2)$$

where

- S_{w+s} is the measured signal from the water and includes both L_w and reflected skylight;
- S_{sky} is the measured signal from the sky;
- S_p is the average measured signal from the white Spectralon plaque;
- *refl* is the reflectivity of the plaque (approximately 99% white; actual measured spectral values are used in the calculation); and
- π (p) converts the reflected radiance values to irradiance for these "Lambertian" diffusers.
- The measured sky radiance is multiplied by $\rho(\theta)$ which is the proportionality factor that relates the radiance measured when the detector views the sky to the reflected sky radiance measured when the detector views the sea surface.

The value of $\rho(\theta)$ is dependent on wind speed and direction, detector FOV, and sky radiance distribution. Only in the case of a level sea surface and a uniform sky radiance distribution does $\rho(\theta)$ equal the average of the Fresnel reflectance over the detector FOV. For our measurement angles under nominal sky and wind conditions, we pull $\rho(\theta)$ from the table of Mobley [2015].

The computed R_{rs} is assumed to be "black" at about 750 nm due to water absorption. If not zero, then it is assumed that the S_{sky} was not estimated correctly. Following the "quick and easy" algorithm [Carder and Steward, 1985], it is further assumed that any error in the skylight reflection term is white (not wavelength dependent) and one may simply subtract the computed $R_{rs}(750)$ from the entire spectrum. In practice, this may lead to negative reflectance values R_{rs} near 750 nm. Therefore, the processing subtracts the smallest $R_{rs}(\lambda)$ in the range from 700 nm to 800 nm.

Figure 20 shows results of the comparison between the NRL HyperPro floating instrument with the handheld above-water SEV.

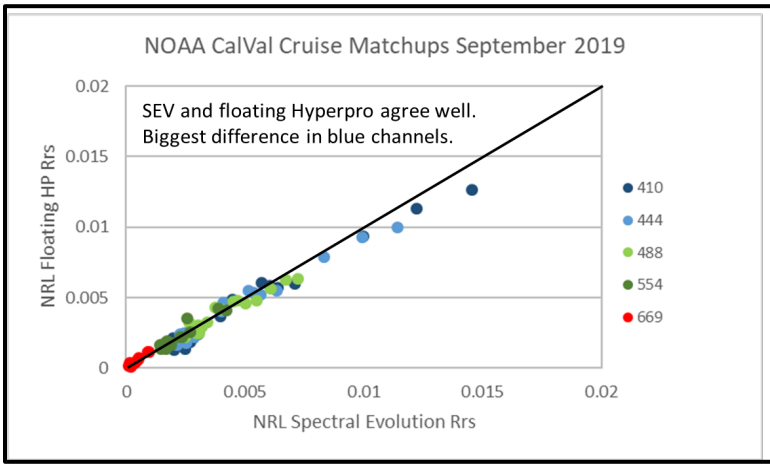

Insitu	Slope	r2	ratio
410	0.90	0.98	1.21
444	0.92	0.98	1.10
488	0.94	0.93	1.05
554	1.01	0.90	1.01
669	1.16	0.95	0.99

Number of valid matchups

NRL	#	SNPP	N20
ASD	13	10	12
SEI	25	20	22
HYP	22	18	20

Figure 20. Comparisons, statistics and number of # valid matchups with NOAA MSL12 VIIRS. The NRL spectral evolution (SEV) above-water and floating HyperPro (HYP) in-water instrument R_{rs} agree well. Note that the biggest differences occur in the blue channels.

Continuous Underway Flow-through Measurements of IOPs

IOP flow-through measurements were collected to address specific objectives as follows but will be used for other analyses as well:

- Characterize the spatial variability of IOPs (a_t, a_g, a_p, b converted to b_b, c) along the cruise track and how the variability impacts the uncertainty of in situ measurements at each station along with sub-pixel variability.
- Evaluate the vertical optical changes within one optical depth (penetration depth of satellite observations) in coastal and offshore waters. The flow-through data at a source depth of 3 m can be different from observed satellite values. Vertical profiles with CTD and IOPs can be used to evaluate the vertical changes and the effect on surface IOP validation.
- Determine the a_t and c properties at specific wavelengths to validate the IOPs derived from the VIIRS ocean color satellites.
- Determine the optical water mass characteristics using spectral scattering and absorption to identify response of ocean color.
- Define coastal/shelf frontal boundaries, ocean processes and water mass types.
- Validate VIIRS SNPP and VIIRS NOAA-20 IOP products.

IOPs were collected continuously using an underway flow-through system on the NOAA Ship *Gordon Gunter* designed and set up by the NRL group including two WetLabs hyperspectral ac-s instruments (one filtered and one non-filtered), WetLabs BB3 backscattering instrument designed with three channels (440 nm, 532 nm, and 650 nm) and a fluorometer connected to the ship's seawater flow-through system where the water intake was located at approximately 3 m below ocean surface. To ensure stability and reliability, both ac-s instruments were placed in controlled temperature water baths to dissipate the instruments' heat and stabilize instrument temperature (Figure 21). A total of 4 ac-s instruments (NRL SN 316, NRL SN024, USF SN 024 and NOAA SN180) were used in the 2 ac-s setup during the cruise due to stability and sensitivity to vibration issues of 2 of the instruments.

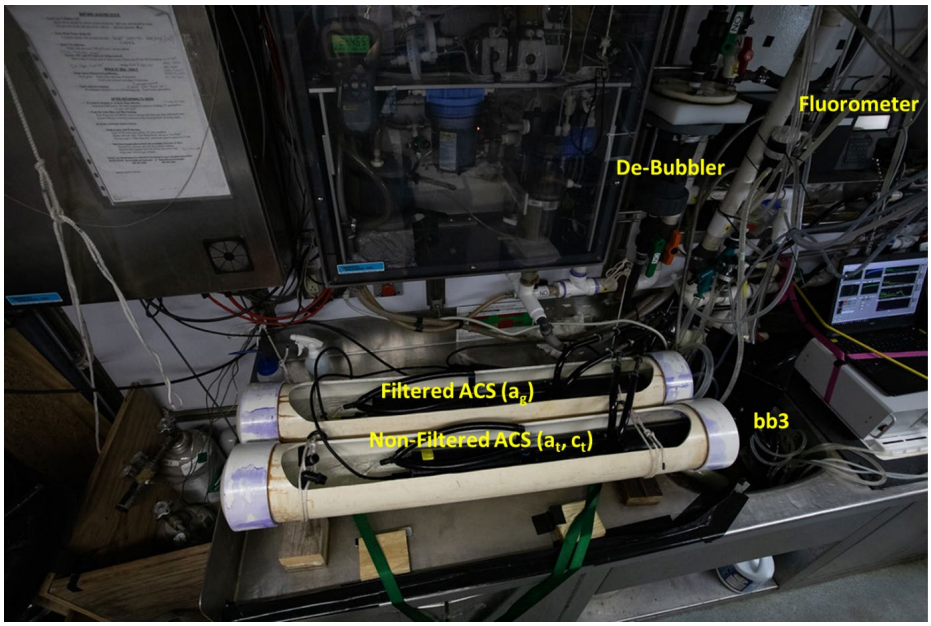

Figure 21. The NRL group's IOP continuous flow-through wet lab setup on the NOAA Ship *Gordon Gunter*, which included two hyperspectral ac-s instruments (one filtered and one non-filtered), BB3 sensor and fluorometer. The two ac-s instruments were placed inside PVC tube water baths to maintain a constant temperature during operation and were calibrated with Nanopure water daily. The BB3 instrument was placed inside a flow cell. Both the PVC tubes and the BB3 flow cells were designed specifically for those instruments.

The two ac-s instruments were interfaced with a WET Labs DH4 data logger with additional inputs from the ship's flow-through system (CTD, Fluorometer and GPS). The ship's flow-through system data stream included position, time, date, heading, water temperature, salinity, and fluorescence (voltage). These inputs are required for the standard processing protocol corrections during the post processing of the ac-s data. The WET Labs DH4 host software was used to combine and store all these data inputs and allowed a display capability in real-time to evaluate the ac-s and BB3 data to ensure the systems were operating correctly and producing reliable and consistent data. The data sample rate of the ac-s meters was 4 Hz. Output data files from the DH4 were saved hourly for the entire cruise.

The two ac-s sensors were cleaned and calibrated daily with new device files during the cruise to correct for sensor drift. Calibration of the ac-s sensors included running Nanopure water through the instruments using a gravity feed. This clean water calibration was done before and after cleaning the absorption and scattering tubes. An update to instrument device files was applied in real-time if it was deemed that new corrections were necessary to assure good quality measurements using a visual display. The BB3 housing was cleaned daily. The BB3 instrument was operated using the WetLabs pre-calibration which did not change during the cruise.

The hyperspectral ac-s instruments (Figure 21) measured $c(\lambda)$, $a(\lambda)$ and $a_g(\lambda)$ from 399 nm to 755 nm at 4.0 nm spacing and the BB3 instrument returns total volume scattering (β), volume scattering of particles (β_p), backscattering of particles (b_{bp}) and b_b at 3 channels (440 nm, 532 nm, and 650nm). Concurrent flow-through measurements of time, latitude, longitude, and temperature, and salinity from a thermo-salinograph (CTD) will be used for correction of the ac-s $a(\lambda)$. Correctly addressing the thermal, salinity and scattering (c-a) corrections that must be applied is important [WETLabs, 2011; Röttgers et al., 2013]. All the flow-through data collected through the DH4 were time merged using WET Labs Archive Processing program (WAP) and hourly output archive files were generated. Hourly WAP archive files

were then combined to create daily files. The daily WAP archive files were binned to 1 minute time bins to reduce the amount of data for spreadsheet import and processing.
The standard order of post processing protocol used (WET Labs 2011).

1. Remove sections of the data collected during the daily ac-s cleaning and pure water calibration.
2. Apply temperature and salinity corrections to ac-s *a* data using the coincident ship thermo-salinograph temperature and salinity data.
3. Temperature correct pure water calibration data for *a* and *c*.
4. Subtract the pure water calibration data from the in situ data.
5. Remove spikes in data due to bubbles, etc., using a σ filter and then interpolate
6. Scatter correct a_t [Röttgers et al., 2013].
7. Add spectral pure water absorption coefficients [Pope and Fry, 1997] to measured $a_{t\text{-}w}$ to yield a_t.
8. Compute spectral scattering $b = c_t - a_t$

Figure 22 shows comparisons of $c(\lambda)$ and $a_t(\lambda)$ measured with the NRL flow-through ac-s system versus those measured by UMB's in-water IOP profiling system.

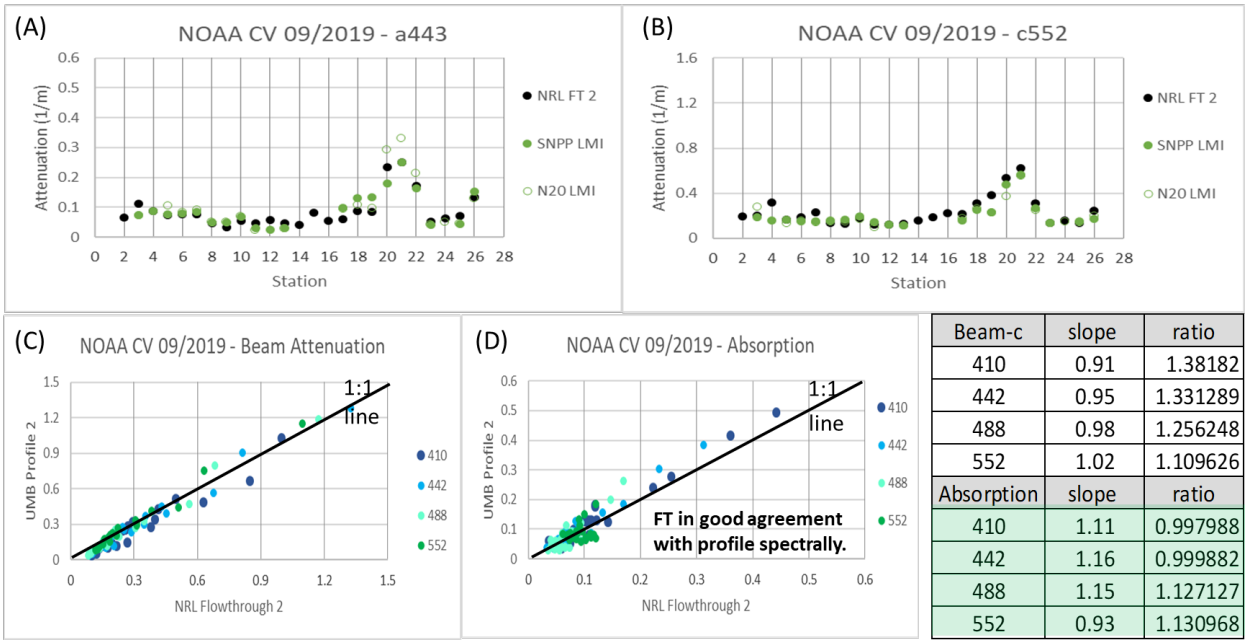

Beam-c	slope	ratio
410	0.91	1.38182
442	0.95	1.331289
488	0.98	1.256248
552	1.02	1.109626
Absorption	slope	ratio
410	1.11	0.997988
442	1.16	0.999882
488	1.15	1.127127
552	0.93	1.130968

Figure 22. (A) Comparison between NRL APS v6.10 processed VIIRS SNPP and VIIRS NOAA-20 (labelled N20) and flow-through a_t at 443 nm at each station from the unfiltered ac-s. (B) Same as (A) but for *c* at 552 nm. (C) Scatter plot of NRL flow-through versus UMB's profile $c(\lambda)$ (wavelength colors in legend) pulled for each station near the depth of the intake (3 m). (D) Same as (C) but for $a_t(\lambda)$. $c(\lambda)$ and $a_t(\lambda)$ are shown in units of m^{-1}. Flow through ac-s is in good agreement with the profile ac-s spectrally. The embedded table shows statistics of slopes and ratios for all station comparisons.

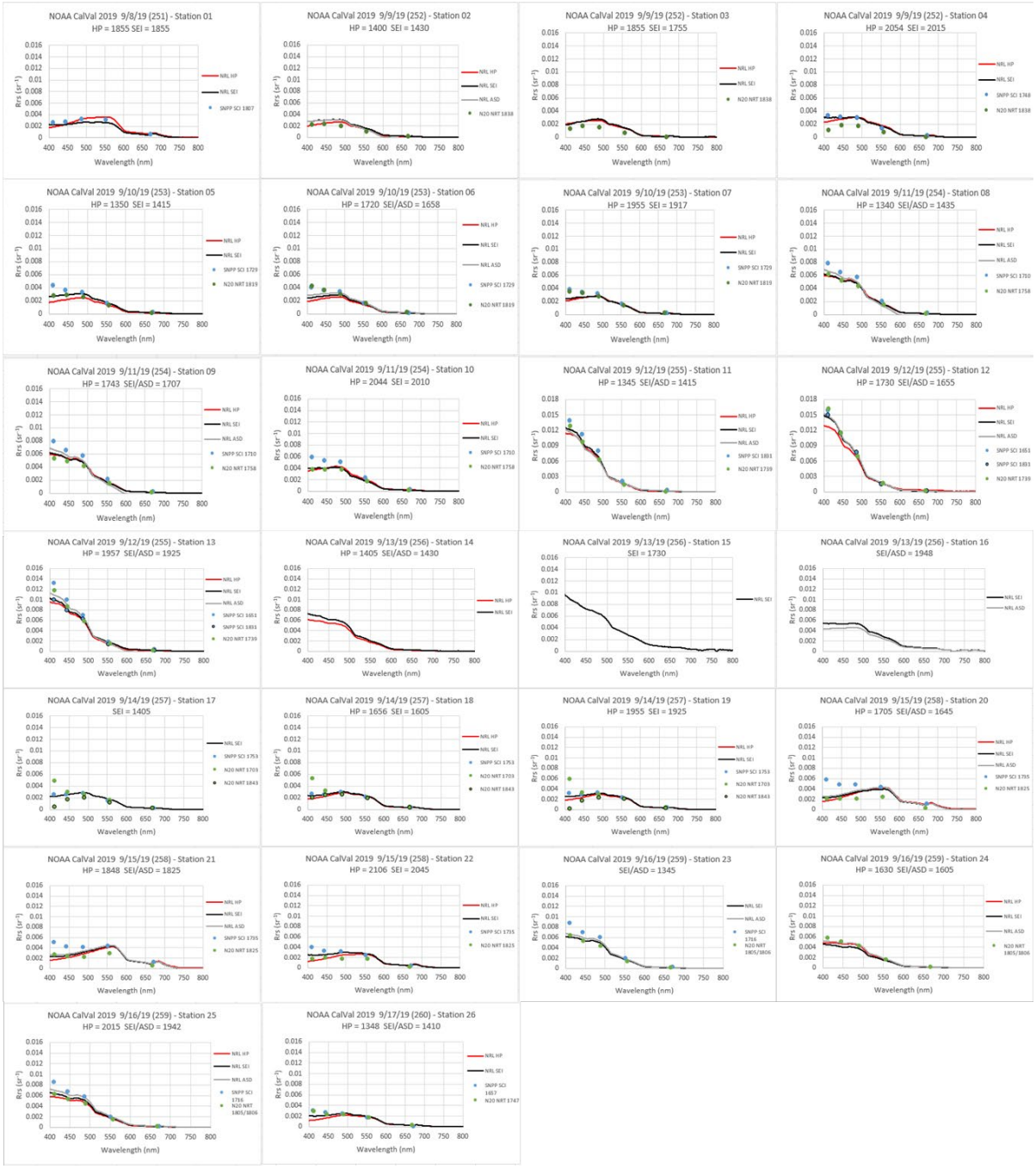

Figure 23. Preliminary matchups between Floating HyperPro, Spectral Evolution and ASD and NOAA MSL12 SNPP (Science Quality processing) and NOAA-20 (near real-time processing): above-water ASD with NRL white plaque (grey line); above-water Spectral Evolution with NRL white plaque (black line); NRL Floating HyperPro (red line); NOAA MSL12 SNPP Science Quality (blue dots); NOAA MSL12 NOAA-20 near real-time (green dots). Horizontal axis is wavelength from 400 nm to 800 nm and vertical axis is R_{rs} in units of sr^{-1}. Note that the extra set of dots with same color with black outline represent a second orbit.

11.7 UMB - Zhongping Lee, Jianwei Wei, Shuai Zhang

In this report, we evaluate the consistency of the L_w measured during this NOAA Cal/Val Cruise with the skylight-blocked approach (SBA) [Lee et al. 2013]. We present the $R_{rs}(\lambda)$ validation results from NOAA SNPP VIIRS and NOAA-20 with collocated in situ measurements from the cruise. And, we describe measurements from our profiling IOP package.

Consistency of water-leaving radiance from SBA and VIIRS validation results R_{rs} products

In situ measurements

Two sets of SBA systems (SBA-UMB and SBA-STAR) were deployed simultaneously at the 26 stations (Figure 24A) sampled during the cruise. Measurements from sixteen of those stations, with favorable sky and sea conditions as demonstrated in Figure 24B were selected for evaluation between the two SBA systems. The median spectra of $L_w(\lambda)$ at each station measured by SBA-UMB are presented in Figure 25 where L_w spectra at UV-visible domain show significant variations, especially for the UV-blue domain (from about 0.0001 μW cm^{-2} sr^{-1} nm^{-1} to 1.5 μW cm^{-2} sr^{-1} nm^{-1}).

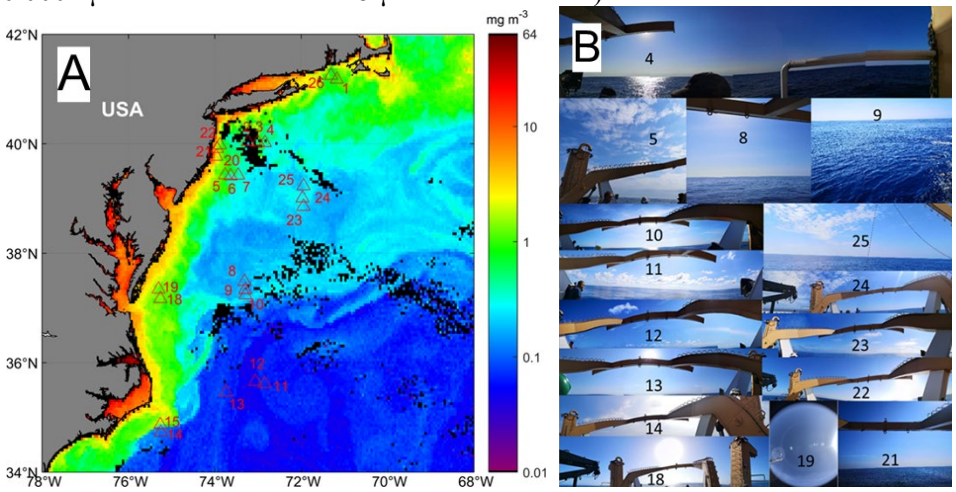

Figure 24. (A) Locations of the 26 sampling stations (red triangle); (B) Photographs of favorable sea and sky conditions at the 16 SBA comparison stations.

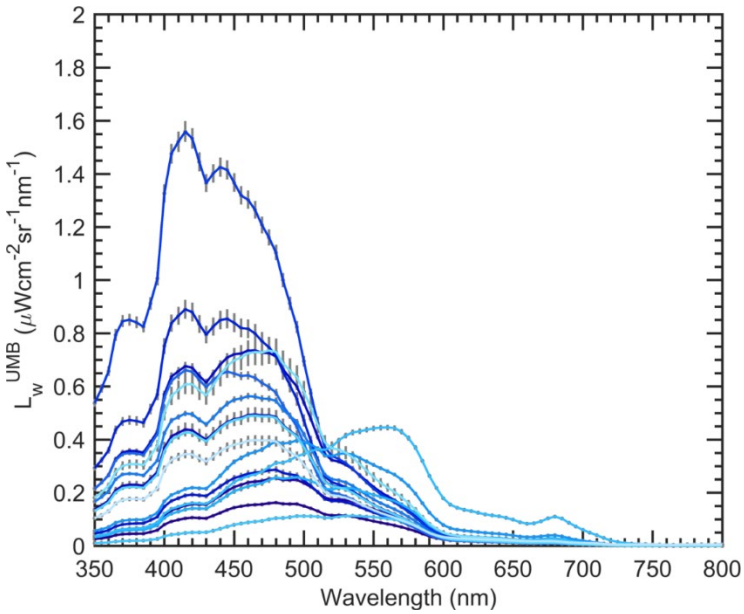

Figure 25. $L_w(\lambda)$ spectra measured by SBA-UMB during the NOAA Cal/Val Cruise.

Results

Comparison of $L_w(\lambda)$ between SBA-STAR and SBA-UMB

$L_w(\lambda)$ were measured directly by blocking off the surface-reflected skylight with the custom-designed cone [Lee et al., 2013]. To quantitatively evaluate the consistency of the $L_w(\lambda)$ measured by two SBA systems, scatter plots between measured $L_w(\lambda)$ by SBA-UMB and SBA-STAR are presented in Figure 26. Statistical parameters are also presented for each subfigure.

As shown in Figure 26, $L_w(\lambda)$ measurements from two SBA systems demonstrate outstanding consistency, especially in the visible domain (Figure 26A). Figure 27 shows the statistic metrics of unbiased percentage difference (UPD), absolute percentage difference (APD), relative percentage difference (RPD), and root-mean-square difference (RMSD) between the two $L_w(\lambda)$, which further confirm the consistency of the $L_w(\lambda)$ measurements in the visible domain (e.g., UPD ~3%). However, the $L_w(\lambda)$ measurements appear to have relatively larger differences (UPD ~26%) in the NIR bands.

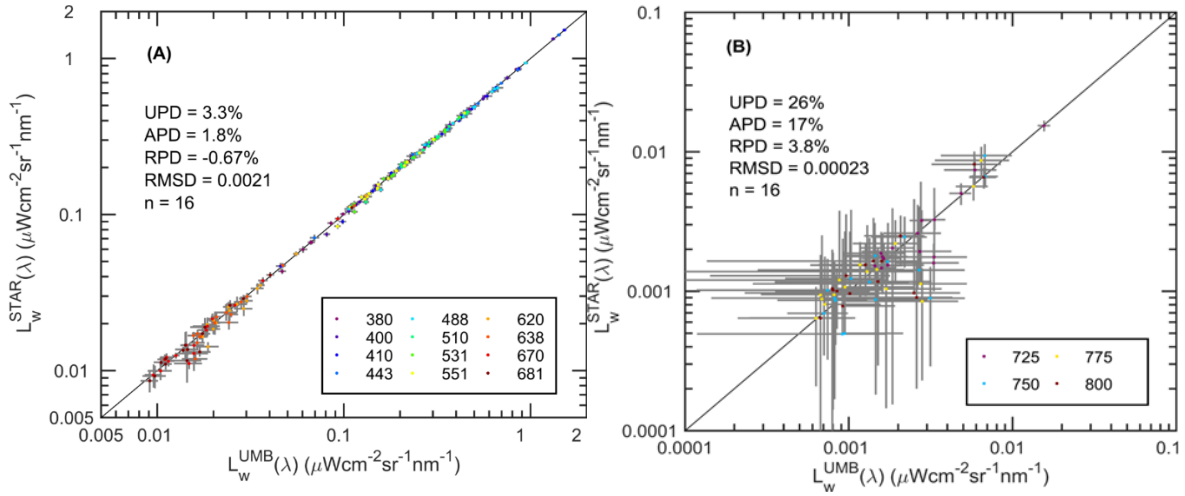

Figure 26. (A) $L_w(\lambda)$ consistency evaluation in the visible bands; (B) $L_w(\lambda)$ consistency evaluation in the NIR bands.

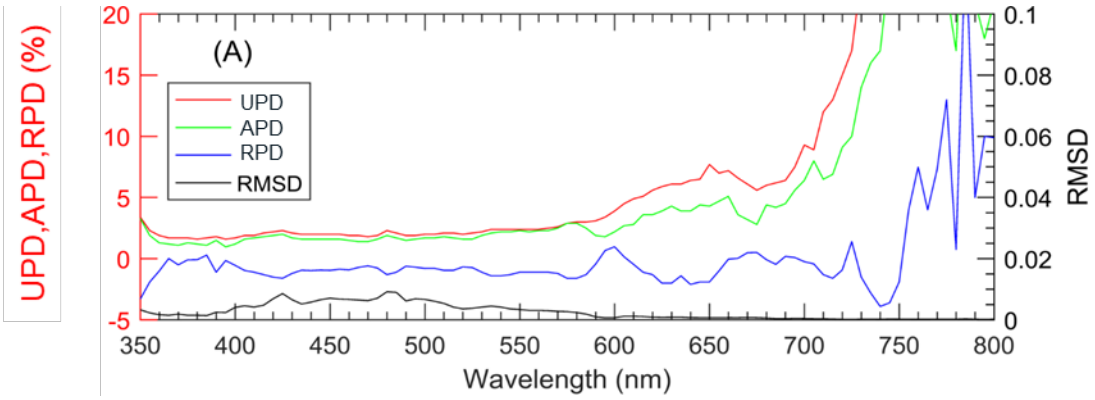

Figure 27. UPD, APD, RPD, and RMSD of the two sets of $L_w(\lambda)$ measurements.

Comparison of $E_s(\lambda)$ between SBA-STAR and SBA-UMB

Consistency of $E_s(\lambda)$ measurements was evaluated using data measured by NRL's radiometer and STAR's radiometer, hereafter referred to as E_s^{umb} and E_s^{star}, respectively. Figure 28 presents the comparison between the two E_s measurements. High consistency of the $E_s(\lambda)$ measurements is observed

(UPD = 7.9%). Furthermore, standard deviations also overlap in Figure 28. Overall, $E_s(\lambda)$ measurements show larger variations in the blue domain compared with the other visible bands with larger standard deviations.

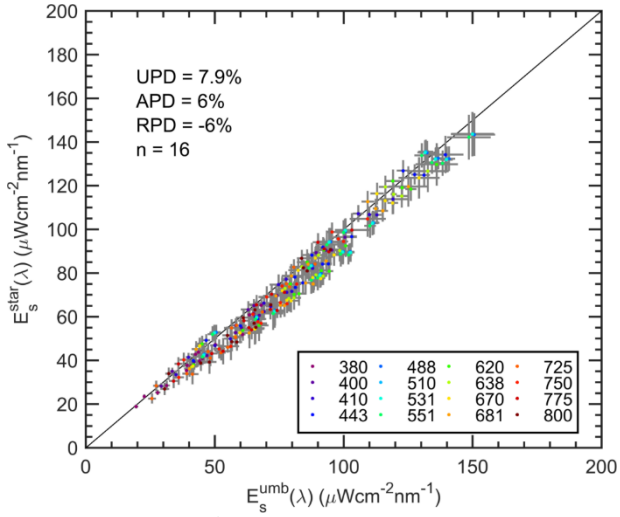

Figure 28. $E_s(\lambda)$ consistency evaluation. E_s^{umb} are measured using NRL's radiometer.

Comparison of $R_{rs}(\lambda)$ between STAR-SBA and UMB-SBA

Consistency evaluation of $R_{rs}(\lambda)$ measurements were conducted using the in situ data collected from sixteen stations with favorable sky and sea conditions. Similar to the $L_w(\lambda)$ measurements, $R_{rs}(\lambda)$ in the visible domain demonstrated higher consistency (UPD = 8.9%) (Figure 29A), in comparison to the NIR domain (UPD = 32%) (Figure 29B). Moreover, the standard deviations of the red bands were larger than other visible bands. Additionally, the statistics between the two sets of $R_{rs}(\lambda)$ measurements in the visible domain are presented in Figure 30, indicating consistency in the $R_{rs}(\lambda)$ measurements.

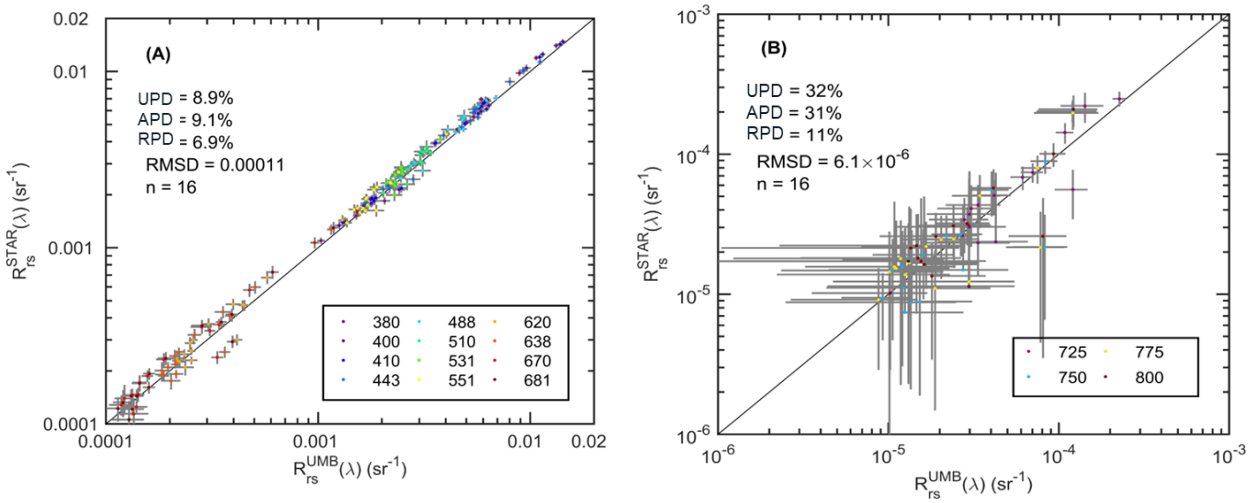

Figure 29. (A) $R_{rs}(\lambda)$ consistency evaluation in visible bands; (B) $R_{rs}(\lambda)$ consistency evaluation in NIR bands.

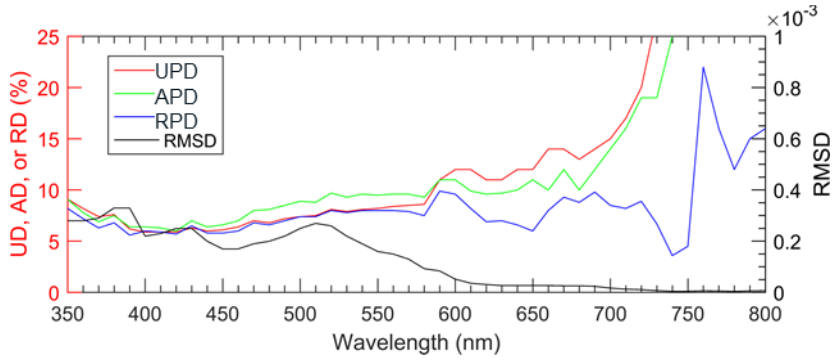

Figure 30. UPD, APD, RPD, and RMSD of the two sets of $R_{rs}(\lambda)$ measurements using SBA.

Validation of SNPP VIIRS and NOAA20 $R_{rs}(\lambda)$ products

To validate the $R_{rs}(\lambda)$ products, Level 2 products of VIIRS SNPP and VIIRS NOAA-20 were acquired from NOAA CoastWatch. Data acquired from VIIRS SNPP and VIIRS NOAA-20 were atmospherically corrected using the NOAA Multi-Sensor Level-1 to Level-2 (MSL12) data processing system. In this report, the combined NIR and shortwave infrared (SWIR) atmospheric correction algorithm (NIR-SWIR) was applied [Wang, 2007; Wang and Shi, 2007].

Satellite match-ups centered at the in situ sampling sites were acquired over a 3 pixel by 3 pixel window. For the VIIRS SNPP match-ups, pixels flagged as 'LAND', 'HIGLINT', 'HILT', 'HISATZEN', 'HIPOL', 'STRAYLIGHT', 'LOWLW', and 'CLDICE' were considered as invalid. In total, 11 pairs of VIIRS SNPP match-ups and 9 pairs of VIIRS NOAA-20 match-ups were obtained. Validation of the VIIRS SNPP and VIIRS NOAA-20 $R_{rs}(\lambda)$ products are presented in Figure 31. Statistical validation parameters results are presented in Table 10 and Table 11.

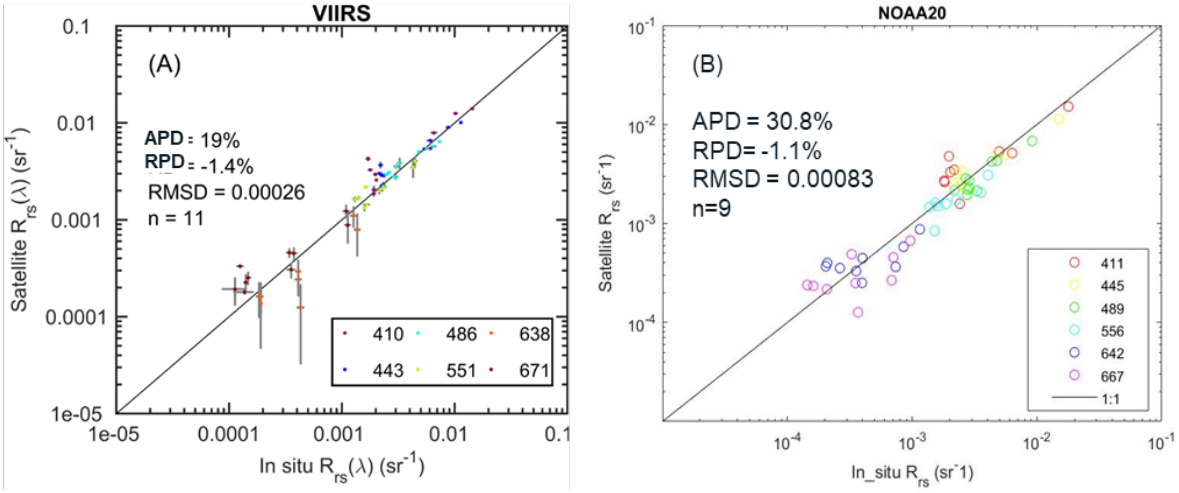

Figure 31. Validation of (left) VIIRS SNPP and (right) VIIRS NOAA-20 $R_{rs}(\lambda)$ product.

Table 10. Statistical parameters for the validation results for VIIRS SNPP.

VIIRS SNPP (N=11)	410	443	486	551	638	671	410/443	443/551
APD (%)	21	13	7.9	8.8	39	36	11	13
RPD (%)	19	9.2	4.6	-3.9	-39	36	9.2	8
RMSD	0.001	0.0006	0.0004	0.0002	0.0001	0.0001	0.12	0.22

Table 11. Statistical parameters for the validation results for VIIRS NOAA-20.

VIIRS NOAA-20 (N=9)	411	445	489	556	642	667	411/445	445/556
APD (%)	48	16	17	19	41	43	30	35
RPD (%)	-33	-5	16	16	-8	6	-24	-29
RMSD	0.0016	0.0013	0.001	0.0007	0.0002	0.0002	0.3289	0.5763

As shown in Figure 31, R_{rs} of the match-ups from VIIRS SNPP and VIIRS NOAA-20 matched well with the field-measured R_{rs} in the visible domain. The APD of satellite-derived R_{rs} in the visible bands are 19% and 30.8% for VIIRS SNPP and VIIRS NOAA-20, respectively, indicating promising results for the Level 2 products from these two sensors. As shown in Table 10 and Table 11, APD of VIIRS SNPP in the listed bands are lower than their VIIRS NOAA-20 counterparts, indicating the better performance of VIIRS SNPP R_{rs} product regarding APD. R_{rs} of VIIRS NOAA-20 has generally larger uncertainties compared with VIIRS SNPP when validated with field measured R_{rs}.

Summary of $L_w(\lambda)$, $E_s(\lambda)$, and $R_{rs}(\lambda)$

Validation results show excellent consistency of $L_w(\lambda)$, $E_s(\lambda)$, and $R_{rs}(\lambda)$ data between the two SBA systems in terms of the UPD of 3.3%, 7.9% and 8.9% respectively. Among the three measurements, $L_w(\lambda)$ measurements showed extremely high consistency. Also, R_{rs} products from VIIRS SNPP and VIIRS NOAA-20 were overall consistent with field-measured R_{rs} (SBA-UMB). However, VIIRS SNPP R_{rs} product performed relatively better in terms of APD.

In situ profiles of the IOP package

The IOP package, including WetLabs ac-s, bb9, and CTD were deployed at 23 stations during the cruise (Figure 32). The maximum deployment depth varied from 12 m to 60 m below the surface. The package was powered by battery packs and the data were recorded by a WetLabs DH4 logger.

The ac-s sensor was calibrated before and during the cruise with Milli-Q water produced on board. The hyperspectral ac-s measured $a_t(\lambda)$ and $c(\lambda)$ (from 402 nm to 732 nm). The WetLabs bb9 measured b_b and b_{bp} at seven wavelengths (412 nm, 440 nm, 488 nm, 530 nm, 595 nm, 695 nm, and 715 nm). Two other channels were for CDOM and chlorophyll fluorescence. The CTD contributed temperature and salinity data (used for the correction of the ac-s), and time, depth, latitude, and longitude for further data processing.

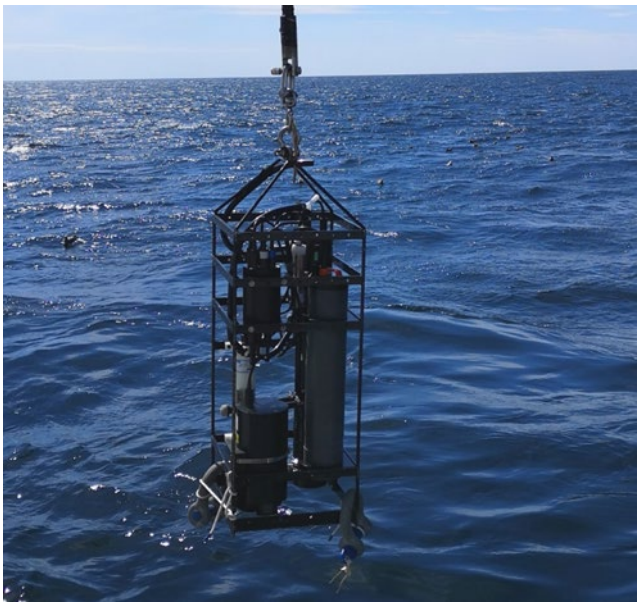

Figure 32. UMB profiling IOP package.

11.8 HBOI - Michael Twardowski* and Nicole Stockley, Christopher Strait

In situ profiles of inherent optical properties

HBOI previously participated in the 2016 cruise [Ondrusek et al., 2017] and again deployed a substantially similar instrument package (Figure 33) to measure profiles of IOPs at each station. As in 2016, the package consisted of instruments to measure absorption, scattering, and attenuation. Measurements of a_t were made with both a WET Labs ac-9 (9 wavelengths) and an ac-s (87 wavelengths). Measurements of total attenuation were made with the ac-s, while the ac-9 had a 0.2 um capsule filtered installed to measure dissolved attenuation. As in 2016, measurements of VSF were made with the MASCOT sensor (WET Labs), including cross- and co-polarization, and several sensors measured $b_b(\lambda)$. The same fluorometer measuring CDOM and chlorophyll fluorescence was also included. The package was again powered by battery packs with power distribution and data recording managed by 2 WET Labs DH-4s. The ac-s and ac-9 units were calibrated at HBOI before and after the cruise as well as onboard the ship during the cruise. The scattering sensors were calibrated at HBOI in August 2019.

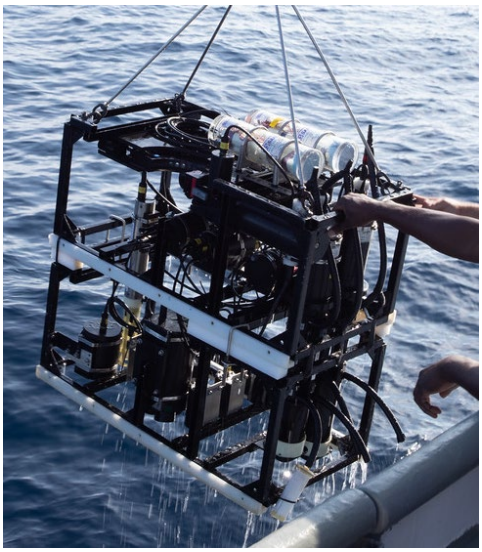

Figure 33. HBOI profiling IOP package.

In situ measurement of scalar irradiance

HBOI deployed a TriOS RAMSES radiometer (Rastede, Germany) to measure scalar irradiance just below the surface of the water. The RAMSES was held in the center of a floating frame (made from polyvinyl chloride tubing) with the height adjusted to keep the sensor head as close to the air-sea interface without breaking the surface (Figure 34). This was deployed from the stern of the ship with the other in-water floating radiometers. The sensor was calibrated by the manufacturer in 2018 and data were recorded directly onto a computer.

Figure 34. The RAMSES was held in the center of a floating frame with the height adjusted to keep the sensor head as close to the air-sea interface without breaking the surface.

Using water collected by the CTD rosette, HBOI used a Point Source Integrated Cavity Absorption Meter (PSICAM), Liquid Waveguide Capillary Cell (LWCC) and filtering for a_p (Figure 35). All measurements were made following the updated Ocean Optics Protocols for absorption [IOCCG, 2018], all sample processing was conducted within 5 hours of collection. PSICAM samples were measured on the boat, a_{pg} and a_g were measured separately. The filtrate from the PSICAM a_g measurement was then measured in the LWCC. The PSICAM was calibrated twice a day for the duration of the cruise. Filtered a_p samples were flash frozen and stored in liquid nitrogen. These will be measured in a Quantitative Filter Technique Integrated Cavity Absorption Meter (QFT-ICAM) and a benchtop spectrophotometer.

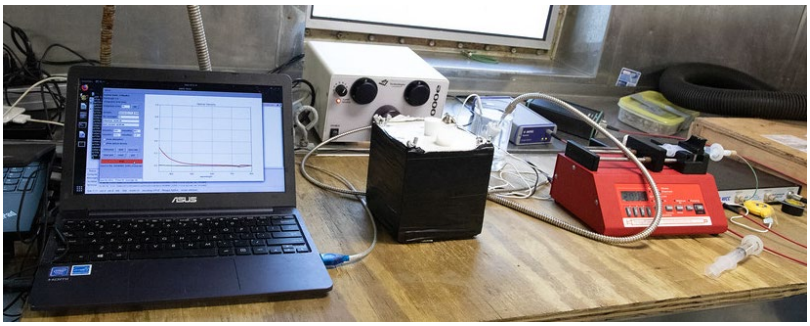

Figure 35. Benchtop arrangement for the PSICAM and LWCC.

All data collected by HBOI is currently being processed for distribution to the VIIRS Cal/Val team.

12 Summary

The fifth dedicated VIIRS Cal/Val cruise took place 8 September to 17 September 2019 aboard the NOAA Ship *Gordon Gunter* in the Atlantic coastal waters of the US East Coast. In situ AOP radiometry and IOP optical measurements were made with multiple instruments deployed in several modes (e.g., in-water profiling, above water, flow-through, etc.) and water samples were collected for later processing to provide measurements of additional ocean properties. Uncertainties in the in situ and satellite validation measurements will be estimated by utilizing pre- and post-cruise calibrations of instruments, simultaneous measurements of parameters utilizing multiple techniques and instruments and evaluation of data processing techniques. Clear weather immediately following the passage of Hurricane Dorian and strategic station planning resulted in a record number of satellite matchups (24 for VIIRS SNPP and 23 for NOAA-20) at the 26 stations occupied.

13 Cruise Data Access

All data collected on this cruise will be formally archived with NOAA/NCEI according to their guidelines and will also be publicly accessible through NOAA CoastWatch/OceanWatch. Data users are strongly urged to communicate with cruise investigators for appropriate collaborations and citations. Some data from this cruise have been or will be submitted to the NASA SeaBASS archive.

14 Acknowledgments

Funding for this project was provided as follows: JPSS VIIRS Ocean Color Cal/Val funding supported most of the science groups' participation; NOAA/NESDIS/STAR Product Development, Readiness and Application (PDR&A)/Ocean Remote Sensing (ORS) program provided additional support to assist in LDEO participation. Groups external to the JPSS VIIRS Ocean Color Cal/Val team also provided their own support. NOAA/OMAO awarded ship time and crew support and we thank the crew of the NOAA Ship *Gordon Gunter* for their support in making data collection possible. NASA/GSFC will perform laboratory analyses on discrete water samples for some parameters. Carol Johnson of National Institute of Standards and Technology provided the primary source used in the HyperPro radiance calibrations at the NOAA optical laboratory.

The scientific results and conclusions, as well as any views or opinions expressed herein, are those of the author(s) and do not necessarily reflect those of NOAA or the Department of Commerce.

15 References Cited

Arnone, R., M. Fargion, P. Martinolich, S. Ladner and e. al. (2012), Validation of the VIIRS Ocean color, *Proc. SPIE 8372*, *Ocean Sensing and Monitoring IV, 83720G*, doi: http://dx.doi.org/10.1117/12.922949.

Arnone, R., R.A. Vandermeulen, S. Ladner, J. Bowers, P. Martinolich, M. Fargion and M. Ondrusek (2014), Sensitivity of calibration "gains" to ocean color processing in coastal and open waters using ensembles members for NPP- VIIRS, *Proc. SPIE 9111*, *Ocean Sensing and Monitoring VI, 911105.* , doi: http://dx.doi.org/10.1117/12.2053409.

Brown, S., S. Flora, M. Feinholz, M. Yarbrough, T. Houlihan, D. Peters, Y.S. Kim, J. Mueller, B.C. Johnson and D. Clark (2007), *The marine optical buoy (MOBY) radiometric calibration and uncertainty budget for ocean color satellite sensor vicarious calibration*, SPIE, https://doi.org/10.1117/12.737400.

Carder, K.L. and R.G. Steward (1985), A remote-sensing reflectance model of a red-tide dinoflagellate off west Florida, *Limnology and Oceanography*, *30*(2), 286-298.

Carrizo, C., A. Gilerson, R. Foster, A. Golovin and A. El-Habashi (2019), Characterization of radiance from the ocean surface by hyperspectral imaging, *Optics Express*, *27*(2), 1750-1768, doi: 10.1364/OE.27.001750.

Chekalyuk, A. and M.A. Hafez (2008), Advanced laser fluorometry of natural aquatic environments, *Limnology and oceanography, methods*, *6*, 591.

Chekalyuk, A.M., M.R. Landry, R. Goericke, A.G. Taylor and M.A. Hafez (2012), Laser fluorescence analysis of phytoplankton across a frontal zone in the California Current ecosystem, *J. Plankton Res.*, *34*(9), 761-777, doi: 10.1093/plankt/fbs034.

Clark, D.K., H.R. Gordon, K.J. Voss, Y. Ge, W. Broenkow and C. Trees (1997), Validation of atmospheric correction over the oceans, *J. Geophys. Res.-Atmos.*, *102*(D14), 17209-17217, doi: 10.1029/96jd03345.

Clark, D.K., M.A. Yarbrough, M.E. Feinholz, S. Flora, W. Broenkow, Y.S. Kim, B.C. Johnson, M. Yuen and J.L. Mueller (2002), MOBY, a radiometric buoy for performance monitoring and vicarious calibration of satellite ocean color sensors: Measurement and data analysis protocols, in *Ocean Optics Protocols for Satellite Ocean Color Sensor Validation, Revision 3, Volume 2.*, Edited by Mueller, J.L. and Fargion, G.S., NASA/TM--2002-21004:138-170 (2002), p.^pp., NASA Goddard Space Flight Center, Greenbelt, Maryland.

Cox, C. and W. Munk (1954), Measurement of the Roughness of the Sea Surface from Photographs of the Sun's Glitter, *J. Opt. Soc. Am.*, *44*(11), 838-850, doi: 10.1364/JOSA.44.000838.

EPA (1971), Methods for chemical analysis of water and wastes, EPA-NERL: 160.2, US Environmental Protection Agency.

Gilerson, A., C. Carrizo, R. Foster and T. Harmel (2018), Variability of the reflectance coefficient of skylight from the ocean surface and its implications to ocean color, *Optics Express*, *26*(8), 9615-9633, doi: 10.1364/OE.26.009615.

Gilerson, A., C. Carrizo, M. Malinowski, P. Groetsch, R. Foster and E. Herrera Estrella (2019), *Multi- and hyperspectral polarimetric imaging of the ocean surface*, SPIE, https://doi.org/10.1117/12.2534055.

Gilerson, A., C. Carrizo, A. Ibrahim, R. Foster, T. Harmel, A. El-Habashi, Z. Lee, X. Yu, S. Ladner and M. Ondrusek (2020), Hyperspectral polarimetric imaging of the water surface and retrieval of water optical parameters from multi-angular polarimetric data, *Appl. Optics*, *59*(10), C8-C20, doi: 10.1364/AO.59.0000C8.

Goes, J.I., H.d.R. Gomes, E.M. Haugen, K.T. McKee, E.J. D'Sa, A.M. Chekalyuk, D.K. Stoecker, P.J. Stabeno, S.-I. Saitoh and R.N. Sambrotto (2014), Fluorescence, pigment and microscopic characterization of Bering Sea phytoplankton community structure and photosynthetic competency in the presence of a Cold Pool during summer, *Deep Sea Research Part II: Topical Studies in Oceanography*, *109*(0), 84-99, doi: 10.1016/j.dsr2.2013.12.004.

Gorbunov, M.Y. and P.G. Falkowski (2004), Fluorescence induction and relaxation (FIRe) technique and instrumentation for monitoring photosynthetic processes and primary production in aquatic ecosystems, (ed.), *Proceedings of Photosynthesis: Fundamental Aspects to Global Perspectives"-Proc. 13th International Congress of Photosynthesis, Montreal, Aug*.

Gordon, H.R. (2010), Some reflections on thirty-five years of ocean-color remote sensing, in *Oceanography from Space: Revisited*, Edited by Barale, V., Gower, J.F.R. and Alberotanza, L., 289-305, Springer Netherlands.

Gordon, H.R., D.K. Clark, J.L. Mueller and W.A. Hovis (1980), Phytoplankton Pigments from the Nimbus-7 Coastal Zone Color Scanner: Comparisons with Surface Measurements, *Science*, *210*(4465), 63-66, doi: 10.2307/1684604.

Gould, R.W., R.A. Arnone and M. Sydor (2001), Absorption, scattering; and remote-sensing reflectance relationships in coastal waters: Testing a new inversion algorithm, *J. Coast. Res.*, *17*(2), 328-341.

Groetsch, P.M.M., P. Gege, S.G.H. Simis, M.A. Eleveld and S.W.M. Peters (2017), - Validation of a spectral correction procedure for sun and sky reflections in above-water reflectance measurements, - *25*(- 16), - A761, - http://www.opticsexpress.org/abstract.cfm?URI=oe-25-16-A742.

GUM (1995), Evaluation of measurement data - Guide to the expression of uncertainty in measurement (ed.), http://www.bipm.org/en/publications/guides/gum.html. http://www.bipm.org/en/publications/guides/gum.html.

Holm-Hansen, O. and B. Riemann (1978), Chlorophyll a determination: improvements in methodology, *Oikos*, *30*, 438-447.

Hovis, W.A., D.K. Clark, F. Anderson, R.W. Austin, W.H. Wilson, E.T. Baker, D. Ball, H.R. Gordon, J.L. Mueller, S.Z. El-Sayed, B. Sturm, R.C. Wrigley and C.S. Yentsch (1980), Nimbus-7 Coastal Zone Color Scanner: System Description and Initial Imagery, *Science*, *210*(4465), 60-63, doi: 10.2307/1684603.

Hunter, C. (2006), Particulate organic carbon, nitrogen and total suspended matter. Methodologies, protocols and analyses used in the development of ocean color product algorithms., Technical Publication 06–1 (ed.), Moss Landing Marine Laboratories.

IOCCG (2018), Protocols for Satellite Ocean Color Data Validation: In situ Optical Radiometry. (ed.), *IOCCG Protocol Series,* No. in preparation, International Ocean Colour Coordinating Group, Dartmouth, NS, Canada.

Jenkins, C., J. Goes, K. McKee, H.d.R. Gomes, R. Arnone, M. Wang, M. Ondrusek, P. Nagamani, T. Preethi Latha, K. Rao and V. Dadhwal (2016), *High-resolution shipboard measurements of phytoplankton: a way forward for enhancing the utility of satellite SST and chlorophyll for mapping microscale features and frontal zones in coastal waters*, SPIE, https://doi.org/10.1117/12.2225875.

Johnson, B.C., J. Rice, H. Yoon and A. Parr (2014), Principles of optical radiometry, in *Optical radiometry for ocean climate measurements*, edited by Zibordi, G., Donlon, C. and Parr, A., pp. 13-67, Academic Press, Waltham, MA.

Kishino, M., M. Takahashi, N. Okami and S. Ichimura (1985), Estimation of the spectral absorption coefficients of phytoplankton in the sea, *Bulletin of Marine Science*, *37*(2), 634-642.

Lee, Z.P., N. Pahlevan, Y.-H. Ahn, S. Greb and D. O'Donnell (2013), Robust approach to directly measuring water-leaving radiance in the field, *Appl. Optics*, *52*(8), 1693-1701.

Lee, Z.P., K.L. Carder, R.G. Steward, T.G. Peacock, C.O. Davis and J.L. Mueller (1997), *Remote-sensing reflectance and inherent optical properties of oceanic waters derived from above-water measurements*, 160-166 pp., Spie - Int Soc Optical Engineering, Bellingham, doi: 10.1117/12.266436.

Mikelsons, K. and M. Wang (2019), Optimal satellite orbit configuration for global ocean color product coverage, *Opt. Express*, *in press.*

Mobley, C.D. (1999), Estimation of the remote-sensing reflectance from above-surface measurements, *Appl. Optics*, *38*(36), 7442-7455, doi: 10.1364/ao.38.007442.

Mobley, C.D. (2015), Polarized reflectance and transmittance properties of windblown sea surfaces, *Appl. Optics*, *54*(15), 4828-4849, doi: 10.1364/ao.54.004828.

Morrow, J.H., C.R. Booth, R.N. Lind and S.B. Hooker (2010), The Compact Optical Profiling System (C-OPS), Advances in Measuring the Apparent Optical Properties (AOPs) of Optically Complex Waters, NASA Tech. Memo. 2010–215856, Morrow, J.H., Hooker, S.B., Booth, C.R., Bernhard, G., Lind, R.N. and J.W., B. (ed.) 42–50 pp, NASA Goddard Space Flight Center, Greenbelt, Maryland.

Mueller, J.L., C.O. Davis, R. Arnone, R. Frouin, K. Carder, Z.P. Lee, R.G. Steward, S.B. Hooker, C.D. Mobley and S. McLean (2003a), Above-water radiance and remote sensing reflectance measurement and analysis protocols, in *Ocean Optics Protocols For Satellite Ocean Color Sensor Validation, Revison 4, Volume III: Radiometric Measurements and Data Analysis Protocols*, Edited by Mueller, J.L., Fargion, G.S. and Mcclain, C., NASA/TM-2003-21621/Rev4-Vol III, p.^pp. 21 - 31, Goddard Space Flight Center, National Aeronautics and Space Administration, Greenbelt, Maryland.

Mueller, J.L., A. Morel, R. Frouin, C. Davis, R. Arnone, K. Carder, Z.P. Lee, R.G. Steward, S. Hooker, C.D. Mobley, S. McLean, B. Holben, M. Miller, C. Pietras, K.D. Knobelspiesse, G.S. Fargion, J. Porter and K. Voss (2003b), *NASA Tech. Memo. 2003-21621/Rev-Vol III*, Ocean optics protocols for satellite ocean color sensor validation, revision 4, Ocean optics protocols for satellite ocean

color sensor validation, Mueller, J.L., Fargion, G.S. and Mcclain, C.R. (ed.), NASA Goddard Space Flight Center, Greenbelt, Maryland.
Ondrusek, M., E. Stengel, C.S. Kinkade, R.L. Vogel, P. Keegstra, C. Hunter and C. Kim (2012), The development of a new optical total suspended matter algorithm for the Chesapeake Bay, *Remote Sensing of Environment*, *119*, 243-254, doi: 10.1016/j.rse.2011.12.018.
Ondrusek, M., V.P. Lance, M. Wang, E. Stengel, C. Kovach, R.A. Arnone, S. Ladner, W. Goode, A. Gilerson, A. El-Habashi, et al. (2019), Report for Dedicated JPSS VIIRS Ocean Color Calibration/Validation Cruise May 2018, United States. National Environmental Satellite, D. and Information, S. (ed.), Washington, D.C., https://repository.library.noaa.gov/view/noaa/20267. doi: https://doi.org/10.25923/scyb-qf42.
Ondrusek, M., E. Stengel, V.P. Lance, M. Wang, K. Voss, G. Zibordi, M. Talone, Z. Lee, J. Wei, J. Lin, et al. (2015), Report for Dedicated JPSS VIIRS Ocean Color Calibration/Validation Cruise, NOAA/NESDIS Technical Report #146, Lance, V.P. (ed.) 60 pp, National Oceanic and Atmospheric Administration, US Department of Commerce, Washington, DC. doi: 10.7289/V52B8W0Z.
Ondrusek, M., V.P. Lance, M. Wang, E. Stengel, C. Kovach, R. Arnone, S. Ladner, W. Goode, A. Gilerson, S. Ahmed, et al. (2017), Report for Dedicated JPSS VIIRS Ocean Color Calibration/Validation Cruise October 2016 NOAA/NESDIS Technical Report #151, Lance, V.P. (ed.) 75 pp, National Oceanic and Atmospheric Administration, US Department of Commerce, Washington, DC. doi: doi:10.7289/V5/TR-NESDIS-151.
Ondrusek, M., V.P. Lance, E. Stengel, M. Wang, R. Arnone, S. Ladner, W. Goode, R. Vandermeulen, S. Freeman, C.J. E., et al. (2016), Report for Dedicated JPSS VIIRS Ocean Color Calibration/Validation Cruise December 2015 NOAA/NESDIS Technical Report #148, Lance, V.P. (ed.) 66 pp, National Oceanic and Atmospheric Administration, US Department of Commerce, Washington, DC. doi: doi:10.7289/V5/TR-NESDIS-148.
Pope, R.M. and E.S. Fry (1997), Absorption spectrum (380-700 nm) of pure water .2. Integrating cavity measurements, *Appl. Optics*, *36*(33), 8710-8723, doi: 10.1364/ao.36.008710.
Röttgers, R., D. McKee and S.B. Woźniak (2013), Evaluation of scatter corrections for ac-9 absorption measurements in coastal waters, *Methods in Oceanography*, *7*, 21-39, doi: http://dx.doi.org/10.1016/j.mio.2013.11.001.
Satlantic (2003), Operation Manual for Profiler II (ed.), Satlantic Incorporated, Halifax, Nova Scotia.
Satlantic (2004), SatView Data Logging / Display Program Users Guide; Version 2.8 (ed.), Satlantic Incorporated, Halifax, Nova Scotia.
Satlantic (2012), Operation Manual for Profiler II (ed.), Satlantic Incorporated, Halifax, Nova Scotia.
Sun, J., M. Wang, L. Jiang and X. Xiong (2019), - NOAA-20 VIIRS polarization effect and its correction, - *58*(- 24), - 6665, - http://ao.osa.org/abstract.cfm?URI=ao-58-24-6655.
Van Heukelem, L. and C.S. Thomas (2001), Computer-assisted high-performance liquid chromatography method development with applications to the isolation and analysis of phytoplankton pigments, *Journal of Chromatography A*, *910*(1), 31-49, doi: 10.1016/s0378-4347(00)00603-4.
Voss, K.J. and G. Zibordi (1989), Radiometric and geometric calibration of a spectral electro-optic "fisheye" camera radiance distribution system, *J. Atmosph. and Ocean. Techn.*, *6*, 652-662.
Voss, K.J. and A.L. Chapin (2005), Upwelling radiance distribution camera system, NURADS, *Optics Express*, *13*(11), 4250-4262, doi: 10.1364/opex.13.004250.
Wang, M. (2007), Remote sensing of the ocean contributions from ultraviolet to near-infrared using the shortwave infrared bands: Simulations, *Appl. Optics*, *46*(9), 1535-1547, doi: 10.1364/AO.46.001535.
Wang, M. and W. Shi (2007), The NIR-SWIR combined atmospheric correction approach for MODIS ocean color data processing, *Optics Express*, *15*(24), 15722-15722, doi: 10.1364/oe.15.015722.
Wang, M., S. Son and W. Shi (2009), Evaluation of MODIS SWIR and NIR-SWIR atmospheric correction algorithms using SeaBASS data, *Remote Sensing of Environment*, *113*(3), 635-644, doi: 10.1016/j.rse.2008.11.005.

Wang, M., X. Liu, L. Jiang and S. Son (2017), The VIIRS Ocean Color Product Algorithm Theoretical Basis Document, National Oceanic and Atmospheric Administration, National Environmental Satellite and Data Information Service, 68 pp., doi: TBD.

Wang, M., X. Liu, L. Tan, L. Jiang, S. Son, W. Shi, K. Rausch and K. Voss (2013), Impact of VIIRS SDR performance on ocean color products, *J. Geophys. Res. Atmos.*, *118*, 10347–10360, doi: doi:10.1002/jgrd.50793.

Wang, M., X. Liu, L. Jiang, S. Son, J. Sun, W. Shi, L. Tan, P. Naik, K. Mikelsons, X. Wang and V. Lance (2014), Evaluation of VIIRS Ocean Color Products, *Proc. SPIE 9261*, *92610E*, doi: 10.1117/12.2069251.

Welschmeyer, N.A. (1994), Fluorometric analysis of chlorophyll-*a* in the presence of chlorophyll-*b* and pheopigments, *Limnol. Oceanogr.*, *39*(8), 1985-1992, <Go to ISI>://A1994QG41300020.

WETLabs (2011), ac meter protocol document, ac meter protocol (acprot); Revision Q 20 April 2011 (ed.).

Zappa, C.J., M.L. Banner, H. Schultz, A. Corrada-Emmanuel, L.B. Wolff and J. Yalcin (2008), Retrieval of short ocean wave slope using polarimetric imaging, *Measurement Science and Technology*, *19*(5), 055503, doi: 10.1088/0957-0233/19/5/055503.

Appendix

Table A-1. Notations, descriptions and units if applicable.

Abbreviation	Description	Typical Units (if applicable)
		m^{-1}
a_d	Absorption coefficient of detrital matter	m^{-1}
a_{nw}	Non-water absorption coefficient	m^{-1}
AOP	Apparent optical property	
APD	Absolute percent difference	
a_{ph}	Phytoplankton pigment absorption coefficient	m^{-1}
		m^2 mg^{-1}
a_t	Total absorption (all components: water; particles (including particulate detritus and phytoplankton); and gelbstoff or CDOM	m^{-1}
b_b	Backscattering (scattering in the backwards direction) coefficient	m^{-1}
BRDF	Bi-directional reflectance distribution function	
		m^{-1}
Cal/Val	Calibration and Validation	
CDOM	Chromophoric dissolved organic material	ppb
Chl-*a*	Chlorophyll *a* concentration	mg m^{-3}
		m^{-1}
CZCS	Coastal Zone Color Scanner instrument aboard the NIMBUS-7 satellite	
E_d	Downwelling irradiance	mW cm^{-2} μm^{-1}
EDR	Environmental Data Record	
EPA	US Environmental Protection Agency	
	Downwelling irradiance from above-water reference sensor	mW cm^{-2} μm^{-1}
ESSA	Environmental Science Services Administration	
		mol e^- h^{-1}
FOV	Field of view	
F_v/F_m		
FWHM	Full width at half maximum	
GIOP	Generalized IOPs algorithm	
IFCB	Imaging Flow CytoBot instrument (see Table B2)	
I_i	integration time used for that reading	s
IOCCG	International Ocean Colour Coordinating Group	
JPSS-2	Joint Polar Satellite System -2 (future satellite mission)	
		mW cm^{-2} μm^{-1} sr^{-1}
Lat	latitude	decimal degrees
		mW cm^{-2} μm^{-1} sr^{-1}
LDEO	Lamont-Doherty Earth Observatory at Columbia University	
L_s	Radiance of sky	mW cm^{-2} μm^{-1} sr^{-1}
		mW cm^{-2} μm^{-1} sr^{-1}
L_u	Upwelling radiance	mW cm^{-2} μm^{-1} sr^{-1}
$L_u(0^-, \lambda)$		mW cm^{-2} μm^{-1} sr^{-1}
L_w	Water-leaving radiance	mW cm^{-2} μm^{-1} sr^{-1}
min	minutes	
MOBY	Marine Optical BuoY	
MSL12	Multi-Sensor Level-1 to Level-2 processing system	
	number (count)	

Abbreviation	Description	Typical Units (if applicable)
n/a	Not available	
n.d.	Not done	
NASA	National Aeronautics and Space Agency	
NASA/GSFC	NASA/Goddard Space Flight Center	
NCEI	National Centers for Environmental Information	
NCOM	Navy Coastal Ocean Model	
NESC	National Environmental Satellite Center	
NESDIS	National Environmental Satellite, Data, and Information Service	
NESS	National Environmental Satellite Service	
NIR	Near infrared	
NIST	National Institute of Standards and Technology	
nL_w	Normalized water-leaving radiance	mW cm^{-2} μm^{-1} sr^{-1}
NOAA	National Oceanic and Atmospheric Administration	
NOAA-20	Satellite platform (JPSS-1 prior to launch)	
NOAA/STAR	NOAA/Center for Science tech, algorithm, research	
NRL	Naval Research Laboratory	
NURADS	New Upwelling Radiance Distribution camera System	
OCR-VC	Ocean Colour Radiometry Virtual Constellation	
OLCI	Ocean and Land Colour Instrument	
OMAO	Office of Marine and Air Operations	
OSU	Oregon State University	
PAR	Photosynthetically Active Radiation	
PI	Principal Investigator	
PSICAM	Point source integrated cavity absorption meter	
PSU	Practical salinity unit	g kg^{-1}
QAAv6	Quasi-analytical algorithm version 6	
QFT-ICAM	Quantitative filter technique - integrated cavity absorption meter	
RFU	Relative fluorescence units	
RMSD	Root mean square difference	
RPD	Relative percent difference	
R_{rs}	Remote sensing reflectance	sr^{-1}
S	Radiometric spectrum measurement	
SeaWiFs	Sea-viewing Wide Field-of-view Sensor	
SGLI	Second Generation Global Imager	
SN	Serial number	
SNPP	Suomi National Polar-orbiting Partnership	
S_p	Radiometric spectrum measurement of NOAA Spectralon white plaque	
S_{sfc}	Radiometric spectrum measurement of surface water	
S_{sky}	Radiometric spectrum measurement of sky	
SST	Sea surface temperature	°C
SPM	Suspended Particulate Material	mg L^{-1}
T	Time	s
U. Miami	University of Miami	
UMB	University of Massachusetts – Boston	
USF	University of South Florida	
USM	University of Southern Mississippi	
UTC	Coordinated Universal Time	
UPD	Unbiased percent difference	
UV	Ultraviolet	
VIIRS	Visible Infrared Imaging Radiometer Suite	
VSF	Volume scattering function	m^{-1} sr^{-1}
β	Total volume scattering	m^{-1}
β_p	Particulate volume scattering	m^{-1}
$\Delta\phi$	Relative azimuth between the sun and the instrument viewing direction	°
$\Delta(\lambda)$	spectrally dependent scalar offset	
λ	Wavelength	nm
ϕ_i	Scatter azimuth, incident	°
ϕ_r	Scatter azimuth, reflective	°
Φ	Relative azimuth of the sensor to the sun	°
P	Reflectance	sr^{-1}
$\rho(\lambda, \theta)$	Fresnel reflectance factor of seawater	
θ_{sfc}	Sensor zenith angle for water surface	°
θ_{sky}	Sensor zenith angle for sky	°
σ_{PSII}	Functional absorption cross-section of Photosystem II	$Å^2$ $quanta^{-1}$ or 10^{-10} m^2 $electron^{-1}$
σ	Standard deviation	

Table A-2. Instrument shorthand, description and manufacturer with modifications when applicable.

Instrument Shorthand	Full Identification/Purpose	Manufacturer or Citation
ac-9	In situ spectrophotometer – 9 wavelength spectral resolution	WET Labs, Sea-Bird Scientific
ac-s	In situ spectrophotometer – high spectral resolution, 87 wavelengths	WET Labs, Sea-Bird Scientific
ADCP	Acoustic Doppler Current Profiler	Teledyne RD Instruments
AERONET-OC	AErosol RObotic NETwork for Ocean Color	
ALF	Advanced Laser Fluorometer	WET Labs, Sea-Bird Scientific
AlgaeOnlineAnalyser	Spectral fluorometer	bbe Moldeanke
ASD	Analytical Spectral Device; HandHeld2-Pro visible and near infrared spectrophotometer	Analytical Spectral Devices, Inc., a Malvern Panalytical company, Boulder, CO, USA
BB3	Backscatter – 3 channels	WET Labs, Sea-Bird Scientific
BB9	Backscatter – 9 channels	WET Labs, Sea-Bird Scientific
C-OPS	In situ radiometer, 3 sensors, 19 channels each	Biospherical Instruments, Inc. San Diego, CA, USA
CTD	Conductivity, Temperature, Depth	Generic, various manufacturers
DH4	Data logger	WET Labs, Sea-Bird Scientific
ECO-Puck Triplet Fluorometer	Fluorescence at 3 channels for determining chlorophyll, CDOM and phycoerythrin	WET Labs, Sea-Bird Scientific
ECO-Puck Triplet Scatterometer	Scatter – 3 channels (443, 550, 860)	WET Labs, Sea-Bird Scientific
FIRe	Variable fluorescence	Satlantic
FL3	Fluorometer	WET Labs, Sea-Bird Scientific
FlowCam	Dynamic imaging particle analysis for species composition and size measurements	Fluid Imaging Technologies, Inc.
FRRF	Fast Repetition Rate Fluorometer	Generic term
Garmin GPSMAP 78sc	Global positioning mapping instrument	Garmin International, Inc., Olathe, KS, USA.
GER	Field portable spectroradiometer	Spectra Vista Corporation, Poughkeepsie, NY, USA.
HyperOCI	Hyperspectral irradiance sensor	Satlantic LP, Sea-Bird Scientific
HyperOCR	Hyperspectral radiance sensor	Satlantic LP, Sea-Bird Scientific
HyperPro, HyperPro-II	Free-falling hyperspectral optical profiler	Satlantic LP, Sea-Bird Scientific
Imaging Flow CytoBot (IFCB)	Automated microscopic imaging instrument	McLane Research Labs
M2450	Polarization camera	Teledyne DALSA, Waterloo, ON, Canada
MASCOT	Multi-angle scattering optical tool	WET Labs, Sea-Bird Scientific
Microtops	Handheld sun photometer (atmospheric aerosols and optical depth)	Solar Light Company
NURADS	Upwelling Radiance Distribution Camera System	Voss and Chapin, 2005
RAMSES	Radiometer	TriOS Mess- und Datentechnik GmbH, Rastede, Germany
RISBA	Radiometer Incorporating the Sky Blocking Approach	Lee et al. 2013
Sartorius CPA 2250	Balance	Sartorius
SBE 49	Conductivity, Temperature, Depth	SeaBird Scientific
Spectralon	White material (used for above-water reference plaques)	Labsphere, Inc., North Sutton, NH, USA
Snapshot Hyperspectral Imager, UHD285	Above water snapshot imaging spectrometer	Cubert GmbH, Germany
SR1900 (Spectral Evolution)	Spectroradiometer, handheld	Spectral Evolution, Inc., Lawrence, MA, USA
VSF-9	Volume scattering function – 9 channels	WET Labs, Sea-Bird Scientific